SYDDANSK UNIVERSITET

UNIVERSITY OF SOUTHERN DENMARK

MADS CLAUSEN INSTITUTE
NanoSYD

Plasmonics for microfluidics sensor application

Master Thesis

Author:

Elzbieta Sobolewska

Supervisor:

Jacek Fiutowski,

James Hoyland

Sønderborg 2014

Table of contents

Acknowledgment

I would like to express my deep gratitude to my supervisors Assistant Professor Jacek Fiutowski and Assistant Professor James Hoyland for every help I received. I will always be grateful to for their patience, knowledge they shared with me and guidance during my master project. I am grateful for all the support I received and for possibility of working with them.. This thesis would not have been possible without their help.

Finally, I own more than thanks to my parents and my sister for all kinds of support and encouragement. That they stand by me even in my moments of weakness and uncontrolled happiness.

I. Introduction

1. Motivation

Microfluidics is a fast developing field of science, which during last decade found use for various applications. Due to the fact that it uses fluids with amounts less than µl gives a great opportunity to decrease the size and costs of measurement and analyses. Microfluidics is the base for miniaturization of laboratories which are used in biology, physics, medicine and many more. These devices are called Lab-On-Chip (LOC) and integrate several different microfluidic structures on a single chip of only millimetres to a few square centimetres in size. Additionally, is possible to design and fabricate construction which allows separating the components of the solution, combining them with another fluid or allowing for existence at the same time in one channel without mixing.

From a long time the light was used in detection, measurements and analysis. An interesting part of this field of study is surface plasmons (SPs). This can be described as coherent electron oscillations that exist at the metal – dielectric interface. It can be excited at special configuration by the light illumination. Excitation of SPs is commonly used as a technique known as surface plasmon resonance (SPR). In this method the power of reflected beam is the measurement signal which is presented as a function of incident light or wavelength. Moreover, approach of any type of plasmons have a high potential for nanoscale light manipulation and is a key for future applications e.g. CMOS- compatible electro-optical plasmonic modulator [1], molecular sensors [2], plasmonic solar cells [3] .

A natural consequence of the development of sensors is a combination of these two fields of science. Taking advantages from microfluidics and plasmonics at the same time give a starting point for new research area which is called optofluidics [4]. Although the term is new, in the past few years bring a lot of experimental devices from different fields e.g. energy applications [5], biosensors [6]etc. However, especially usage of surface plasmons polaritons (SPPs) is not common in Lab on chip.

High sensitivity of SPPs to changes of dielectric properties is the biggest advantage of this phenomenon in terms of microfluidics sensors. Many experimental setups which use SPPs are under investigation and were a main inspiration for approach of this project e.g. alcohol sensor [7], research about Kretschmann surface plasmon resonance (SPR) sensor configuration [8], differential plasmon resonance sensor [9].

2. Project description

The aim of this project is to investigate abilities of the plasmonic nanostructure to perform optical measurements of the microfluidic flow (the ability of usage of SPs in order to build LoC sensor platform). The detection system is constructed and arranged for sensing any change of the refractive index in the microfluidic channel.

The goal of the project is to construct a system which allows placing fluids in microscale on the plasmonic structure and collecting the reflected light. This step includes fabrication of the PDMS chip and adapting it to the optical detection system.

Moreover, to verify the effectiveness of the sensor the design of the chip is droplet-based microfluidics system. It allows introducing additional bubbles of a gas or droplets of a liquid in the continuous flow of the medium. The project should present characteristic features of the optical sensor.

II. Background principles

This chapter presents the main theoretical aspects which are related to the field of optics and microfluidics. These principles are the base for performing entire concept of building the plasmonic sensor applications.

1. The evanescent wave

Starting point for understanding the light phenomenon which occurs on the boundary of two mediums with different refractive indices are Fresnel's equations. Due to the fact that the light is an electromagnetic wave, there can be selected two perpendicular propagating waves (of electric and magnetic field). So, there can be distinguished two extreme cases: when electric field is perpendicular to the interface (TM) and when electric field is parallel to it (TE). These types are called the polarization modes and give different properties for the boundary conditions (Figure 1). They are connected with the location of electric and magnetic wave with respect to the plane of incidence. Definition of the plane of incidence is that it is a plane which contains the incident and reflected k-vectors. Also, the plane of the interface (the boundary) is the plane between the two mediums and is perpendicular to the incidence plane.

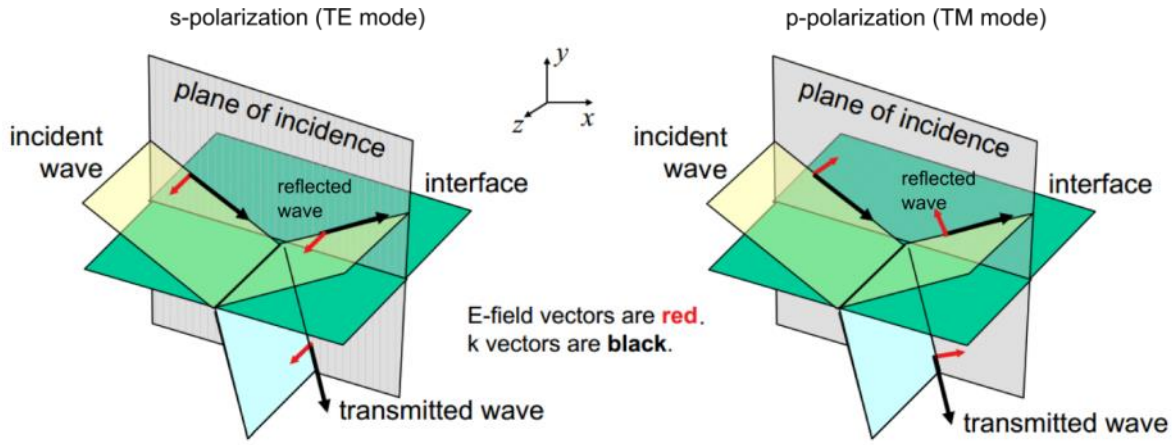

Figure 1 Presentation of two polarization modes and their physical interpretation on the interface of two mediums [10].

For perpendicularly polarized light (s-polarized) the electric field vector is perpendicular to the plane of incidence and the magnetic field is parallel to it. Moreover, all parallel components to the boundary must continue at the boundary [11]. In this case the electric field can be simplified to the equation (1.1). However, boundary conditions require taking into account all geometrical connection between incidents, reflected and transmitted beam of the magnetic field. This results with equation (1.2).

$$E + E_r = E_t \tag{1.1}$$

$$B_i \cdot \cos\theta - B_r \cdot \cos\theta_r = B_t \cdot \cos\theta_t \tag{1.2}$$

Combining these equations with the Snell's law of refraction (1.3) give coefficients of reflection and transmission (1.4). These equations are known as the Fresnel's equations for s-polarized light.

$$n_r \cdot \sin\theta_r = n_t \cdot \sin\theta_t \tag{1.3}$$

$$r_{TE} = \frac{E_r}{E_i} = \frac{\cos\theta - n \cdot \cos\theta_t}{\cos\theta + n \cdot \cos\theta_t} = \frac{\cos\theta - \sqrt{n^2 - \sin^2\theta}}{\cos\theta + \sqrt{n^2 - \sin^2\theta}} \tag{1.4}$$

$$t_{TE} = \frac{E_t}{E_i} = \frac{2\cos\theta}{\cos\theta + n \cdot \cos\theta_t} = \frac{2\cos\theta}{\cos\theta + \sqrt{n^2 - \sin^2\theta}} \tag{1.5}$$

Similar situation can be considered for parallel polarized light (p-polarized). In this case the vector of the magnetic field is perpendicular to the plane of incidence and the electric field is parallel to it. These results in the opposite situation for boundary conditions, the magnetic field can be simplified (1.6) while geometrical relations must be taken into account for electric field (1.7). Repeating the process of combining these equations give as results the Fresnel's equations for p-polarized light (1.8, 1.9).

$$-B_i + B_r = -B_t \tag{1.6}$$

$$E_i \cdot \cos\theta + E_r \cdot \cos\theta_r = E_t \cdot \cos\theta_t \tag{1.7}$$

$$r_{TM} = \frac{E_r}{E_i} = \frac{-\mathrm{n} \cdot \cos\theta + \cos\theta_t}{n \cdot \cos\theta + \cos\theta_t} = \frac{-n^2 \cdot \cos\theta - \sqrt{n^2 - \sin^2\theta}}{n^2 \cdot \cos\theta + \sqrt{n^2 - \sin^2\theta}} \tag{1.8}$$

$$t_{TM} = \frac{E_t}{E_i} = \frac{2 \cdot \mathrm{n} \cdot \cos\theta}{n^2 \cdot \cos\theta + n \cdot \cos\theta_t} = \frac{2 \cdot \mathrm{n} \cdot \cos\theta}{n^2 \cdot \cos\theta + \sqrt{n^2 - \sin^2\theta}} \tag{1.9}$$

The plot of relations between reflection coefficients for glass-to-air interface and incident angle (Figure 2), gives a lot of information about light-matter interaction. Relationships at the air-to-glass interface have been omitted due to the fact that they do not contribute to developing of the project.

Regardless of the polarization mode, at the Critical angle (θ_c) reflection coefficient tends to 1 or -1. For each angle above the limit angle, total internal reflection occurs. This phenomenon has also mathematical base which come from the Snell's law (1.3). Solution of this equation for θ_t is (1.10) shows that there is no "real number" solution for arcsine of a number larger than one. In this case the critical angle exists when sin θ_i is equal 1. The physical interpretation of this is that the entire incident light is reflected back into the first medium from the interface [12].

$$\theta_t = \sin^{-1}\left(\frac{n_i}{n_t}\sin\theta_i\right) \tag{1.10}$$

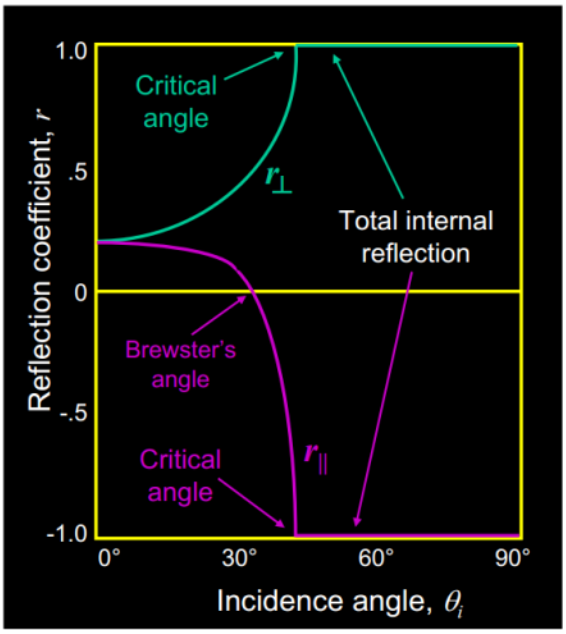

Figure 2 An exemplary presentation of the relationship between reflection coefficient (r) and angle of incidence (θ_i) for glass-to-air interface [10]. It can be noticed that there exists the angle for which r of both polarization modes are equal 1 or -1. This is the limit angle for which total internal reflection occurs.

However, when total internal reflection (TIR) occurs, there must be still continuity of the electromagnetic field at the boundary of two mediums. This "transmitted wave" is called the evanescent wave and its wave equation can be written (1.11) with two (x- and y) components (1.12). In case of the TIR the $\cos(\theta_t)$ becomes purely imaginary and gives new exponential factor (1.13) which results in a new wave equation (1.14).

$$E_t = E_{0t} e^{i(\overrightarrow{k_t}\cdot\vec{r}-\omega t)} \tag{1.11}$$

$$\overrightarrow{k_t}\cdot\vec{r} = k_t(-x\sin\theta_t - y\cos\theta_t) \tag{1.12}$$

$$\overrightarrow{k_t}\cdot\vec{r} = -k_t x\frac{\sin\theta}{n} + ik_t|y|\sqrt{\frac{\sin^2\theta}{n^2}-1} \tag{1.13}$$

$$E_t = E_{0t} e^{-i\omega t} e^{-ixk_t\frac{\sin\theta}{n}} e^{-k_t|y|\sqrt{\frac{\sin^2\theta}{n^2}-1}} \tag{1.14}$$

This presents that the evanescent wave is decreasing exponentially in y- direction. The penetration depth can be calculated from the last part of the wave equation (1.15).

$$|y| = \frac{\lambda}{2\pi\left(\frac{\sin^2\theta}{n^2}-1\right)} \tag{1.15}$$

Due to the fact that the evanescent wave is an exponential function it gives great possibilities of application. If dielectric material is located in distance smaller than the penetration depth, then the TIR can be "frustrated". This phenomenon is called Frustrated Total Internal Reflection (FIR). The most common application nowadays is fingerprint

sensors, multi-touch [13] screens and Total internal reflection fluorescence (TIRF) microscopy [14]. The idea is that the second surface is very close to the place of the evanescent wave; however it is not touching (Figure 3).

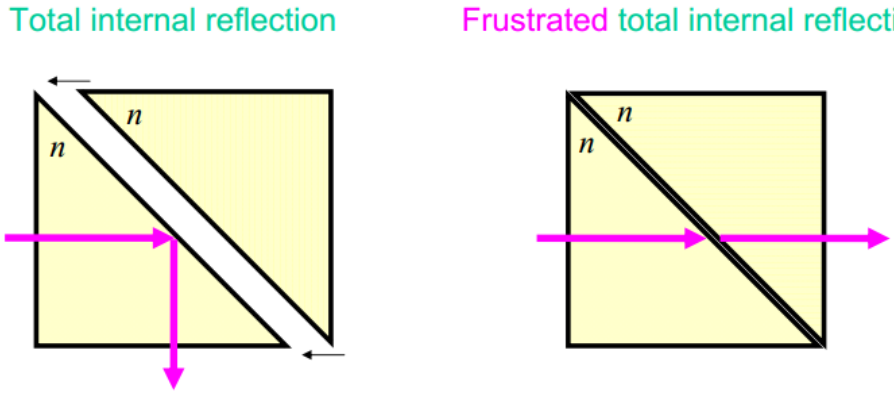

Figure 3 Presentation of the phenomenon TIR and FIR. The idea is that both substances have got the same or similar refractive index and are placed in distance smaller than the penetration depth. In that situation, created evanescent wave will penetrated through the space gap and go to the second surface.

2. Surface plasmon polaritons

Considerations about the incident light on the boundary of two dielectrics with different refractive index, lead to the next stage which is the interface between dielectric and metal. Interactions of electromagnetic fields with the matter can be described by Maxwell's equations (1.16 -1.19), which are the basic formulas in the electrodynamics [15].

$$\nabla \cdot \vec{D} = \rho_{ext} \tag{1.16}$$

$$\nabla \cdot \vec{B} = 0 \tag{1.17}$$

$$\nabla \times \vec{E} = -\frac{\partial \vec{B}}{\partial t} \tag{1.18}$$

$$\nabla \times \vec{H} = \vec{J}_{ext} + \frac{\partial \vec{D}}{\partial t} \tag{1.19}$$

These equations are the combination of four macroscopic fields which are necessary to describe the phenomenon at the metal-dielectric interface. In the equations (1.16 -1.19) E[V/m] is a electric field intensity, H[A/m] is a magnetic field intensity, D[C/m^2] is the dielectric displacement, B[Wb/ m^2] is the magnetic induction. Where, ρ_{ext} is the external charge and J_{ext} is current density which can be treated as sources of the electric and magnetic field, respectively. To solve the set of equation, there must be added constitutive relations which combine together $\vec{H}$ vector with $\vec{B}$ vector and also $\vec{E}$ vector with $\vec{D}$ vector. Thus, the system of equations can be associated with the material constants ε (electric permittivity) and μ (magnetic permeability) (1.20 and 1.21).

$$\vec{D} = \varepsilon \vec{E} = \varepsilon_0 \vec{E} + \vec{P} \tag{1.20}$$

$$\vec{B} = \mu \vec{H} = \mu_0 \vec{H} + \mu_0 \vec{M} \tag{1.21}$$

$\vec{P}$ in this case is the vector of electric polarization and $\vec{M}$ is the vector of magnetic polarization which can be omitted if it is considered non-magnetic surface.

In the wide range of the optical frequency, the metal properties can be described by the Drude model. It was presented by Paul Drude in 1900 and assumed that the microscopic behaviour of electrons in the solid material can be described as a sea of constantly moving electrons above the stable plane of positive ions [16] [17]. Electrons collide with themselves and other ions etc. with probability equal to $\gamma = 1/\tau$ (τ is mean free time between ionic collisions [16]) and they can bounce even out from the metal. Therefore, above the metal surface there exists a cloud of electrons oscillating with the so called plasma frequency ωp [15] (1.22).

$$\omega_p = \sqrt{\frac{ne^2}{\varepsilon_0 m}} \tag{1.22}$$

Combining this relation with the polarization density and dielectric displacement it is possible to obtain the formula for dispersion relation which can describe most of the metal parameters.

$$\varepsilon(\omega) = 1 - \frac{{\omega_p}^2}{\omega^2 - j\gamma\omega} \tag{1.23}$$

These relations are necessary to determine the dispersion relation of the plane wave in metal. To achieve this, there must be some general assumptions added to already known relations. The starting point for any calculation connected with light is the wave equation (1.24). Next thing is general formula for dispersion relation of plane wave (1.25). The last required equation is connected to the definition of ideal metal (1.26) where damping does not exist.

$$\nabla^2 \mathrm{E} - \frac{\varepsilon}{\mathrm{c}^2} \cdot \frac{\partial^2 \mathrm{E}}{\partial \mathrm{t}^2} = 0 \tag{1.24}$$

$$\left|\vec{k}\right|^2 = k^2 = \varepsilon(\omega)\left(\frac{\omega}{c}\right)^2 \tag{1.25}$$

$$\varepsilon(\omega) = 1 - \left(\frac{\omega_p}{\omega}\right)^2 \tag{1.26}$$

Combining all presented equations give as a result the dispersion relation of the plane wave in metal (1.27).

$$\left|\vec{k}\right|^2 = k^2 = \left[1 - \left(\frac{\omega_p}{\omega}\right)^2\right]\left(\frac{\omega}{c}\right)^2 \Rightarrow \omega^2 = \mathrm{c}^2\mathrm{k}^2 + {\omega_\mathrm{p}}^2 \tag{1.27}$$

Graph which presents the dispersion relation give a lot of information about the light phenomenon at the metal-dielectric interface.

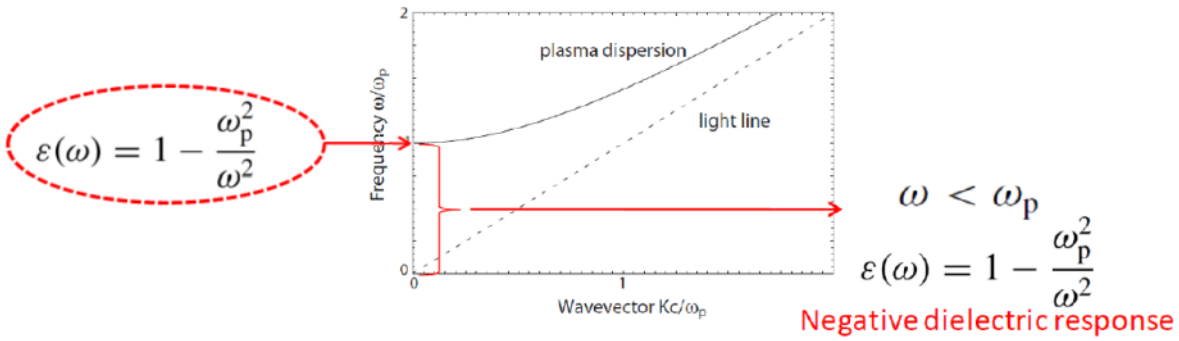

Figure 4 The dispersion relation of the free electron gas [15]. Dotted line corresponds to the white light dispersion. Because, it does not cross the plasma dispersion line which means that direct illumination of the white light does not have any influence on the free electron's oscillation. Moreover, it shows that electromagnetic propagation is allowed only for frequency higher thanω_p.

The presented dispersion formula is useful for considerations about reflection from metals, where can be selected and discussed three parts.

- For $\omega < \omega_p$ the dielectric function (ε) is imaginary and the wave is totally internally reflected.
- For $\omega = \omega_p$ the dielectric function is equal to 1 which corresponds to a resonant state. In this case there is no reflection of the wave; however the excitation of volume plasmons (VPs) occurred. VPs are collective longitudinal oscillations of the free electrons within the metal bulk which cannot be excited by transverse wave (no crossing points on (Figure 4)).
- For $\omega > \omega_p$, the ε(ω) is real and transmission of the light is possible which can be described by the reflectance (1.28).

$$R = \left|\frac{\sqrt{\varepsilon} - 1}{\sqrt{\varepsilon} + 1}\right|^2 \qquad (1.28)$$

However, there occurs also another phenomenon which takes place only at the surface and is called surface plasmons polaritons. They are collective oscillations of electrons that propagate on the boundary between metal and dielectric. The electromagnetic field of propagating SPPs can be determined in each of the media using the classical solutions of Maxwell's equations with taking into account the relevant boundary conditions. To obtain the solution of the surface wave, boundary conditions must assumed the continuity of tangential components of electric and magnetic fields on the border and the exponential decay of fields as the distance from the border [17] (Figure 5).

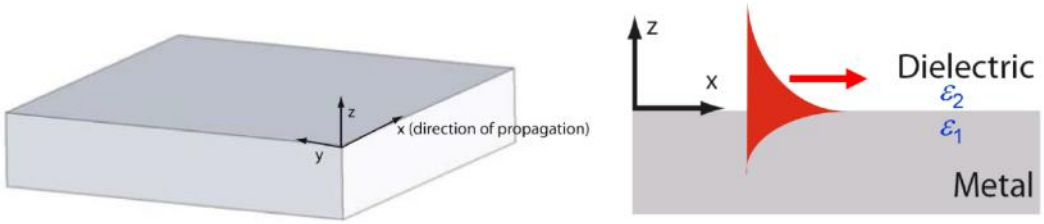

Figure 5 Representation of coordinate system used in the calculation of the SPPs properties.

To investigate SPPs it is assumed that monochromatic light is used as the light source and according to presented coordinate system the direction of propagation is the x-axis. Under this conditions components of two curl-equations are presented (1.29)(1.30). The time harmonic dependence is assumed and constitutive relations are applied to equations (1.31, where $\beta=k_x$ is propagation constant). Both curl-equations must be combine with the others, but in respect with all direction separately (1.32)(1.33).

$$\nabla \times E = -\frac{\partial B}{\partial t} \tag{1.29}$$

$$\nabla \times H = J_{ext} + \frac{\partial D}{\partial t} \tag{1.30}$$

$$\frac{\partial}{\partial t} = -i\omega \quad \frac{\partial}{\partial x} = i\beta \quad \frac{\partial}{\partial y} = 0 \quad D = \varepsilon\varepsilon_0 E \quad B = \mu_0 \mu H \tag{1.31}$$

$$\nabla \times E = -\frac{\partial B}{\partial t} \Rightarrow \begin{cases} \dfrac{\partial E_y}{\partial z} = -i\omega\mu_0 H_x \\ \dfrac{\partial E_x}{\partial z} - i\beta E_z = i\omega\mu_0 H_y \\ i\beta E_y = i\omega\mu_0 H_z \end{cases} \tag{1.32}$$

$$\nabla \times H = J_{ext} + \frac{\partial D}{\partial t} \Rightarrow \begin{cases} \dfrac{\partial H_y}{\partial z} = i\omega\varepsilon_0\varepsilon E_x \\ \dfrac{\partial H_x}{\partial z} - i\beta H_z = -i\omega\varepsilon_0\varepsilon E_y \\ i\beta H_y = -i\omega\varepsilon_0\varepsilon E_z \end{cases} \tag{1.33}$$

Further considerations must be performed for two polarization states (TE and TM) separately.

TE mode	TM mode	
The following formulas present axial components of the light for different polarization states		
$\frac{\partial^2 E_y}{\partial z^2} + (k_0^2\varepsilon - \beta^2)E_y = 0$	$\frac{\partial^2 H_y}{\partial z^2} + (k_0^2\varepsilon - \beta^2)H_y = 0$	(1.34)
$H_x = i\frac{1}{\omega\mu_0}\cdot\frac{\partial E_y}{\partial z}$	$E_x = -i\frac{1}{\omega\varepsilon_0\varepsilon}\cdot\frac{\partial H_y}{\partial z}$	(1.35)
$H_z = \frac{\beta}{\omega\mu_0}\cdot E_y$	$E_z = -\frac{\beta}{\omega\varepsilon_0\varepsilon}\cdot H_y$	(1.36)
Continuity of E_y and H_x at z=0 must be preserved, hence: $A_1=A_2$ and $A_1(k_1+k_2)=0$	Continuity of H_y and $\varepsilon_i E_z$ at z=0 must be preserved, hence: $A_1=A_2$ and $\frac{k_2}{k_1} = -\frac{\varepsilon_2}{\varepsilon_1}$	(1.37)
Confinement to the surface requires Re[k1] > 0 and $Re\ [k2] > A \Rightarrow\ A = 0$ If the amplitude is equal 0 there is no excitation → **SPP cannot be excited at TE mode**	Combining the second condition with $k_1^2 = \beta^2 - k_0^2\varepsilon_1$ $k_2^2 = \beta^2 - k_0^2\varepsilon_2$ gives formula for propagation constant and therefore, dispersion relation of SPP $\beta = k_0\sqrt{\frac{\varepsilon_1\cdot\varepsilon_2}{\varepsilon_1+\varepsilon_2}}$ and $k_{SPP} = \frac{\omega}{c}\sqrt{\frac{\varepsilon_m(\omega)\cdot\varepsilon_d}{\varepsilon_m(\omega)+\varepsilon_d}}$	(1.38)

Dielectric constant of metal (ε_m) and other medium (ε_d) are very important parameters in the dispersion relation of SPPs. For both materials this factor is directly connected with its refractive index$\sqrt{\varepsilon} = \eta$. However, metals have complex refractive index which results with the complex dielectric constant.

In conclusion, to excite SPPs the x component of the wavevector of the incident light has to be equal to the wavevector of SPPs. Additionally, due to the longitudinal nature of SPPs, only TE mode of polarization can be used in excitation process. Moreover, SPPs wavevector is always larger than wavevector of the incident light, this results that direct illumination of the metal-dielectric interface will not excite SPPs (Figure 6) .

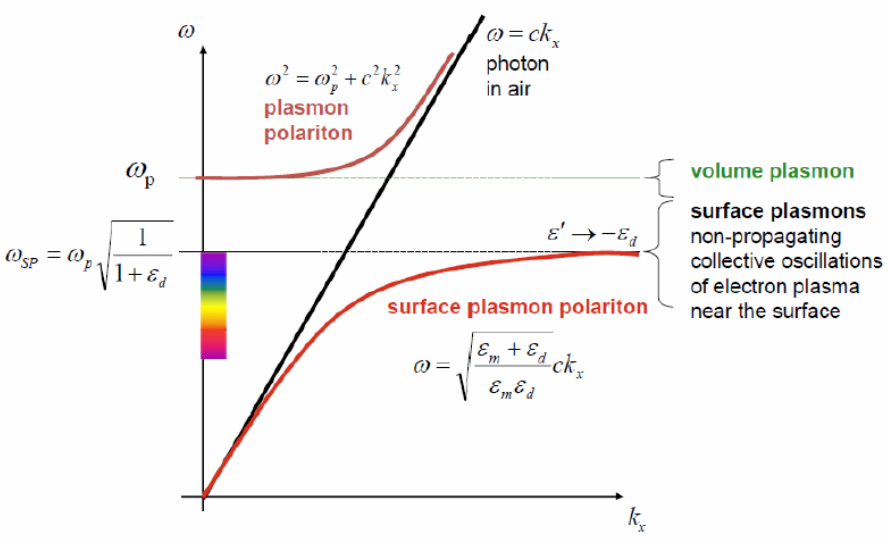

Figure 6 Dispersion relation of surface plasmon polaritons. Straight black line corresponds to the direct light illumination. It shows that there are no common points for the light and plasmon polaritons (SPs), this means that direct illumination of light cannot excite any kind of the SP [18].

Further analyses of SPPs can provide more information about their features like propagation length, penetration depth etc. However, due to losses inside a metal, the energy of SPPs is decreasing exponentially with the propagation along the metal-dielectric interface. The following equations describe wavelength, propagation length and penetration depth of SPPs respectively. Moreover, example of the length of the propagation path at the interface between gold and two dielectrics with different refractive indices is presented in Figure 7.

$$\lambda_{SPP} = \frac{2\pi}{Re(k_{SPP})} \quad L_{SPP} = \frac{1}{Im(2k_{SPP})}$$
$$d_{d(m)} = \left|k_{z,d(m)}\right|^{-1} = \frac{\lambda}{2\pi}\sqrt{\left|\frac{\varepsilon_m + \varepsilon_d}{\varepsilon^2{}_{d(m)}}\right|} \qquad (1.39)$$

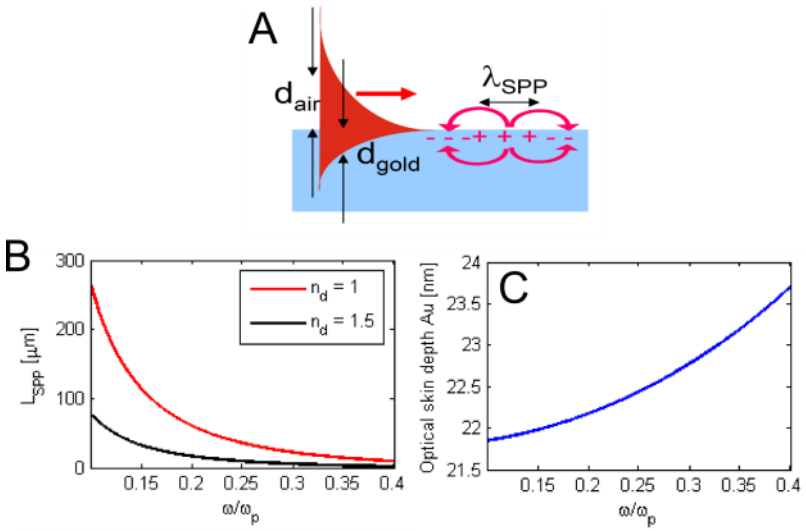

Figure 7 A) imaging abbreviations from (1.39) formula, B) The length of the propagation path of SPPs at the gold-dielectric interface with two different the frequency of the incident wave ε=1 and ε=2,25, C) The depth of penetration of the SPPs electromagnetic field in the gold, depending on the frequency of the incident wave [17].

Localized electromagnetic excitation can also exist on curved surfaces e.g. on nanoparticles, on edges of cavities on the smooth surfaces etc. The characteristic property of localized surface plasmons (LSPs) is that they are not propagating along the surface. Moreover, LSP can be excited by resonance wave of appropriate frequency. Due to that fact, it explains the fact of strong diffraction of SPPs on the uneven surface. Dimensions of the object a material properties (dielectric function) have strong influence on frequencies of LSPs. However, if their frequency is close to SPPs frequency, they have got much influence on the SPPs behaviour. One of LSPs features is that their behaviours are not specified for a particular wavelength and they are very difficult to excite at desire place.

Excitation of surface plasmon polaritons

Due to the fact that direct illumination of the light cannot excite the SPP on the plane surface, it must be applied special configuration. Many methods of SPPs excitation have been developed so far e.g. prism coupling, grating coupling, excitation using highly focused optical beams and many more [19]. Due to approach of this project, only short description of Kretschmann configuration is presented.

It is one of the most common prism coupling methods, which are use to excite SPPs on the plane metal surface. In this case, the plane layer of metal is deposited on the prism's surface. Then the light beam "*impinging from the glass side at an angle greater than the critical angle of total internal reflection tunnel through the metal film and excite SPPs at the metal/air interface*" [19]. One of the requirements for this method is that the thickness of metal' layer must be thin enough to allow tunnelling of photons. Due to the fact that the prism is optically denser, it results with increasing the wavevector of the light.

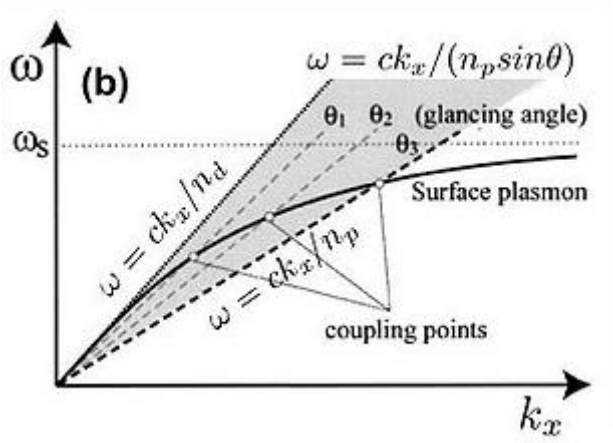

Figure 8 Schematic diagrams of dispersion relation of the light using the Kretschmann configuration. On the graph there are presented four different values of the wavevector of the light, three of them are able to excite SPPs [20].

The in-plane component of wave vector of the light can be changed by adjusting an incident angle according to the following formula (1.40).

$$k = \frac{\omega}{c} n_p \sin\theta \quad (1.40)$$

n_p – refractive index of the prism
θ – the incident angle

3. Basic principles of microfluidics

Microfluidics is a multidisciplinary field of science which combines many scientific disciplines like physic, chemistry, engineering, biology etc. Results of this combination are systems which are able to use a very small amount of fluids to measure, detect or control many processes. However in each of them, there are some laws that must be satisfied in order to successfully design Microfluidics system. Some of basic principles are presented and briefly described.

Reynolds number

Types of the fluid flow are described by the Reynolds number which determines if the flow is laminar or turbulent. The same principles can be used to describe the flow of fluids along microfluidic channels [21] (1.41).

$$R_e = \frac{L \cdot V_{avg} \cdot \rho}{\mu} \quad (1.41)$$

Where, L is a typical length scale in the system, μ is dynamic viscosity, ρ is the density of the fluid and V_{avg} is the average velocity of the fluid in SI units. In microfluidics channel the length is usually equal to 4A/P, where A is the cross section area of the channel and P is the wetted perimeter of the channel.

Because of small dimensions of microfluidics channel, the Reynolds number is usually around 100. According to the definition of the turbulent flow, it occurs when the number exceeds 2000. In that case, the microfluidic flow can be assumed as completely laminar and no turbulence occurs. Laminar flow of the fluid ensures that a small quantity of the substance (even at molecular dimensions) can be transported in a relatively predictable manner along microchannels. However, it is still possible to design system to make usage of all advantages of fluidic flow, because many parameters are because the number of parameters also depends on the shape, length and design of microchannels.

Poiseuille's Law

In case of laminar flow when viscous and incompressible fluid is used, the effective resistance (R) and the flow rate can be calculate using the Hagen–Poiseuille equation in standard fluid notation (1.42) [22] or in physical notation (1.43).

$$\Delta P = \frac{8\mu L Q}{\pi r^4} \tag{1.42}$$

$$R = \frac{8\eta \Delta x}{\pi r^4} \tag{1.43}$$

Where: ΔP is the pressure loss [Pa], Q is the volume flow rate [m^3/s], r is radius of channel [m], η is dynamic fluid viscosity in Pascal-second, Δx is distance in direction of flow,

Methods of flow generation

We can select two methods for generating the fluid's flow through microchannels: pressure driven flow and electrokinetic flow [21] [23]. However, the most simple and common way is first one, which pumps the fluid through the device using e.g. syringe pump.

Moreover, the basic law of fluid mechanics for pressure driven laminar flow is assuming that the fluid velocity on the wall must be equal zero and is increasing non-linear in direction of the channel's middle point. That makes the velocity profile of the channel similar to parabolic shape.

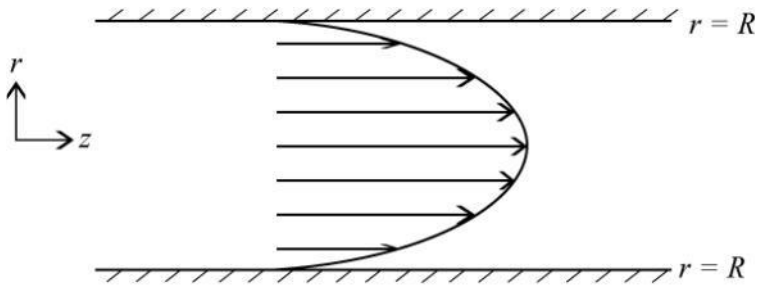

Figure 9 "*The parabolic velocity profile for flow driven by a constant pressure gradient in a circular pipe*" [24].

The parabolic velocity profile is very important in view of distribution of molecules during fluid flow. Moreover, the shape of the channel and pressure value has significant implications for the shape of velocity profile.

Microfluidics droplet device

Microfluidics is the foundation to build miniaturized laboratories which are called Lab-on-Chip (LOC). However, the main principles of operation with fluids in the microscale start from designing microfluidic structure which are dedicated to some special tasks. In LOC many different microfluidics systems are combined together to perform desire analyses or measurements.

One of the key applications is a droplet-based microfluidics. It manipulates at least two flows of fluid to generate the bubble or droplet in a continuous liquid stream. However, the laminar flow is still a requirement for the fluid flow. This type of systems is a great opportunity for building the sensors for fast organic reactions [25]. Basics of a droplet-based microfluidics system are briefly described and presented on the exemplary structure (Figure 10).

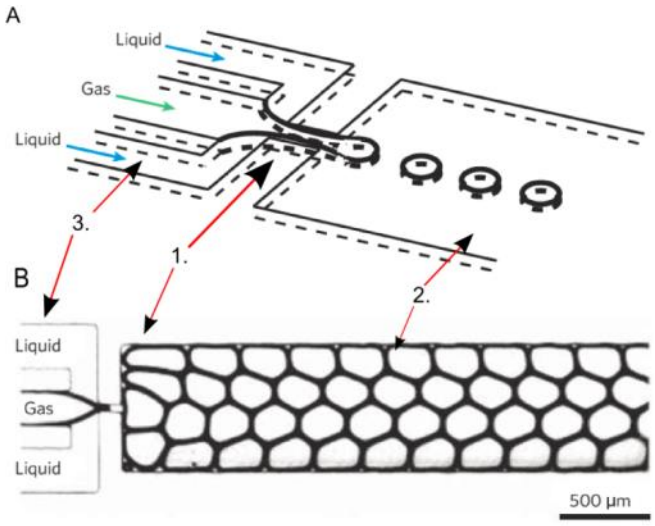

Figure 10 (A and B) Presentation of the principles of a droplet-based microfluidics system. (1.) Focusing channel which is significantly smaller than rest of channels in the system. Here flows of liquid "squeeze" the flow of the gas and produces the bubbles. (2.) Channel which plays the role of bubble chamber and collects all created bubbles and droplets. It is also a area of investigation. (3.) Channels which are responsible for the impact of mediums. The flow rate of liquid and gas control the size and frequency bubbles [25].

Speed of flow of bubbles can be estimated by taking into account the flow speed of each medium and size of the channel. Due to the fact that gases are compressible it is difficult to predict the pressure of the air in the bubble. However, after assumption about the resistance of the liquid flow, the pressure create by the liquid in the channel is around 10% of the atmospheric pressure. This will not have a significant impact on the compressibility of the air. In that case, all calculations are just approximation and the velocity of the bubble can be expressed by equation (1.44).

$$v_b = \frac{Q_g + Q_l}{A} \tag{1.44}$$

Where: Q_g- is a volume flow of gas [m^3/s],

Q_l- is a volume flow of liquid [m^3/s],

A- is a cross section area of the channel [m^2],

III. Approach and experimental setup

This section describes the approach to the problem and its realization. Experimental setup, materials and used fabrication process are here presented with details necessary to understand the entire projects. For some elements of this section it is essential to give the recipe to recreate the process, these can be found in the relevant appendices.

1. Approach

The main idea of the sensor which utilizes the phenomenon of surface plasmon polaritons (SPPs), is to build a structure which combine two fields of science: optics and microfluids. To achieve this, the idea is to excite SPPs on the surface of the prism with a metal layer. The microfluidic chip structure is placed on the top of the prism. To make the system flexible and also easy to replace, the chip is sealed by the glass slide made by the same glass type as the prism. Connection between them is provided by the index matching oil, which correspond to the refractive index of the prism and in the same way to the cover of the chip. A laser light is guided by the optical cage system which allows to freely adjusting the position of the beam. The aim of the laser beam is to reach the prism at specific angle, where phase matching conditions are fulfilled and SPPs are excited at the gold surface. If SPPs are excited inside the channel structure, it will be possible to monitor the dielectric constants of the flowing fluids in classical attenuated total reflection (ATR) configuration. Where any change of refractive index will cause the shift of the angle of the plasmonic resonance.

Reflected beam is measured by the photo diode and collected data presents how the signal is changing depending on flowing medium inside the channel. The sensor should be able to detect small and fast objects in the chip channel. Additionally it will allow for the most accurate detection of difference in flowing liquids. Under consideration, there are two lasers with 633nm and 795nm wavelength. The laser source will be chosen after calculations concerning the incident angle of the plasmon resonance. This stage will also determine the thickness of the metal layer, as well as give the information about the geometric relationships that must be established in the system.

The detection of disturbing objects is made by the flow the small bubbles of air through the channel filled with the liquid. Size of bubbles and speed of flow should be in direct relation with the time and changing the value of the detected light. As a basic design is used a structure with two separated dropled-based maker.

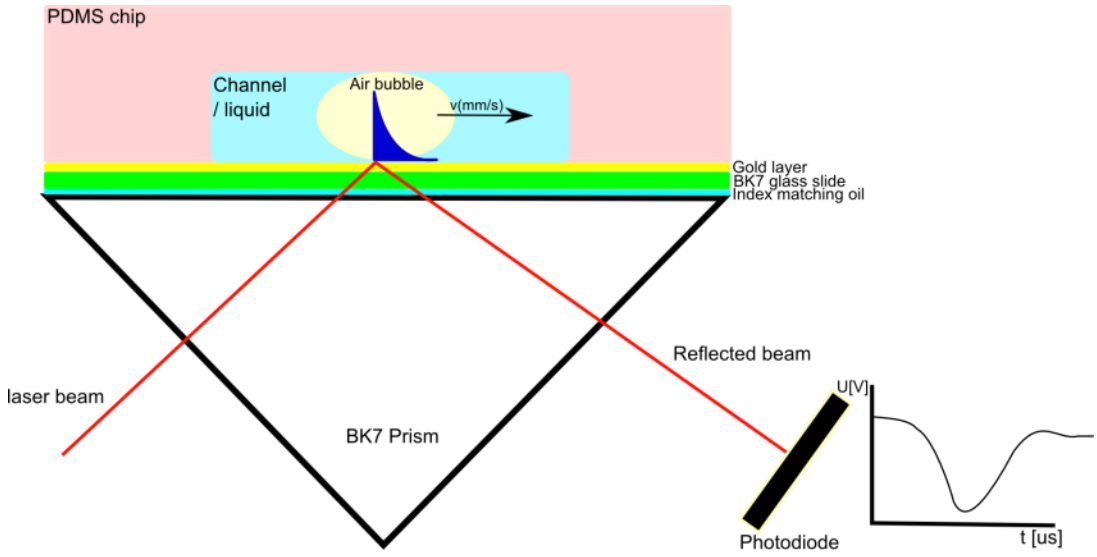

Figure 11 Schematic representation of the microfluidic sensor's idea. A thin layer of gold film is fabricated on the glass slide in place which corresponds to the channel area in the chip. A liquid is given by the two syringe pump and the speed of flow can be controlled. The reflected light from the gold layer is detected by the photodiode which measure the difference in the beam's power relative to the time. This dependence is connected to the presence of substances in the channel.

2. Experimental setup

The entire experimental setup was built and used in the dark optic lab which is situated in the basement to provide constant darkness. To perform experiments correctly, the system consists of optical elements, microfluidic devices, data gathering part and an observation system. The already existing cage system was used as the starting point for this project. The schematic presentation of the entire system shows clearly the connection between elements and the flow of the information (Figure 12). The setup consists of the following parts:

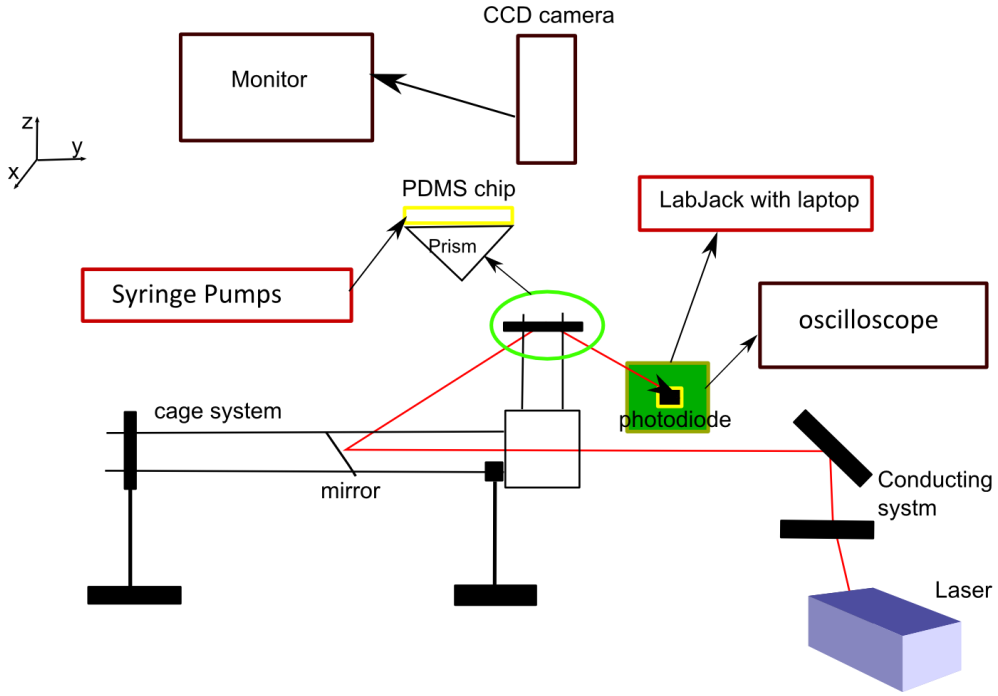

Figure 12 Schematic drawing of the setup and connection between devices.

Laser source with the conducting system – For this project two different lasers were available. First one, which was used in prototyping stage was helium-neon laser emitting light at 633nm and maximum power of 5mW. Second one is the diode laser *(Sacher laser – Tec Series Littrow)* at 795nm wavelength and adjustable power of the beam, up to 60mW. The optical path goes through two mirrors with a protecting silver side (Thorlabs ϕ25,4) recommended for used wavelength. These mirrors provide the ability to adjust the position of beam, both vertically and horizontally. Next elements of the optical system are half-wave plate and polarizer. These components allow reach desire polarization state of the light.

The cage system – In main idea of the project is that the light after passing the conducting system goes through the L-shape cage system. This construction is made from the Thorlabs components: construction rods, clamps, mounting elements and the pivoting optic mount with mirror. At the upper end of the construction is held down the prism with elements to carry out experiments. Rods are easy to exchange or to connect together more than one. The prism holder had to be changed due to the size of the prism. It was made in accordance with given design and with high precision of manufacturing by the university workshop. The mirror is mounted in the Gimbal Mount (Thorlabs) for mirror which allows the movement through rods and rotation with respect to X and z direction.

The microfluidic stage – The right angle prism made from BK7 glass is used as a base for conducting the laser beam to place where surface plasmons polaritons can be enhanced. The hypotenuse wall has dimensions 20mm x 25mm and allows to fit the PDMS chip on its surface. Connection between the chip and the prism is sured by the index matching oil with 1,5000±0,0002 (Cargille Labs, USA) refractive index.

Fluid Control – Two syringe drivers (SK-500I Syringe Pump, SK Medical), are used to control volumetric flow through the chip. There are connected to the motor by pins and rubber tubes which fall within earlier prepared places in the chip.

Observation stage – Non-commercial stage to hold and position CCD camera (JAI CV A60) is used to observe the flow of the medium through channels. Moreover, it helps to adjust the place of laser illumination that fit to the channel. The camera is equipped with a objective with manual shutter (Schneider Optics, Germany), which allows to adjust the right exposure light. Real time observation is possible by the combination the CCD camera with the analog monitor (Colour Video Monitor, Panasonic).

Electronics and data analysis – To measure the reflected beam, the non-commercial light sensor is used. The photodiode has a relatively large area (16mm2). The sensor incorporates a transimpedance amplifier to convert the photocurrent into the voltage signal. The light sensor characterized of a few microseconds response and has direct connection to the oscilloscope (Hewlett Packard, Mega Zoom, 54645D), which allows to immediate

inspection of the signal amplitude and shape. However, to collect data, the photodiode must be connected to the analogue-to-digital converter (the LabJack U12, Low Cost Multifunction DAQ with USB). Then, it is connected to the laptop by standard USB port. To control and collect data, the build-in software is used (LJscope). It works with the same principles as the traditional oscilloscope. One wire is reference and is connected to the ground in the LabJack DAQ card and the second wire reads the current from the photodiode and converts it to voltage. The data is loaded continuously and shown at the user screen (Figure 13 - i). There is possible to connect two channels and load their signals independently (ii - iii). The range of voltage and time can be control by changing the parameters of scanning – scan rate and number of scans (iv). There is also possible to save data, turn on trigger (v), the average of data is automatically calculated (vi) and also there is possible to change the presentation of data (vii).

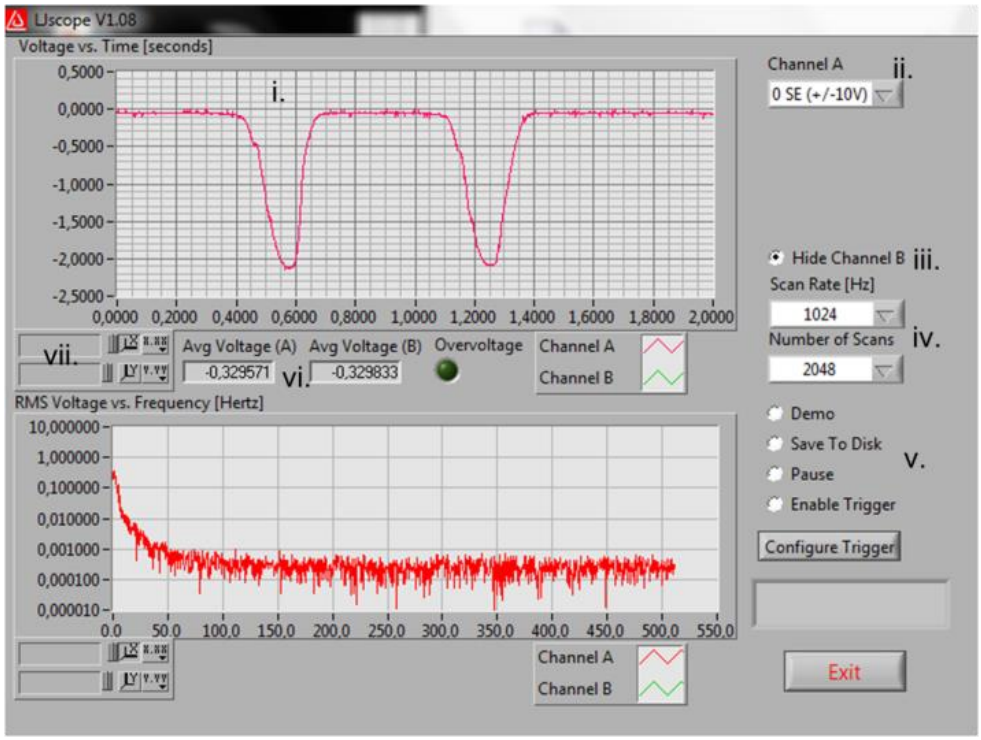

Figure 13 The screenshot of the LJscope software's user window during measurement.

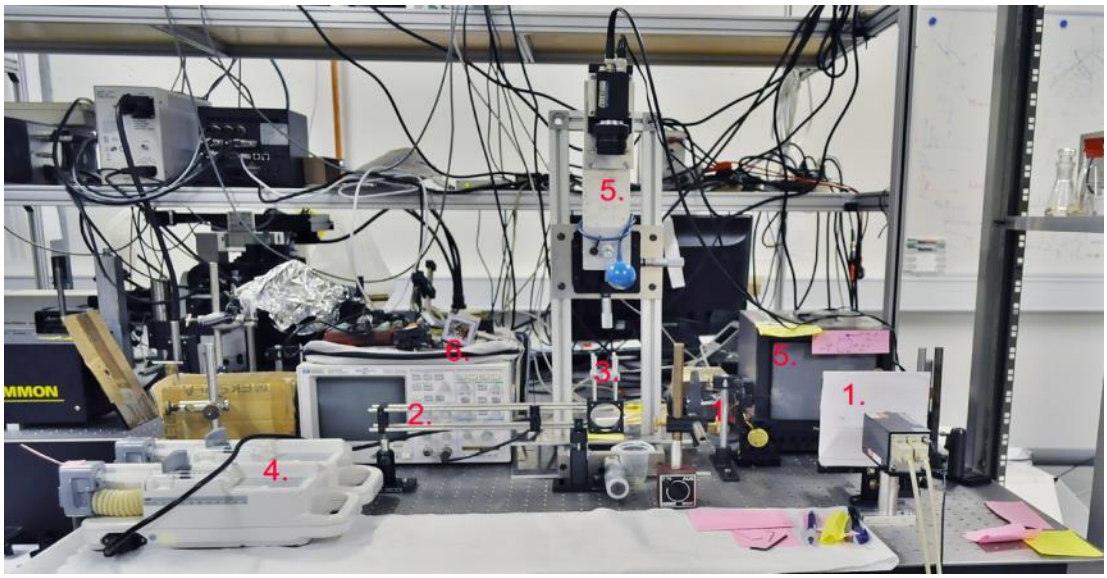

Figure 14 Overview of the setup with marked elements. (1) Laser source with the conducting system, (2)the cage system, (3) The microfluidic stage, (4) fluid control, (5) observation stage, (6) electronics and data analysers.

3. Design and fabrication of the chip

This chapter describes process of fabrication of the PDMS chips which are used in the experimental part. It contains a brief description of all the preparation, cleaning, sealing processes. A detailed recipe for the fabrication process can be found in the appendix 2 (p. 76).

Design

The entire process of the lab-on-chip fabrication starts from designing and preparation of the mask for photolithography with the pattern of channels, which then will be used for replication molding of PDMS.

First of all, because the project concerns fabrication of the droplet-based microfluidics (DBM), the design of channels should enable to make droplets or bubbles, regardless of substances and their physical properties. A suitable template was already designed at the University of Southern Denmark. The next step is to prepare the contact mask for photolithography. To achieve high quality of the master, the mask for the lithography is usually made of chromium plated fused silica [26]. However, the design used in this project has the smallest dimensions equal to 100µm. This mean, that good resolution mask can be obtained by conventional black and white photographic negative films.

This method is suitable to create fast, cheap and flexible photo-lithography masks. First step, is to draw the structure using one of a commercial software which allows to make the design in vector format e.g. CorelDraw [26], DraftSight [27]. Next step is to print

the structure in black and white. After a lot of tries, it was design in the way that does not require any special format of the paper. Special marks in the corners ensure correct positioning of the design and results with proper scaling of the design to the photographic film. To provide high resolution of the negative, many different photographic films have been tested [26].

The image is taken using the Pentax MZ30 SLR camera with the monochrome photographic film Agfa Copex Rapid (AGFA). To reduce camera shake, the camera is mounted on tripod and pictures are taken with a delay shutter. The high contrast provides good resolution and quality of the photolithography mask. The high contrast depends on the developer, but the exposure time is the main parameter to consider during taking a picture. Too long-time can reveal imperfections of the printed design, where too short time can be not sufficient to mark edges. Therefore, the best contrast can be seen in the display. The exposure time was automatically measured by the camera. A few pictures were taken with recommended time and also with slightly different values.

The last step of the designing process is to develop the photo-negative film according to the specifications for selected photographic films and their developers. The film is taken out in completely darkness to avoid overexposures. The process of developing is carried out in the chemical lab. For AGFA film, the SPUR Docu SHC is used as the developer and entire process is taking according to its specification [28]. As it is recommended, first step is developing in mixture of SPUR developer and DI water with ratio 1:9, respectively. This process takes around 8 min and entire mixture must be shaking up every 30s. After that, the developer solution is replaced with acid stop bath (ILFOstop) for 1 min and it terminates the development process. Finally, the film is placed for 4 min in the fixing agent (Ilford Rapid Fixer), which is mixture with DI water in ratio 1:4, respectively (Figure 15-A). It is recommended to use 300ml of solutions in each of these steps. After developing, the film is left to dry and then the best negative frame is chosen as the photolithography mask (Figure 15 – B-E).

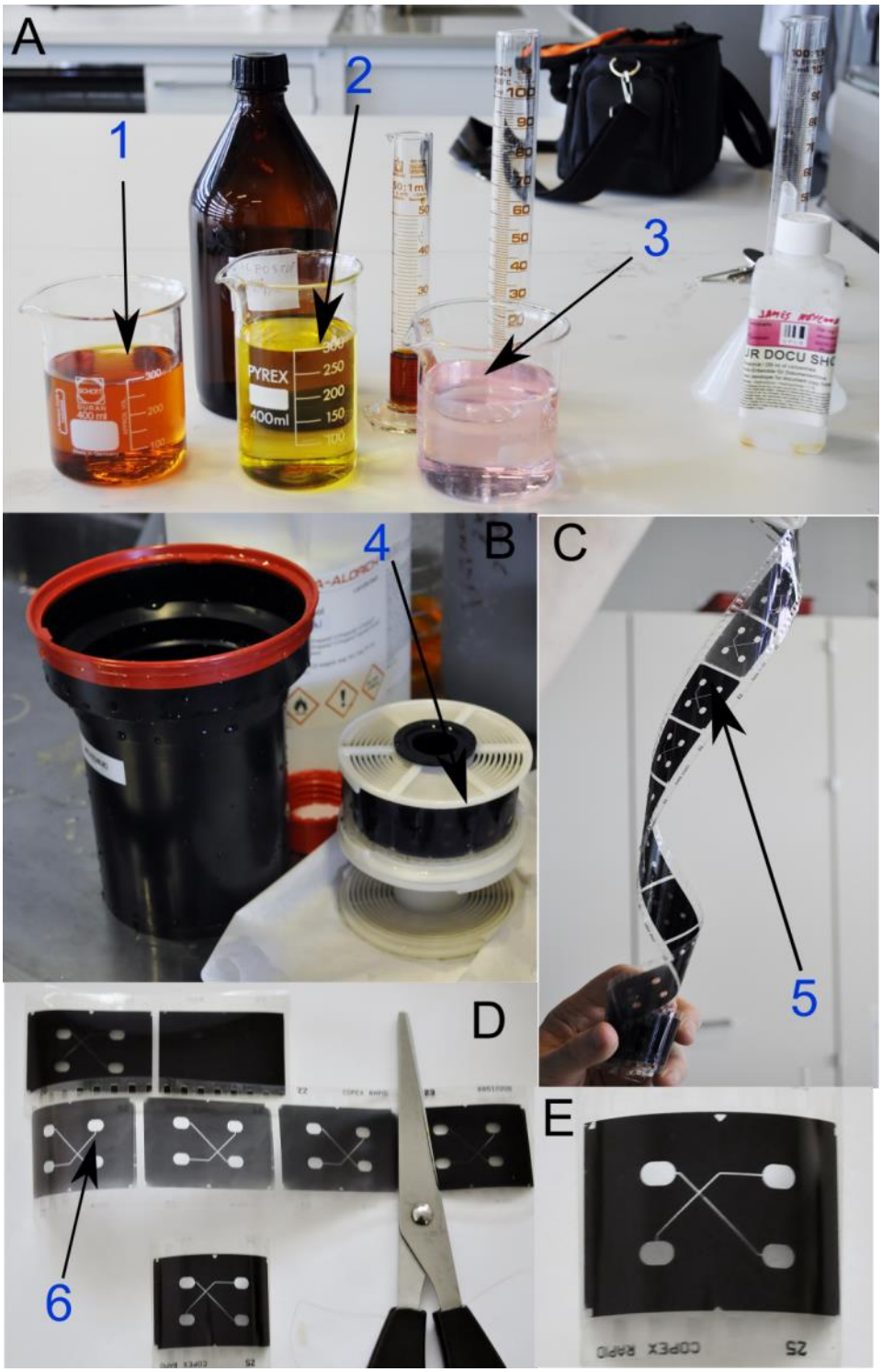

Figure 15 Some of the steps of fabrication the design. (A) process of developing the photographic film, 1- SPUR developer, 2- acid stop bath, 3- the fixing agent. (B) Equipment for carrying out film development and keeping it in the dark for the entire process, 4-the roll for uniform distribution of the film. (C -E) Process of choosing the proper mask for further process. Some imperfections e.g. overexposure or underexposure of the film eliminate a frame from using (6).

SU8 Masters

Standard photolithography processes are used to fabricate SU8 masters for the PDMS chip. All steps of this process are performed in the cleanroom to ensure that the structure is made with the greatest thoroughness. Each process of master's fabrication includes the following steps:

- SU-8 2050 negative photoresist is spincoated on the previously cleaned Si wafer. The thickness of the epoxy is determined by the spin-speed [29]. Thickness of the film should be around 100µm which corresponds to speed 1500rpm for 60s (Figure 16 - A).

- Next step is soft baking to harden the photoresist and evaporate some of the solvent. First bake for 5 min at 65°C, than bake for 10 min at 95°C (Figure 16 - B).

- After that, the wafer is exposed to UV light for around 75s. It is performed in the mask aligner using the photo-negative mask (Figure 16 - C).

- The post exposure baking is made in order to evaporate the rest of the solvent. It consists also two steps, first bake for 3 min at 65°C, than bake for 10 min at 95°C.

- UV exposure, make exposed part of the structure insoluble which after development will stay on the wafer. To develop photoresist, use SU-8 developer mixed with isopropanol IPA and develops for around 5-7min with agitation gently (Figure 16 – D-E).

- Hard baking (15 min at 150°C) is performed to remove remaining solvent and make the photoresist irreversibly solid and mechanically stable.

Spin-speed and time of baking is more or less imposed by the photoresist specifications. But time of exposure and developing should be investigate and adapted to the design and properties of used equipment. Moreover, before hard baking the structure should be investigated under the optical microscope (Figure 16 F - H). Especially, to check if shape of channels is correct and other defects of the structure did not appear. Fabricated masters can be cut using dicing saw (Disco DAD 2H5, Jongshiann Enterprise Ltd.). Dimensions of the master are predefined by the size of the metal mold, which allows mounting the substrate in size 25.8×37.8mm.

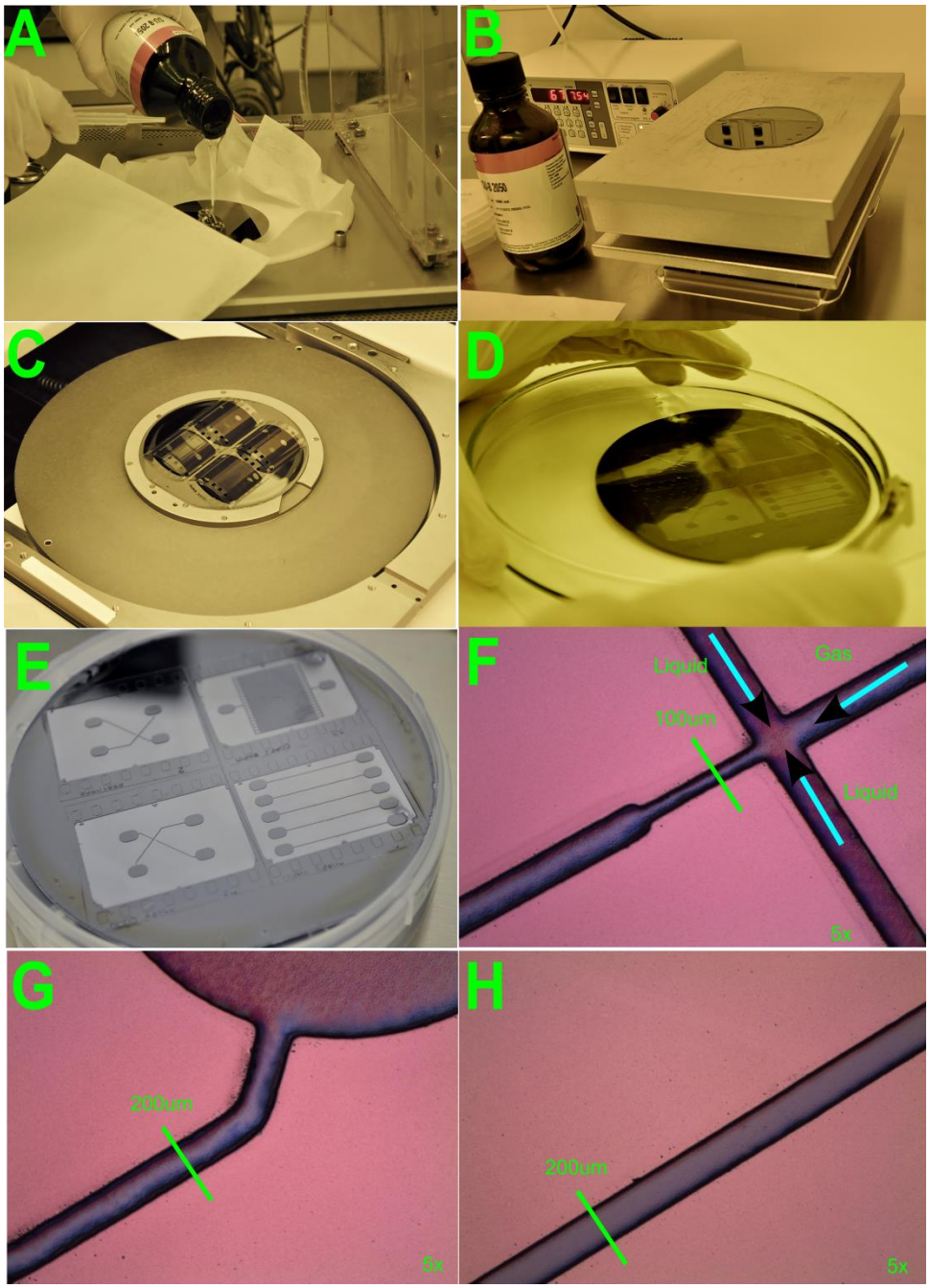

Figure 16 Some of the steps of fabrication the master for PDMS chip. A-C present steps of photolithography process: spinning the SU-8 2050(A), baking (B) and proper photolithography with photographic mask(C). (D) Shows the development process and result of it (E). Investigation under optic microscope is presented on pictures (F-H). On the picture (F) is shown the droplet maker system, where the all inputs are combined in the cross which make the droplet in liquid. (G) Picture presents the output from the chamber with liquid, moreover there can be seen that edges of the channel are not smooth. It can make some problems with fabrication the PDMS chip. On picture H is presented the high quality shape of channel.

PDMS chip

Next step is the preparation of the target chip. The PDMS (*Dow Coring Sylgard 18)* is used as a main material, which consists two ingredients: the base and the curing agent which should be mixed in ratio 10:1, respectively. For preparation one chip it is enough

to use 7g of the polymer. Both ingredients are measured out accurately and stirred well. During mixing, a large amount of air gets into the polymer, which must be removed before curing. So to eliminate air from PDMS, the mixture is placed for 30 min in a glass vacuum bell (pressure 75mBar) to out-gas.

Cut wafer with SU8 structure is placed inside the stainless steel mold, which have been made by Sønderborg Værktøjsfabrik. The master is mounted in the recess and clamped down with the inner part with O-ring around the cavity. Next positioning pins are placed on the opposite side and then the lid is put on and screwed. In that prepared mold, small steel pins are placed in every hole, but only part of them are pushed all the way thought. They ensure correct execution of inputs and outputs for chambers. The orifice in the assembled mold is a place for pouring out-gassed PDMS and then entire mold is again out-gassed for 10min. To prevent inducing a lot of air during pouring, it is recommended to pour the polymer slow and in small portions. To cure the PDMS the mold is placed on a hotplate with temperature of 100°C for at least 30min. After curing and cooling down to room temperature, the PDMS chip can be removed from the mold in the opposite order then during assembling.

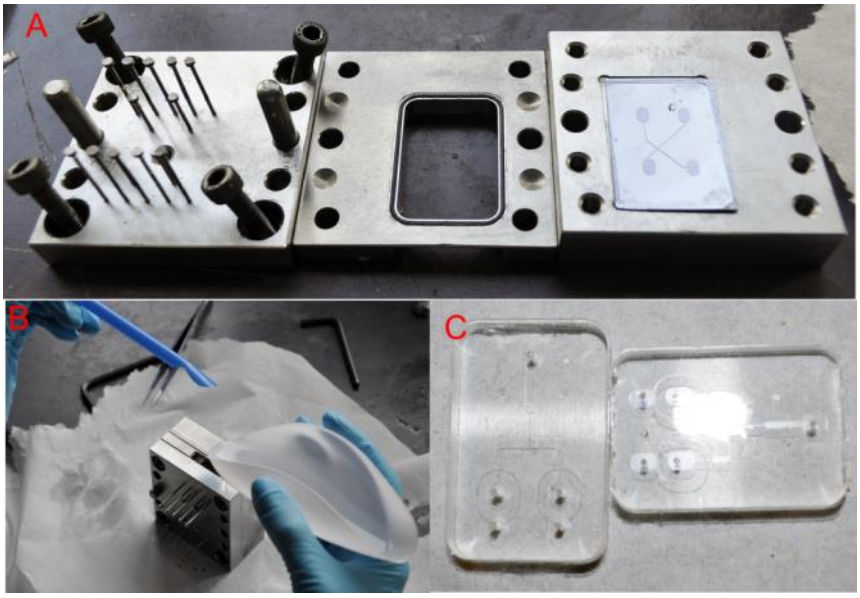

Figure 17 Picture (A) shows the steel mold for preparation the chip, step of filling the chuck is presented (B) and picture (C) shows the PDMS chips.

Deposition

One of the parts of this project is enhancing surface plasmons polaritons on the interface between gold layer and chosen dielectric material. To obtain desire thickness of layer, a physical vapour deposition was used. The gold layer is deposited on freshly clean surface of BK7 glass by Electron Beam Evaporation (e-beam) under high vacuum conditions. This process takes place in cleanroom in order to preserve possible the purest surface of elements. In this project, the gold layer was deposited on two different elements which required special mounting process to avoid theirs destruction or pollution.

The element for deposition is BK7 glass slide with 0,13 – 0,16 mm thickness, which made them easy to break. Because of that, they could not been attached directly to the mounting plate with carbon pads. The thicker piece of glass was used as the support. To avoid fracture, the cover glass was taped to the support piece with the aluminium tape.

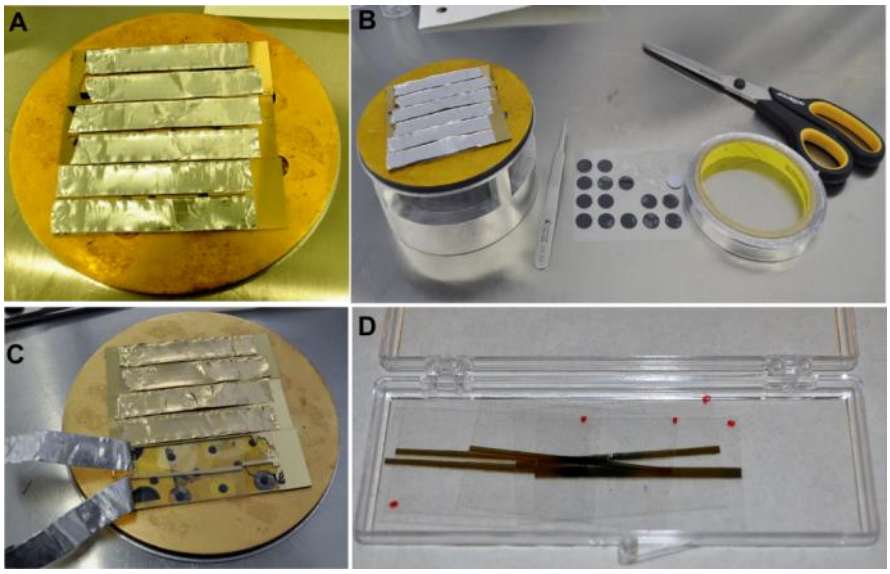

Figure 18 Preparation the sample for deposition process. (A –B) presents the method of mounting the glass slide onto the Cryofox plate. (C-D) show results of this process. The red dots are signs which help in identification the side with gold layer.

Sealing

The last step in the fabrication process of the PDMS chip is sealing of channel structures. The fast and simple way is to bond the chip and the lid using the plasma cleaner (Harrick Plasma Cleaner), which shall arrange for the plasma bonding. PDMS gives an ability to be bond to many different materials as glass, silicon and other materials [30]. As a lid for the chip, the slide made by PDMS is usually used. However, in this project, the aim is to create system for enhancing the surface plasmon polaritons on the prism. To achieve that, the chip must be sealed to the same material as the prism. For this project, the cover glass (LLG - LabLogistics Group, Germany) made with BK7 is used without as well as with additional gold layer. The activation of bonding is done using low pressure oxygen plasma for 1 min on both the chip and the lid. After that, surfaces of both elements are manually connected to each other. After a few tries, it occurred that pressing the lid to the chip is causing a distortion of the chip. The best way is to place the chip on top of the activated glass slide and left it to the action of gravity. No rigid investigations have been made into the strength of the bond, but from experience, the bonding between PDMS and glass is irreversible. Removing the slide without violating the chip is hard and requires using the ethanol bath. However, this process must be controlled in every 5 min to avoid swelling of the chip, because of absorption of the ethanol by PDMS.

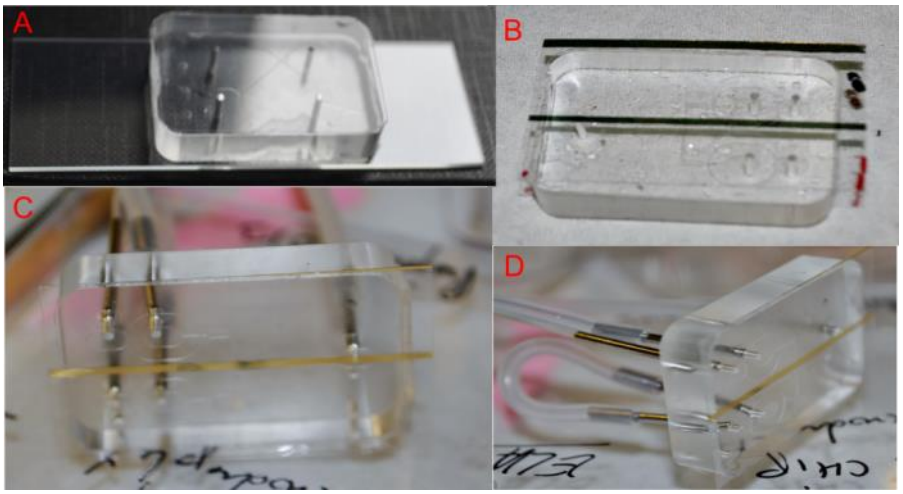

Figure 19 Presentation of the preparation for the sealing process (A-B) and results with ready PDMS chip (C-D).

Droplet-based microfluidics (DBM)

Before making droplets in the channel, the good idea is to check if ingredients are possible to make droplet without mixing. To do that, use Petri glass and pour first ingredient and then small droplets of the second ingredient can be put on it. If they are mixing, change concentration of one of the components until it is possible to make droplets.
Regardless of the used ingredients, procedure to create proper droplets should be preserve as below. Recipe presents making droplets of mineral oil in a solution of 5% Triton X-100.

1. Every pin holes must be plugged by pin with rubber pipe
2. Plug syringes with Triton X-100 and set the flow speed at around 1,3 ml/h and wait until all channels will be filled with Triton X-100 (it takes around 8-10 min)
3. Then change the solution to the mineral oil in the syringe which is connected to the inside chamber
4. Adjust the speed of ingredients, depends on the size and speed of desire droplets
5. After all process spare syringe with mineral oil on Triton X-100 to clean all channels
6. Triton X-100 will evaporate spontaneously, so it does not have to be removed

When using any type of alcohol is required to use de-ionized water to clean all channels. It is caused the fact that PDMS absorbed the alcohol and lab-on-chip swells.

4. Materials

The parameters of different materials are collected to prepare appropriate grounds for experiments. Experimental part starts from calculations of incident angle for the evanescent wave and surface plasmon polaritons. This entails consequences in terms of changes the geometry of the setup as well as provides an appropriate arrangement of other elements. For the evanescent wave phenomenon the most important parameter

is the real part of the refractive index of all layers. However, for SPPs is important the complex refractive index as well as the wavelength of incident light. Additionally physical parameters of materials depend indirectly on the wavelength of the light. That is why, before calculations all parameters are combined and also features of the evanescent wave ad SPPs are presented. This data set allows for the selection of appropriate parameters for experiments.

Table 1 The set of the most important parameters of available materials for experiments. There are chosen regards to the used laser source. Most of features come from the web page which which is a collection of data from many books and publications. [31] Elements with additional signs came from their datasheets or are based on other sources.

	Material	633nm		795nm	
		n	k	n	k
1	Gold (Au)	1,834E-01	3,433E+00	1,520E-01	4,866E+00
2	Silver (Ag)	5,621E-02	4,278E+00	3,599E-02	5,533E+00
3	Titanium (Ti)	2,704E+00	3,766E+00	3,126E+00	4,010E+00
4	SiO2	1,543E+00	0,000E+00	1,538E+00	0,000E+00
5	PDMS [i]	1,412E+00	0,000E+00	1,407E+00	0,000E+00
6	BK7	1,515E+00	1,213E-08	1,511E+00	9,249E-09
7	Air	1,000E+00	0,000E+00	1,000E+00	0,000E+00
8	1st Index matching oil [ii]	1,500E+00	0,000E+00	1,500E+00	0,000E+00
9	2nd Index matching oil [iii]	1,517E+00	0,000E+00	1,517E+00	0,000E+00
10	Water	1,332E+00	1,470E-08	1,329E+00	1,296E-07
11	Ethanol	1,360E+00	0,000E+00	1,358E+00	0,000E+00
12	Methanol	1,326E+00	0,000E+00	1,323E+00	0,000E+00
13	Triton X-100 [iv]	1,490-1,494	0,000E+00	1,490-1,494	0,000E+00
14	Rhodamine 800 [v]	1,619E+00	0,000E+00	1,620E+00	0,000E+00

[i] Weiping Qiu, “PDMS Based Waveguides for Microuidics and EOCB”, Master thesis, Louisiana State University, USA, August 2012, p.13

[ii and iii] The label from the bottle,

[iv] Sigma-Aldrich, Purchase of Triton X-100, available online, used December 2013

[v] Sebastian Wuestner, Andreas Pusch, Kosmas L. Tsakmakidis, Joachim M. Hamm and Ortwin Hess, “Gain and plasmon dynamics in negative-index metamaterials”, Imperial College London, UK, used May 2014, p. 3,15

Despite the fact that the index of refraction is nonlinear function, it can be assumed that usually one percent of concentration corresponds to approximately 0.002 in n [32]. However, in the experiment the solution of Rhodamine 800 (Rh800) is used in concentrations smaller than 1mM. Exactly under consideration are taken concentrations: 100nM, 10nM, 1nM and 0,01nM. Which due to relatively small amount of ethanol or water and cannot change significantly the refractive index of the solvent.

IV. Preparation for experiments

1. Geometry of the prism

Preparations start from carrying out necessary calculations. The main task of this part is to prepare the basic information about incident angles which are necessary to create the evanescent wave as well as surface plasmon polaritons. This information is also important in terms of the appropriate position of elements in the system. Because of the limited geometry of the system, some of the angles may not be achieved. That is why, appropriate materials should be chosen with respect to the possibilities of the device.

Geometry of the prism

For both phenomena the point of interest is the incident angle. However, during the work with the prism there is always present divergence between the notions of the incident angle. That term can be understand as an angle at which the beam is incident on the front wall of the prism (outside the prism) or on the rear wall (inside the prism). Geometrical relations are even more difficult when you can only move the incident beam, which take place at this set.

In the experimental setup, the prism is mounted on the desired height and does not have ability to move or rotate during measurement. This additionally makes the measurement harder, because it is only possible to adjust the angle of the mirror in the cage system. In this case, all geometrical relations must be known (Figure 20). In addition, since on each boundary between the two media there occured the phenomenon of refraction, they must be taken into account in order to achieve accurate calculation.

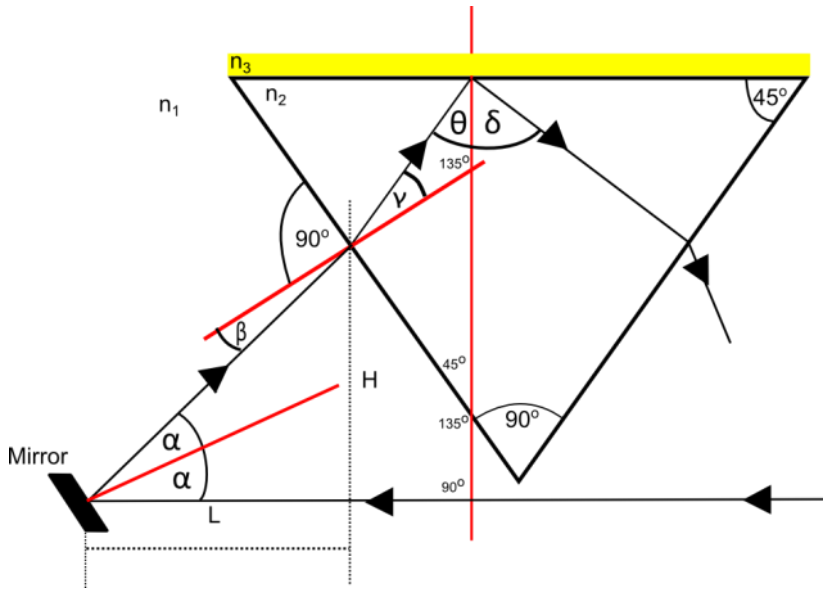

Figure 20 Geometrical relations in the used prism. There are marked the angles that result from the simple mathematical relationships. α, β, γ, θ are sought angles which change depending on the mirror's distance and angle.

In this figures, angles which are results of the simple geometrical relations of the right triangle are already marked. Furthermore, this shows a simplified configuration in which n_3 is the factor associated to each of the medium above the prism. Red lines correspond to perpendicular axes and the way of the beam is signed with arrows. In the used setup, there is possibility to change only angle of the mirror which is directly connected to the 2α. However, according to the reflection law the angle of incidence and the angle of the reflection respect to the perpendicular axis of the mirror are equal. This means that total angle which can be adjusted is equal to α.

The starting point for calculations of the evanescent wave is that the δ is equal to 90° which means that θ is critical angle for this configuration. Using the Snell's law it can be calculate as presented below:

$$sin\theta \cdot n_2 = \sin 90° \cdot n_3 \;\Rightarrow \theta = \sin^{-1}\left(\frac{n_3}{n_2}\right)$$

Next calculations include the relationship between triangles and the refraction law at the boundary.

$$\gamma = 180° - 135° - \delta$$

$$\beta = \sin^{-1}\left(\frac{\sin(\gamma) \cdot n_2}{n_1}\right)$$

$$2\alpha = 45° + \beta$$

$$\alpha = \frac{45° + \beta}{2}$$

Following this way of calculations each time there is a need to change the incident angle; it is possible to find the mirror's angle with high precision. Additionally, from these dependences it is possible to calculate the height (H) - distance between the laser beam and an incident place and the length (L) – distance between mirror and the incident place. These are important information due to the fact that nor rods neither than mirror has the measure for the distance. All mathematical formulas were implemented to the excel file to speed up calculations.

2. Calculations for surface plasmon polaritons

For SPPs calculation of the incident angle is much more complicated. It takes into account the wavelength and the refractive index of each of the layer. Simplification of this phenomenon can lead to wrong results of calculations. Moreover, abilities of the excel file is not sufficient for all necessary formulas for SPPs. Due to this fact, the recommended software (EM Explorer Studio) is used. Furthermore, the code for main calculations for SPPs in Kretschmann configuration was offered and adapted to the project.

However, this project is based on researching the best parameters of the multilayer structure. Because of that, there is more than one arrangement of layers and the best for

available device should be used. That is why; the code of the program was modified to satisfy requirements of the project. Main part of the SPPs calculation was taken from the software company. However, the idea is to check which thicknesses of the layers are the best for used system. To achieve this, the calculation should be provided in the loop and thicknesses must change. In that construction there is possibility to compare incidence angles for SPPs for different parameters of layers and chose the one which shows the highest drop of the light power and simultaneously possible to achieve the incidence angle. Modified code with explaining commands is presented in the appendix 1 (p.72). However, a description of how to calculate the incident angle with the software is shown (Figure 21).

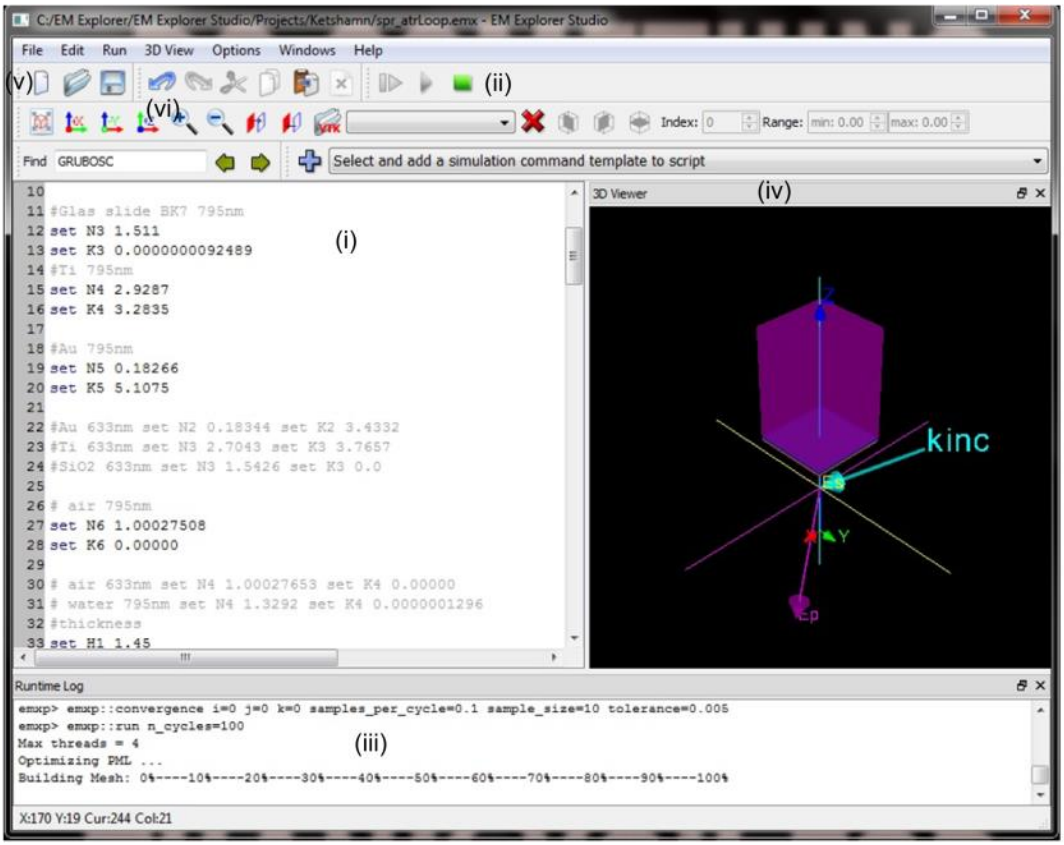

Figure 21 Presentation of the user's window. Main functions of software to compile code for the calculations was marked (i-vi): (i) main area for the code, (ii) these buttons allow to run, pause and stop the calculation, (iii) runtime log which shows the progress of calculations and errors if occurred, (vi) visualization of SPPs of designed structure, (v) and (vi) main operations on the file and visualization.

To get the correct results of the calculations a few parameters should be applied to the basic code. First, the wavelength of the light and the complex refractive index for each of used layer. Every layer thicker than 1,45µm is considered as an infinite layer or the bulk. Mode in the loop requires defining the step with which the thickness of layer is increasing and number of loops which will be done. Also there are a few parameters which are connected to the precision and time of calculation e.g. step for angle (set at 0.5°), tolerance of calculation (0.005). However, the higher precision of calculation the longer the process will take. So there must be keep balance between the precision and time. The range of

angles taken into account has been set from 40° to around 70°. These parameters should cover all possibilities for enhancing SPPs. All results are written in the .txt file. The code was modified in the way that the overwriting the files will not occur.

The purpose of the calculations for this project was the selection of the proper thickness of the layers so that the angle of incidence was possible to achieve in our system. Moreover, there are available two lasers with 633nm and 795nm wavelength. This results with significantly different angle for surface plasmons resonance (SPR). Basic idea for the sensing system is to use multi-layer structure build from: BK7 prism, index matching oil, BK7 glass slide, adhesive layer of titanium (Ti), gold layer, SiO2 and some dielectric medium. Because, from assumption the BK7 prism, index matching oil and glass slide have got the same or very close refractive indices, they are treated in calculation as a one substance. Ti is used to increase the adhesion of the gold to the surface of the prism. However, the thickness of adhesive layer is around 0,002µm, that is why is not taken into account during the calculation process. At first, the idea was to cover the gold layer by SiO2 which protects the main layer from degradation caused by the flow of the liquid. That is why; one of the step is to decide about the thickness of its layer. As the dielectric medium taken into account, we choose air, water and ethanol.

The first step of the calculations is to check what the incident angle is for SPR under illumination by the light with 633nm wavelength and how it is changing with the thickness of gold layer. It is assumed that the thickness of SiO2 is equal to 0 and a dielectric material is air. After that, the dielectric is changed for water and results are compared in both cases for two wavelengths 633nm and 795nm. The thickness is chosen based on the best results for both lasers and both dielectrics. This is caused because the system should be flexible. Both light sources can be used without changes in the sensor or additional fabrication steps.

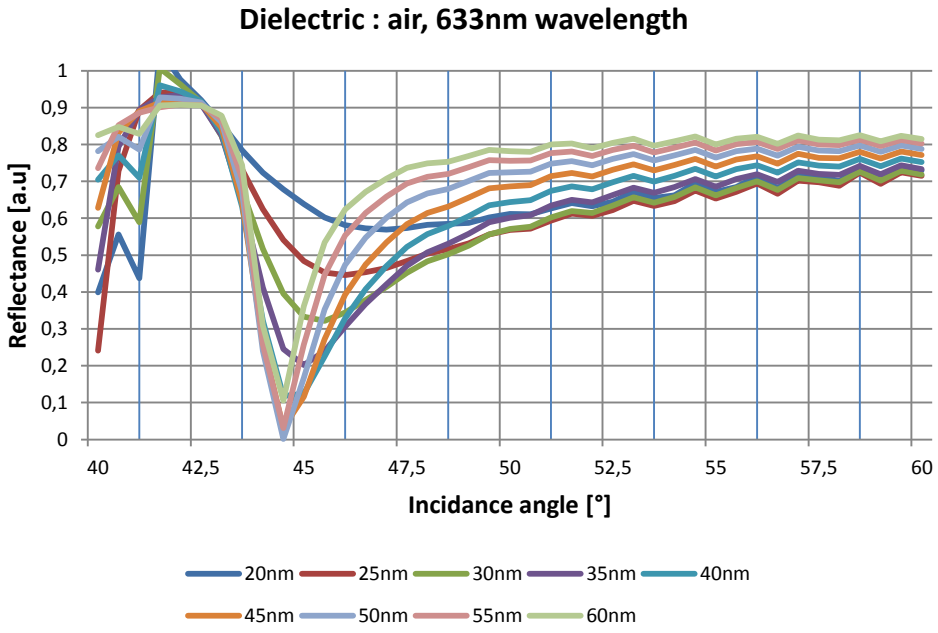

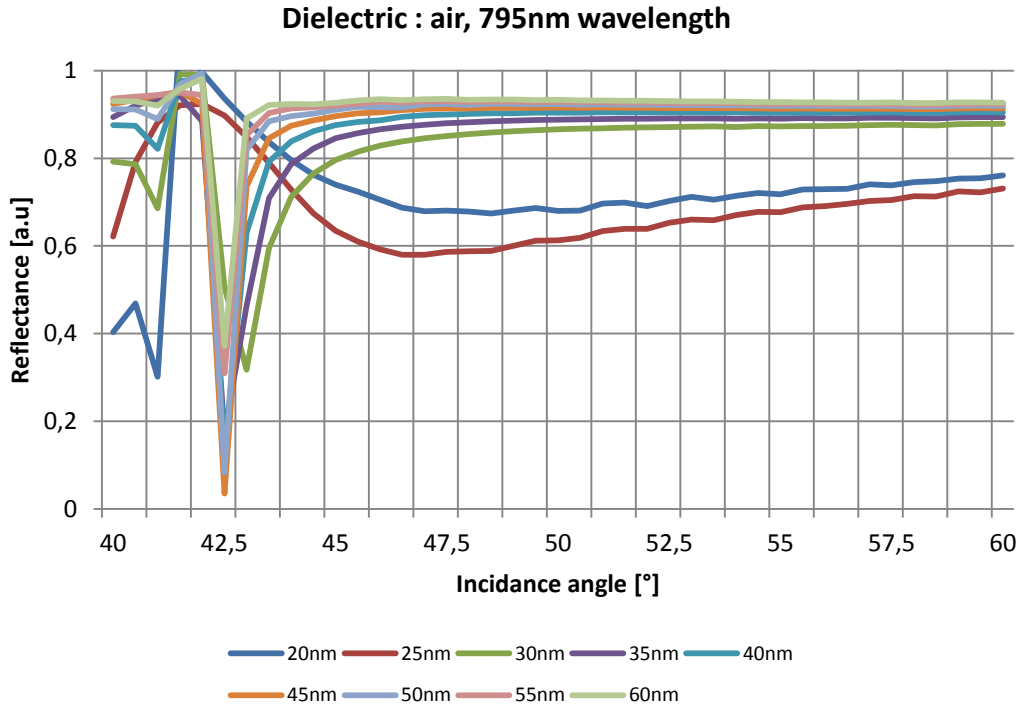

Graph 1 Calculated reflectance curves for the gold strip with different thickness. The dielectric medium is air and there is no division into glass slide, prism and index matching oil. (a) Presents the result for 633nm wavelength laser. (b) shows calculations for the same position of the environmental, however the wavelength of the lease is 795nm. The thickness of the gold around 20-30 nm is useless, because the SPR and it too small to enhance SPPs in visible way.

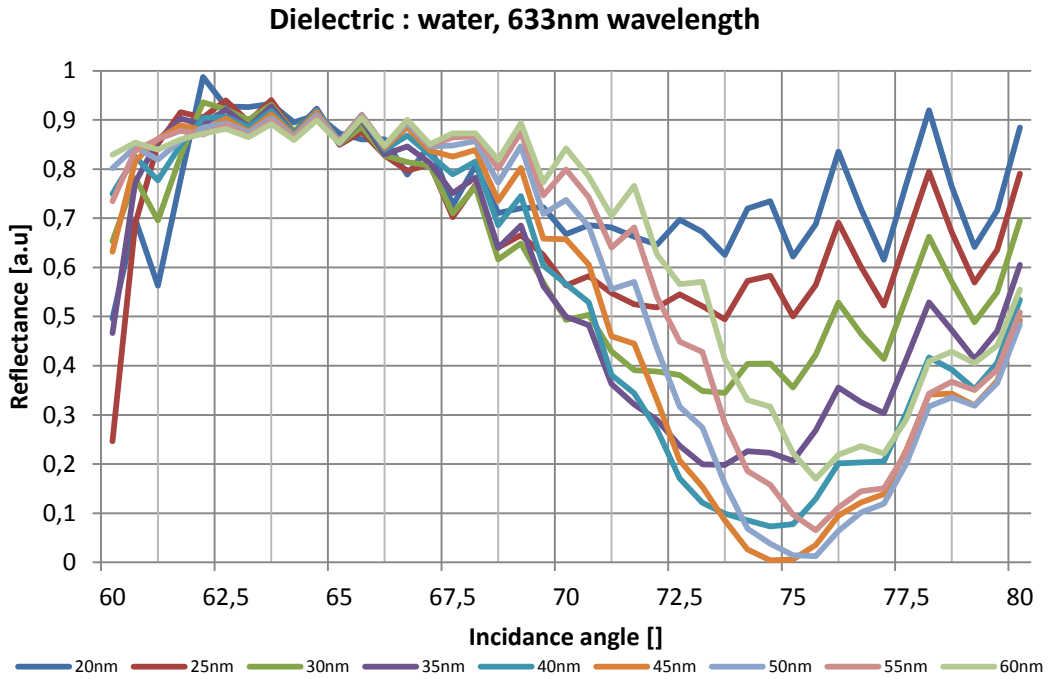

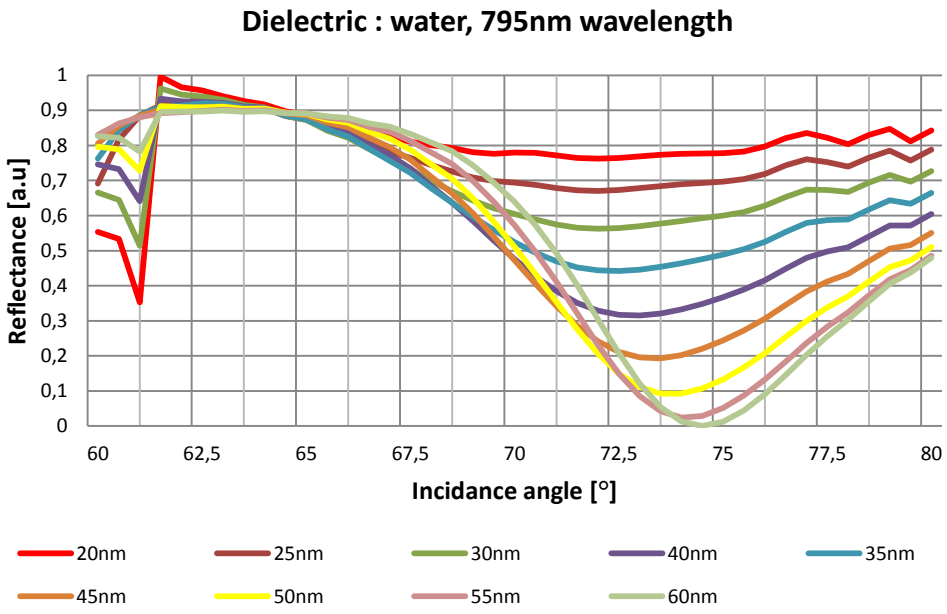

Graph 2 Results of calculation of SPPs with water as a dielectric. Graph shows the results for different thickness of gold layer under illumination 633nm laser light and different angles of incidence. In these calculations there no protective layer (SiO2) and the prism, index matching oil and the glass slide are assumed as a one system. However, results for 633nm wavelength are highly distorted, which is a result of limited version of the commercial software used for compilations.

The angle that corresponds to the SPR occurs when the power of reflected light is dropping only for specific angle of incidence. After that the power rises to the basic level. Due to the calculation was taken in range of angle from 20° to 70°, results are presented from smaller range. It is caused, because the values below and above this angle are not giving more information about the phenomenon. Putting all results would make the graph unreadable and unclear.

Comparing all diagrams give the information that the best results can be seen for thickness of gold around 45-50nm. Moreover, these show that the angle for SPR increases with increasing the dielectric constant of medium. However, changing the light source caused that the searched angle decreases with the higher wavelength. Next step in calculations is to check if the protecting layer from SiO2 has an influence to the angle of incidence and in the value of the power. In this case only 50nm thickness is taken into account and air as a dielectric and the laser light with 633nm wavelength.

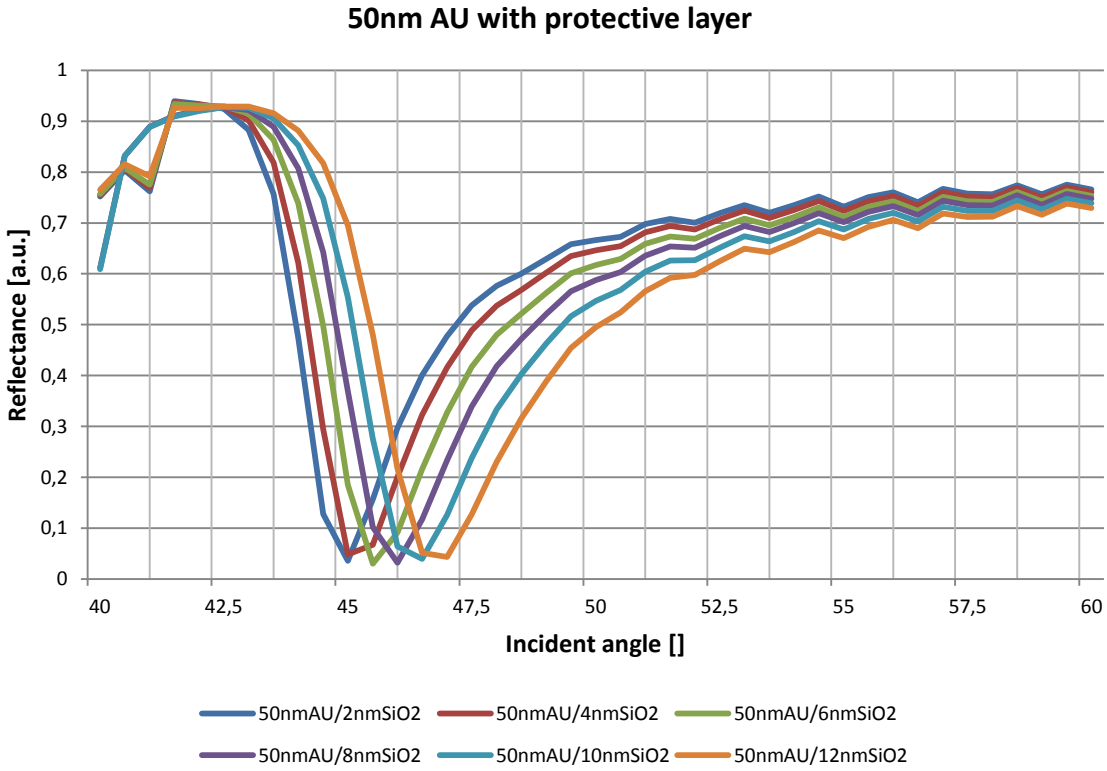

Graph 3 Results of calculation of SPPs with air as a dielectric. Graph shows the results for different thickness of protective layer under illumination 633nm laser light and different angles of incidence.

In this case, the thickness of SiO2 occurs to have slightly influence on the incident angle of SPR. It means that using the protective layer should be considered carefully and the thickness should be adapted to the metal layer. Since the previous calculations were carried out with an accuracy of 0.5 degree. More precise results should be performed to obtain the entire range of angles for SPPs.

Despite the fact, that basic assumptions defined that the prism, index matching oil and the glass slide is one system with the same refractive index. To check that the thickness of the adhesive layer does not influence the phenomenon, additional calculations were performed. In this case, all layers were defined separately in the software as well as theirs thickness.

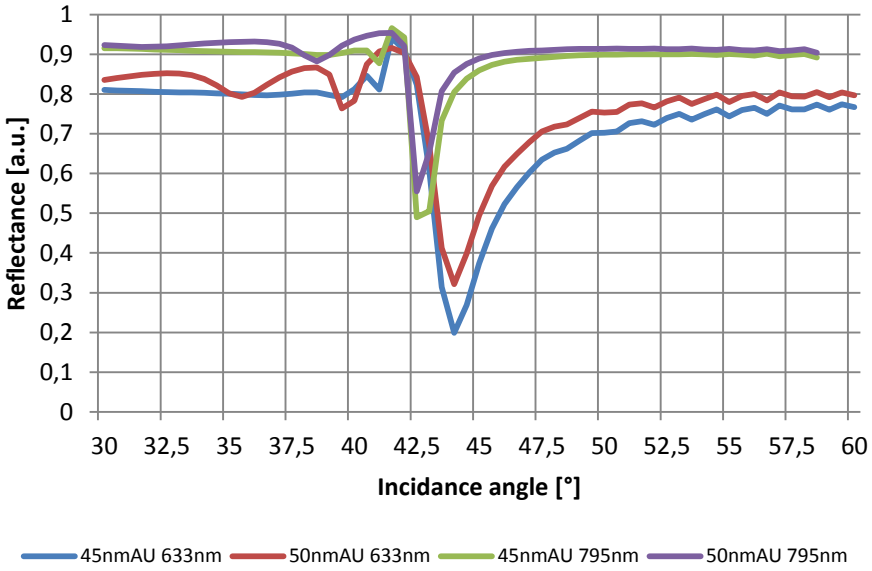

Graph 4 Representation of the results for defining each of the layer: BK7 prism, index matching liquid, glass slide, Ti protective layer, gold and air as a dielectric. In these calculation only two thickness of gold were taken into account: 45nm and 50nm and both available wavelength.

Graph 4 shows that defining all layers with precise refractive index and thickness did not demonstrated any significant changes in the required angle of incidence. It means that, calculations which were provided with simplified system can be assumed as precise as the detailed one.

3. Preparation of the setup

Next step of the project is to customize the setup to the calculated values. Information about critical angles and angles for SPR is the starting point for preparation experiments. Using previously presented geometrical relations in the prism (Figure 20). The distance of the prism (height and length) can be estimated. Basic cage system consist rods with length 200mm in both horizontal and vertical direction.

From first calculations it occurred that, required angles cannot be reach on this setup. It demand changes and only available rods where in length 75mm and 100mm. The results obtained after the initial calculations (Table 2) show that the adaptation of 100mm rods in the horizontal direction will allow obtaining the critical angle only for air as a dielectric. Moreover, because the PDMS chip is a bit wider than the space between rods, there is possibility to place the prism only at the top of the rods. In this case, the horizontal rods would not provide enough space to place the mirror. Additionally, 75mm rods were performed by the university workshop and their features allow placing the PDMS chip between the rods. In this case, the 100mm were connected to the horizontal rods and extended range for the position of the mirror. In the horizontal direction, 75mm rods

were used (

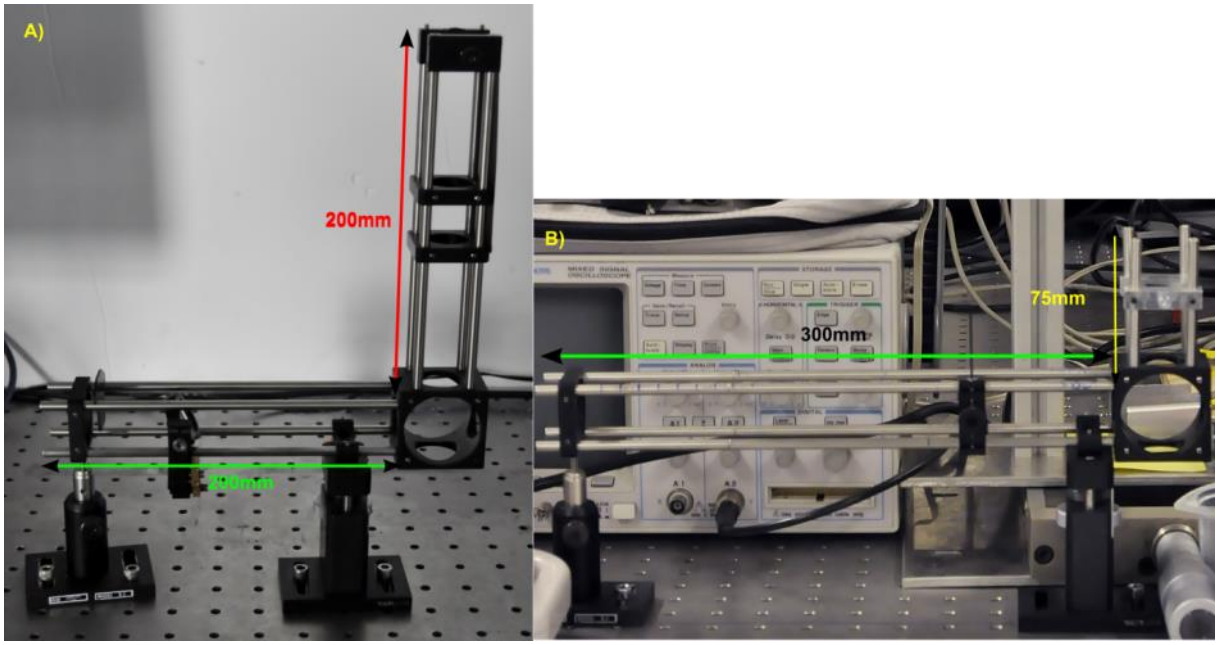

Figure 22).

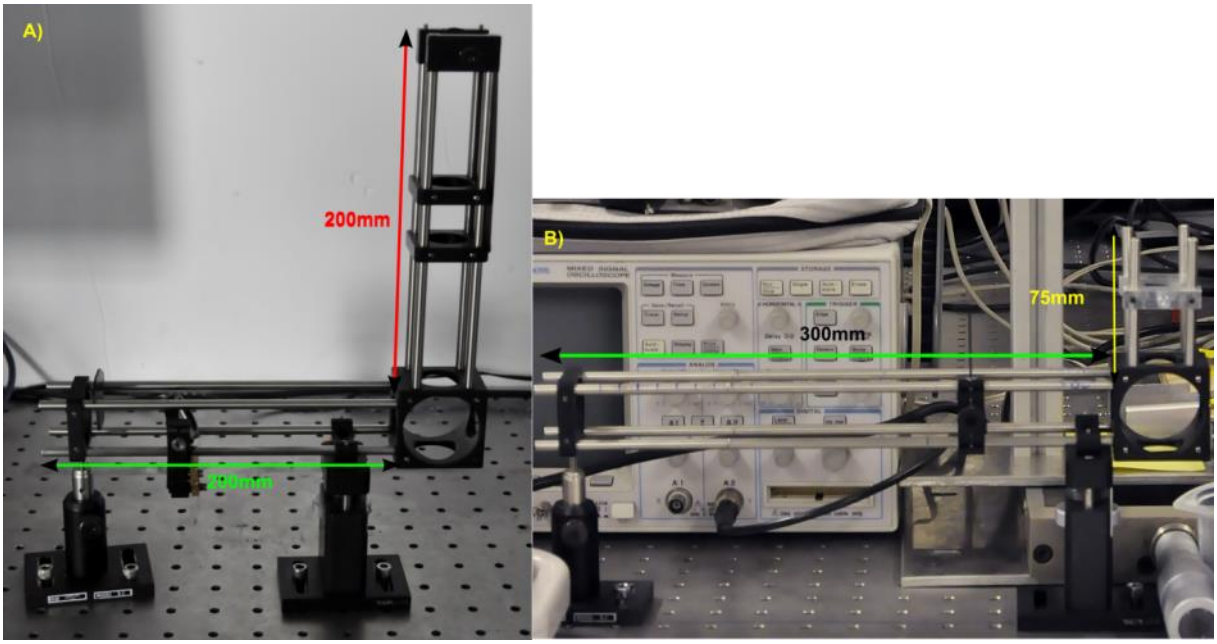

Table 2 The initial calculations for rods with 75mm and 100mm length assembled in vertical direction. These results take into account the difference in refractive indices depending on used wavelength. According to the presented sketch of the prism, 2α angle is the angles which can be adjust by the mirror rotation.

	Critical angle		for H = 75mm	for H=100mm
		2α [°]	L [mm]	L [mm]
633nm				
air	41,3	50,6	61,6	82,2
water	61,5	19,6	210,6	280,8
ethanol	63,9	15,7	266,0	354,7

methanol	61,1	20,3	202,7	270,2
PDMS	69,9	5,6	767,3	1023,1
795nm				
air	41,5	50,4	62,1	83,1
water	61,3	19,9	207,3	275,9
ethanol	64,0	15,6	269,5	359,3
methanol	61,1	20,3	202,7	270,2
PDMS	70,3	4,8	891,1	1190,7

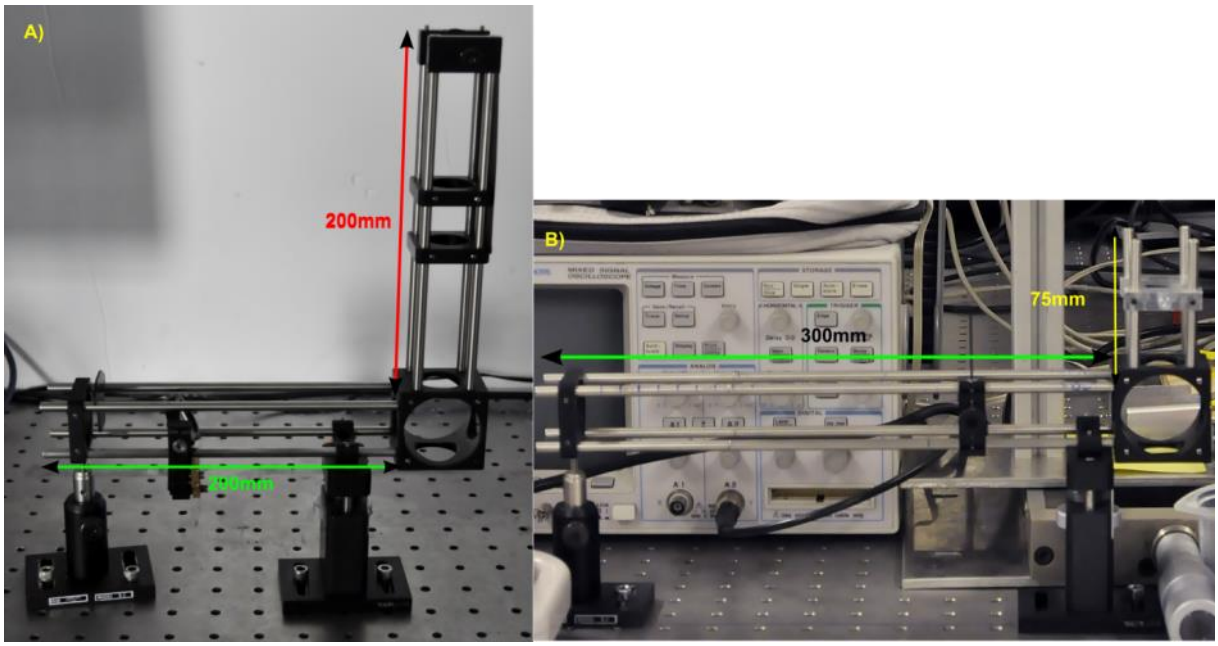

Figure 22 Presentation of the basic cage system (A) and after modification (B). Due to performed calculations vertical rods were changed for 75mm and horizontal rods were connected together with 45mm rods.

Due to the fact that chosen prism is a few millimetres wider than commercial holder allows. It was necessary to find a way to mount the prism with PDMS chip in stable position. First of the option was to use the chip chuck to mount the PDMS chip (Figure 23). Because the chuck is designed for using rods it allows to easy assembling the device. However, during preparation of the experiment it occurred that the chip is bending by the chip chuck. It results that the front layer is curved and it is not possible to make smooth connection with the prism.

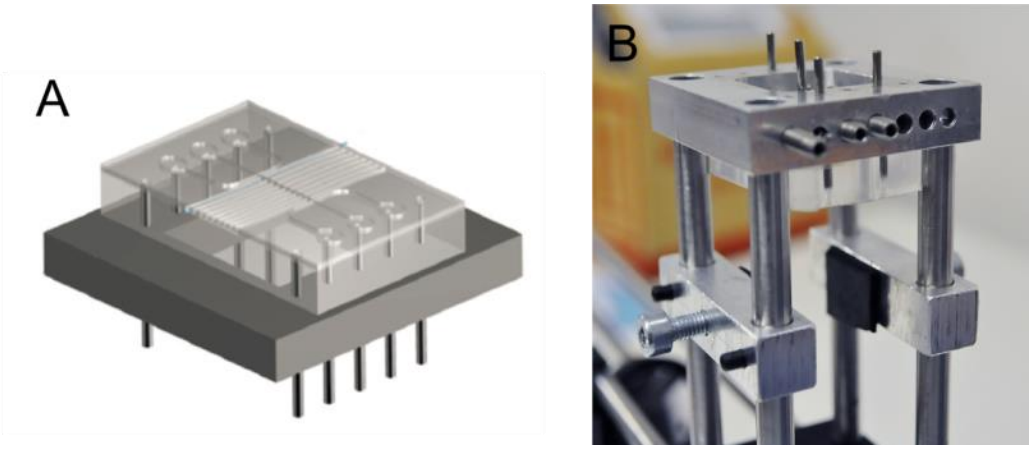

Figure 23 The chip chuck to mount the PDMS chip on rods, (A) 3D concept drawing [26], (B) application in the system.

Next idea was to use the glue gun for connection the chip to the substrate (Figure 24). Advantage of this solution is that the chip will not change the position relative to the prism. It also allows tilting the prism if it necessary and the connection layer will be flat and stable. However, after a few tries it occurred that this process is not repeatable. It means that, during gluing process there can occur different problems e.g. the glue enters between the chip and the prism, too much index matching oil is trapped between elements and makes the connection layer curved.

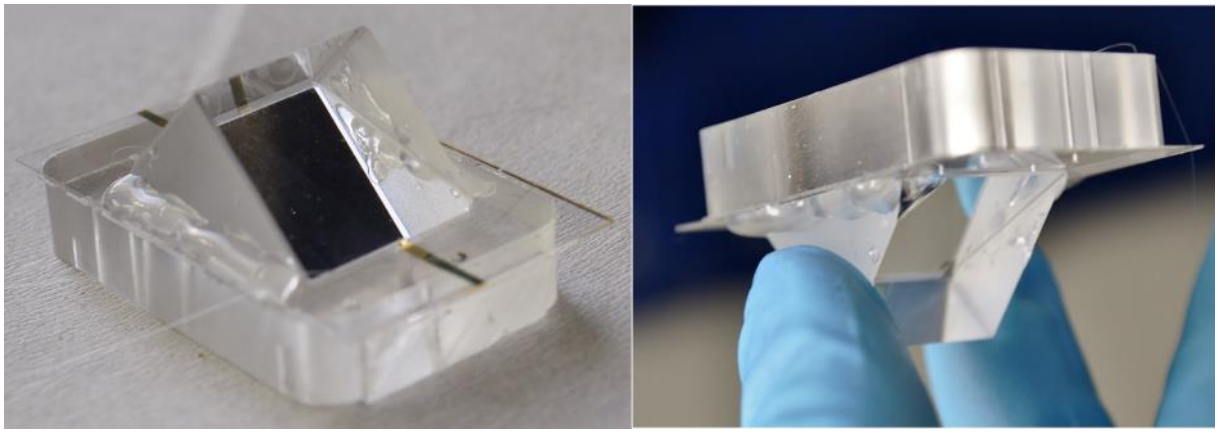

Figure 24 The prism with the PDMS chip on top. Prism has been glued using the glue gun. Quality of the connection is good and strong. Moreover, removing the glue does not leave any stains on the prism or the chip and it is easy to clean.

The final solution was to manufacture the additional element for rods which will be able to hold the prism with PDMS chip on top (Figure 25). Two elements from aluminum were made in accordance to dimensions of rods and the cage system.

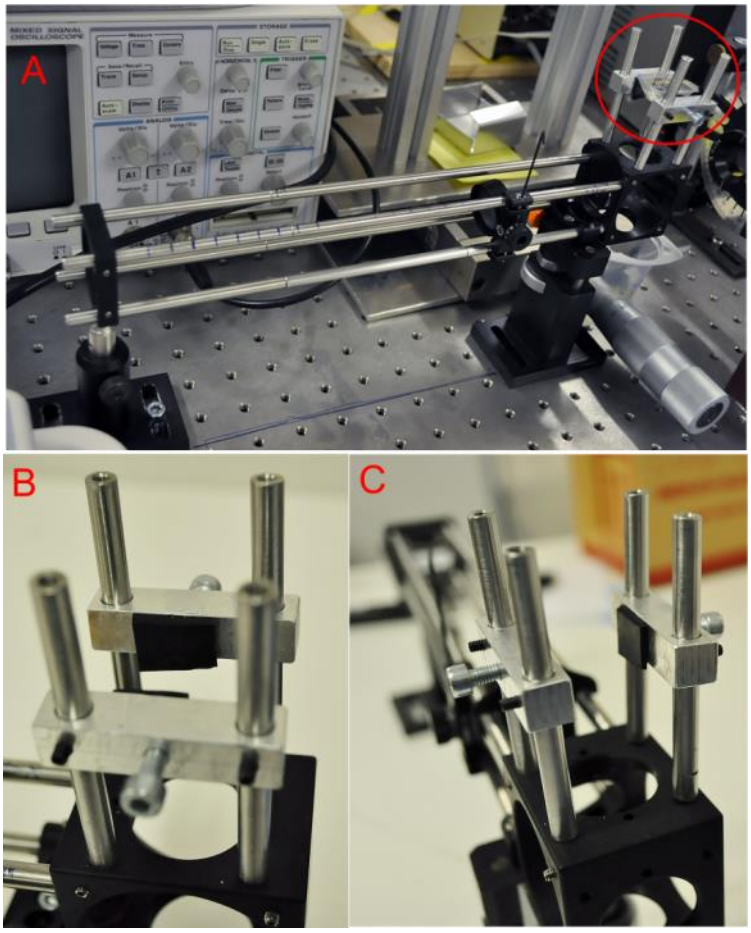

Figure 25 Presentation of the cage system with marked solution to hold the prism (A). These elements were adjusted to the spacing of rods, but they are thinner and smaller than commercial ones. Additional rubber tiles were added to prevent uncontrolled rotation of the prism (B and C).

After obtaining the stable system for microfluidic elements, the next stage is to adjust the laser beam. To achieve this, the optical periscope idea is used. The simplest way to control the light is to adjust it directly in the middle of rods in the cage system. In order to lead the laser beam directly to the centre of mirror it is recommended to use an alignment target (Figure 26). This device can be placed on the upper rods and allows the light to be set directly into the aperture located on the target. Afterwards, the alignment target has to be moved along the rods and entire operation has to be repeated. If the beam passes through the aperture in two distant positions, it is certain that the beam is guided to the centre of mirror. With such adjusted the laser beam, the rotation of the mirror correspond to the movement only in one direction.

Figure 26 The alignment target (a – picture from datasheet) and presentation of principles of adjusting process (b).

Based on the theoretical background to properly enhance SPPs, the good solution is to adjust the system so that the laser beam which incident the prism is directly in TM mode. This allows measurement of higher difference in power between and an angle which corresponds to SPR and one that does not. To obtain the desired mode the polarizer and half-wave plate were used. However, before adjusting components to the right mode, the power of the laser beam must be measure. It allows for estimation of the state of optical components and detection of the largest losses in the beam path. The measurement was taken by the power meter after each of the system element (Figure 27). Thereby it is detected that two from three mirrors were worn out or unsuitable for this wavelength. There were changed and after that the power of the laser beam didn't drop more than 50% after passing all mirrors.

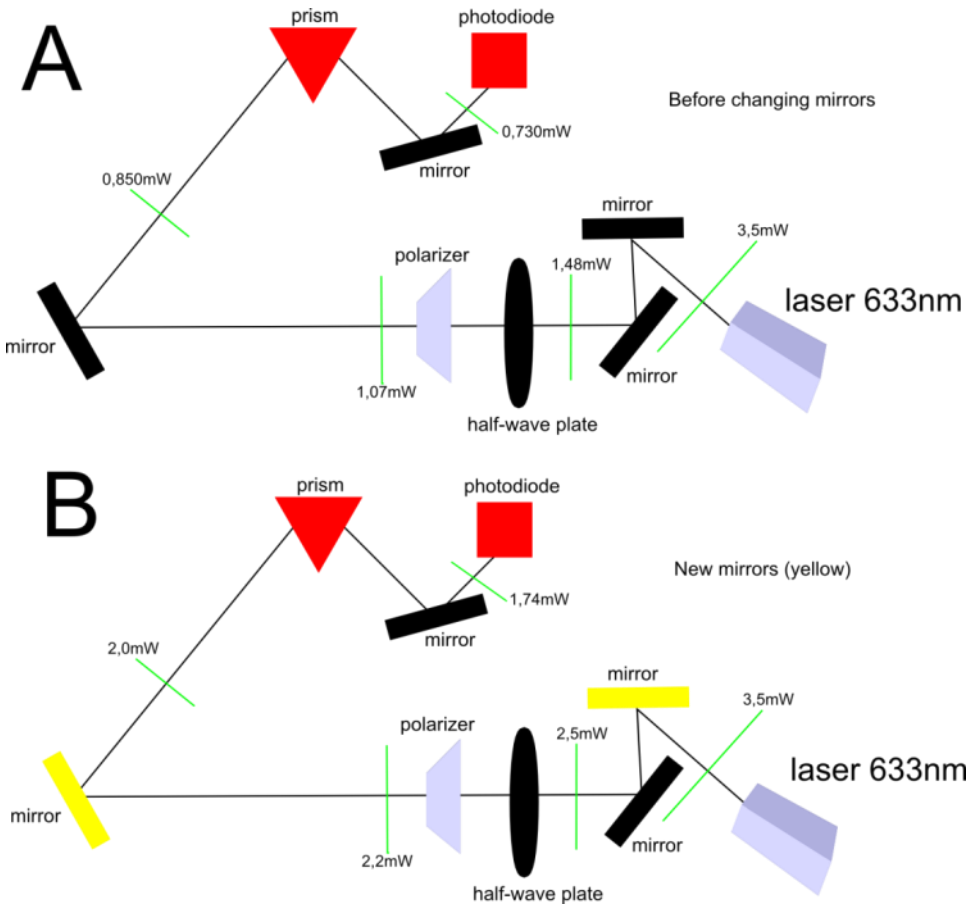

Figure 27 Distribution of the laser beam power after passing through elements of the system. Power of the beam with old mirrors (A) and after changing crucial components (B).

Next step was adjusting the polarization mode. Because used half-wave plate was suitable for different wavelengths, the adjusting process was more difficult and time consuming. Adapting the half-wave plate (Alphalas) for desire wavelength is done by tilting and rotation. Then the right angle is found by rotating the device. The power meter allows knowing if the right polarization is obtained if the power of the laser beam is close to the measured before.

Last step in preparation the setup for carrying out experiments is to mount the photodiode in stable position. Because, used diode is non-commercial device it was necessary to build a special dedicated holder (Figure 28). It keeps the photodiode in stable vertical position. Moreover, it is a great isolator from the cover shell which is made from aluminium profile. Additionally, the front wall was made from aluminium sheet to protect the sensor from the environmental light.

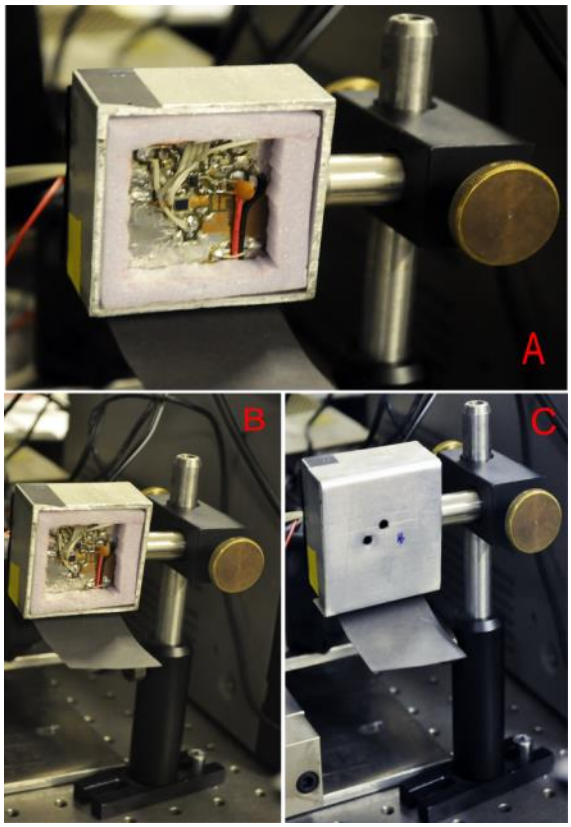

Figure 28 The photodiode inside the box-holder (A). Presentation of the sensor installed in the system, without the cover lid (B) and with it (C).

V. Optics for microfluidics sensor

The aim of this project is to apply the optical (plasmonics) methods into microfluidic system to obtain measurement with high sensitivity. Due to this description, in the project cannot be directly separated experimental part. Entire process of constructing the microfluidics sensor is based on small but relevant steps which show strengths and weaknesses of the setup.

Principles of optofluidics system

Starting point for constructing the sensor was to fabricate the PDMS chip according to presented recipe (p.21). Design of the channels was droplet-based microfluidic system. This structure consists of two separate droplet maker system, which allows to producing the droplet of a gas or a liquid in continuous flow of the medium. However, the requirement for this system to work was that both used mediums do not mix. Presented design has got two separate droplet-based structures (Figure 29), where from the container with basic fluid are coming out two outputs, which than surround the chamber with the second fluid. Principles of making the droplet are based on “squeezing phase” [26]. The main flow of liquid squeezes the air (in this case) and “intersects the stream of the gas into portions”.

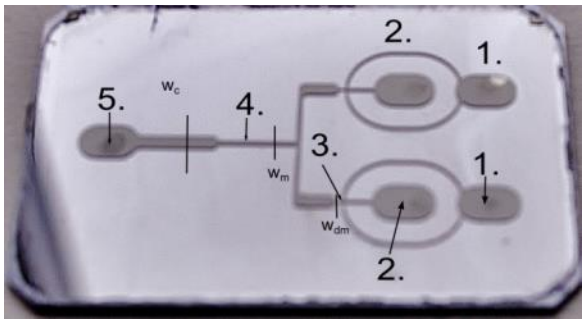

Figure 29 Presentation of the microfluidics design. (1.) The chamber for the main liquid which outlet is divided into two channels and "squeezes" the flow of the gas (2.) in the place where all three channels meet up (3.). (4.) is a place of detection the air bubbles by the laser beam illumination. (5.) is a output chamber.

This part of experiment was conducted in order to verify the approach of the sensor and to check the expected sensitivity. At first, principles of the evanescent wave were used as a base for detection. The idea was to create the bubbles of air in the flow of pure ethanol. Next, the laser beam was adjusted under the desire angle to the place in the PDMS chip (Figure 29 – 4.) where bubbles were flowing. After solving problems with mounting the prism, presented setup (p.18) was used as an experimental device.

The illumination by the laser beam should be obtained in the middle of the channel and set to the angle which corresponds to the critical angle for a particular medium. Then the reflected light is targeted to the photodiode which measures the intensity of the beam. The opto-microfluidics system is based on the project's approach. It means that, the prism and the PDMS chip with glass slide (as a sealing part), are connected to each other by the thin layer of index matching oil with refractive index similar to the prism and the glass slide (Figure 30). Used mirror does not have scale for controlling the angle rotation. However, the evanescent wave occurs at any angle larger than the critical angle. In that case, calculations based on the geometrical relations of the prism and the cage system is sufficient to obtain desired phenomenon. Results of this experiment should present changes in the reflected light caused by changes in the composition of the liquid.

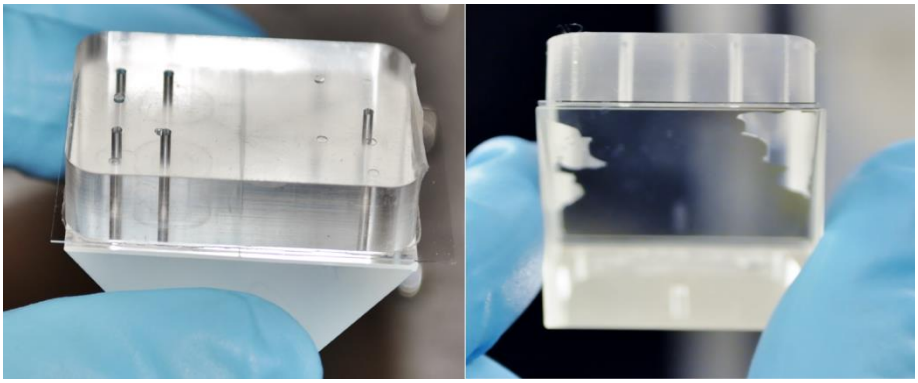

Figure 30. The first idea of microfluidics system. The PDMS chip with sealed glass slide is connected to the prism by the index matching oil. It can be also seen that Due to the curvature of the chip surface, the connection is not homogeneous at all surface.

In these experiments the laser with 633 nm wavelength is used and the incident angle is set to the critical angle for air (41,3°). LabJack with build-in software was used to measure and collect data. First step before the actual measurement is to check the speed of reaction of the photodiode. For this purpose the electric fan was placed in the way of the laser beam. The frequency of the fan is not precisely known, but significantly exceeds possibilities of appearance of air bubbles in the channel. In this stage, the critical angle for air was adjusted on the prism without the chip.

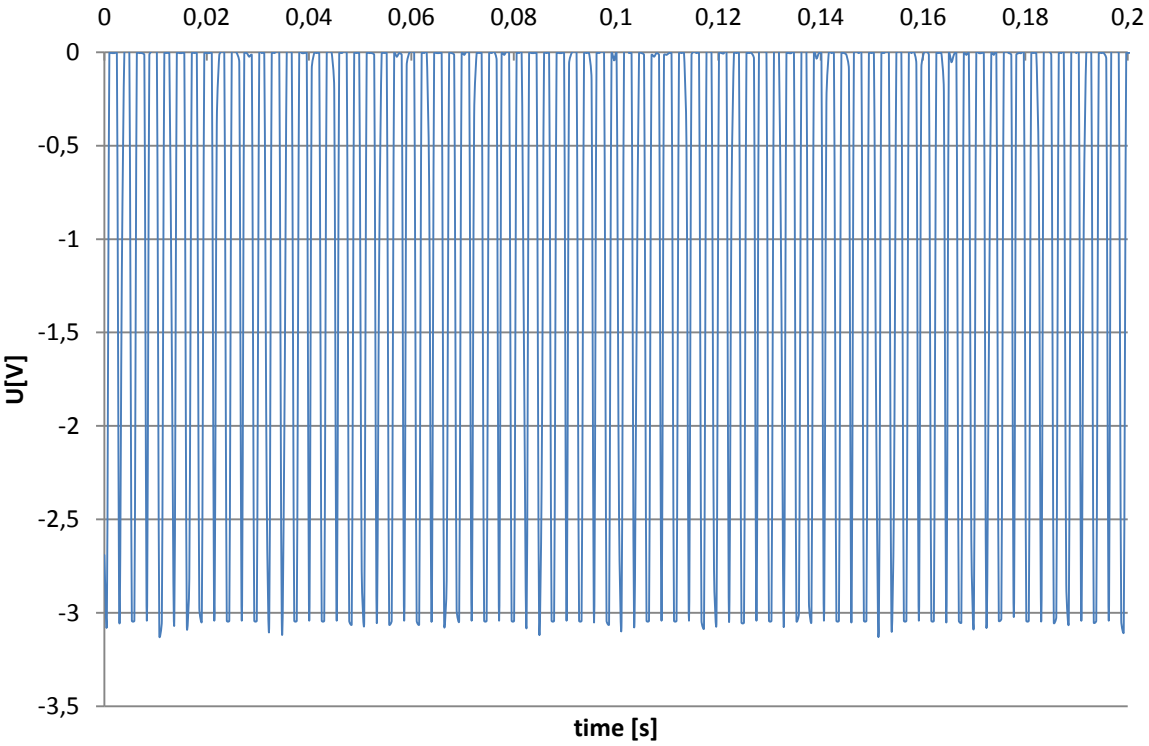

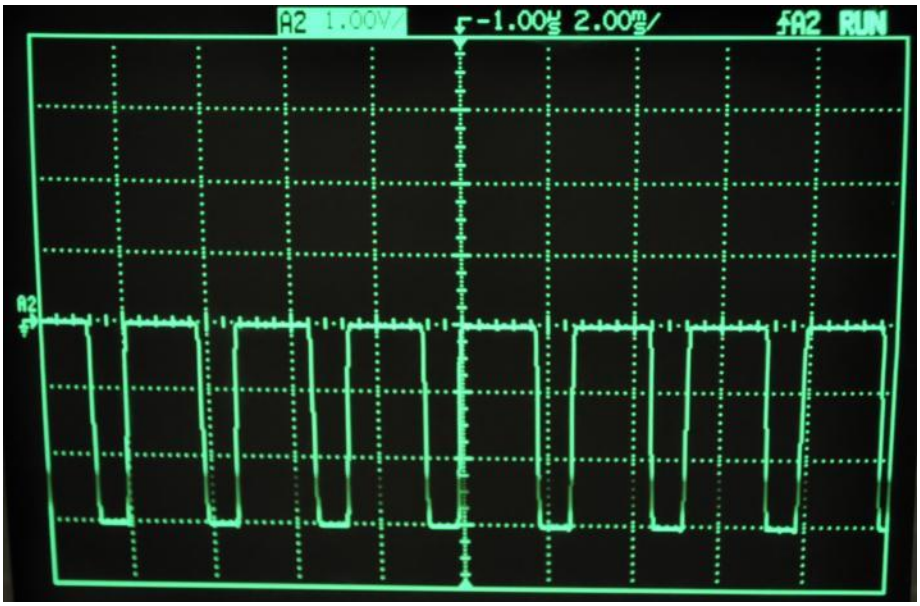

Graph 5 Presentation of results of experiment with fan. The additional picture from oscilloscope is added due to the limitation of the software. It is not possible to set ms resolution in the used software.

These results show that used photodiode is working with the reverse bias, which means that the measured light is expressed in the voltage with a negative sign. Additionally, when the laser light does not fall on the photodiode, the signal from the photodiode still indicates some value. This means that, used sensor is very sensitive and it is measuring also the light from the environment which must be taken into account during measurements.

Next stage is to obtain values of the signal for three cases: noise from environment (necessary to determine the degree of disruptions), signal of total internal reflection (TIR) for air (which takes place on desired place in the channel) and TIR for ethanol which fills the entire channel. These cases give the information about the expected value of the signal. Moreover, the power of the reflected light at TIR for air was measured by the power meter to get the value of the power as a reference. It was equal to 1,74mW.

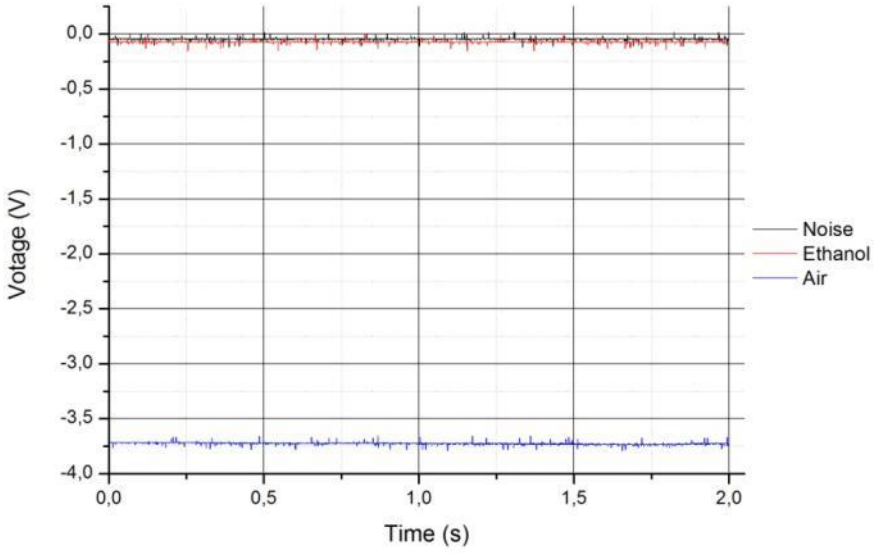

Graph 6 Results of measurements of environmental noises, the reflected light of pure ethanol in the channel and from channel filled with air. Table represents mean value with standard deviation obtained from 2048 scans for each of the medium.

Table 3Presentation of the signal's value of the reflected light for ethanol and air. Moreover, the measurement of noises was performed. Also because, the standard deviation was calculated. It presents that the signal for TIR is not much greater than value of noises. However, it presents more stable signal, because the standard deviation is significantly lower.

	N total	Mean value [V]	Standard Deviation [V]
Noise	2048	-0,04644	0,01086
Ethanol	2048	-0,07329	0,00934
Air	2048	-3,72612	0,01141

After basic measurements, the target experiment was performed. The laser beam was adjusted to the critical angle for air. The channel was filled with the ethanol and the air flow was connected to PDMS chip. Flow rates of these mediums were adjusted to performed air bubbles. Having established appropriate flow rates, the measurement was performed and repeated at least 10 times. The flow rate for air was 1,1ml/h and for ethanol 1,1ml/h.

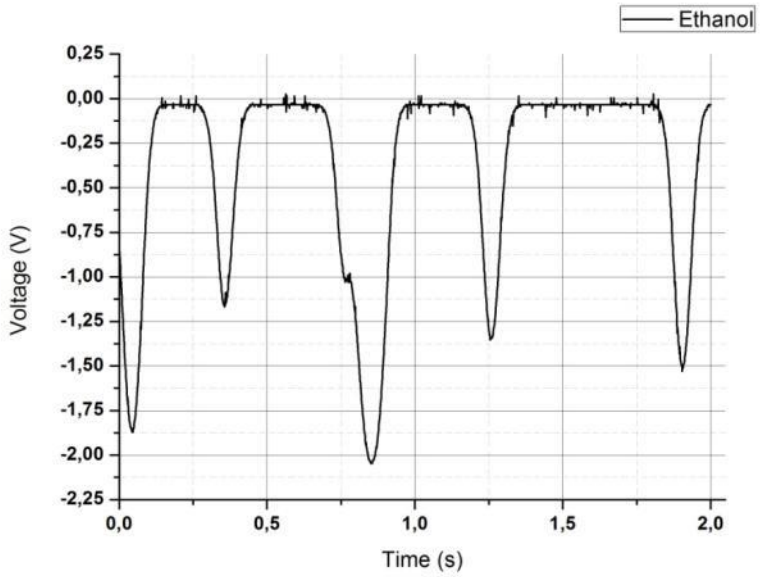

Graph 7 An example of measurement results. When the value of the signal is close to 0 this refers to the presence of ethanol above the place of illumination. Any changes in the signal are connected to the presence of bubble air and refer to the evanescent wave phenomenon.

Obtained results (Graph 7) show low reproducibility over time. This requires calculations of the average value of the duration of the phenomenon and the power of the signal obtained during the presence of air bubbles. The time was measured as a distance between two the half-heights of the peak and the power was assumed from the peak value to the flat line of signal.

Table 4 Presents the mean value of the time and voltage (which corresponds to the power of the laser beam). Total number of measurements corresponds to the number of peaks. Frequency is calculated as the ratio of number of peak and time of the measurement. These measurements correspond to the experiment with pure ethanol and flow of air bubbles thought the channel.

	U [V]	Time EW [s]
Total no. of measurements	77	
Mean value	1,61	0,08
Standard deviation	0,32	0,03
Time [s]	20	
Frequency [no./s]	3,85	

Next stage was to change the fluid from ethanol to the Rhodamine 800. This substance shows the fluorescent properties for under the light illumination with around 600nm wavelength. Rhodamine 800 (Rh800) was dissolved in pure ethanol to obtain a solution with a molar concentration of 100uM. The aim for this part of experiment is to check if the differences in flow rates of mediums have a significant influence on the value of the signal. Measurements and analyses of data were performed in the same way as before.

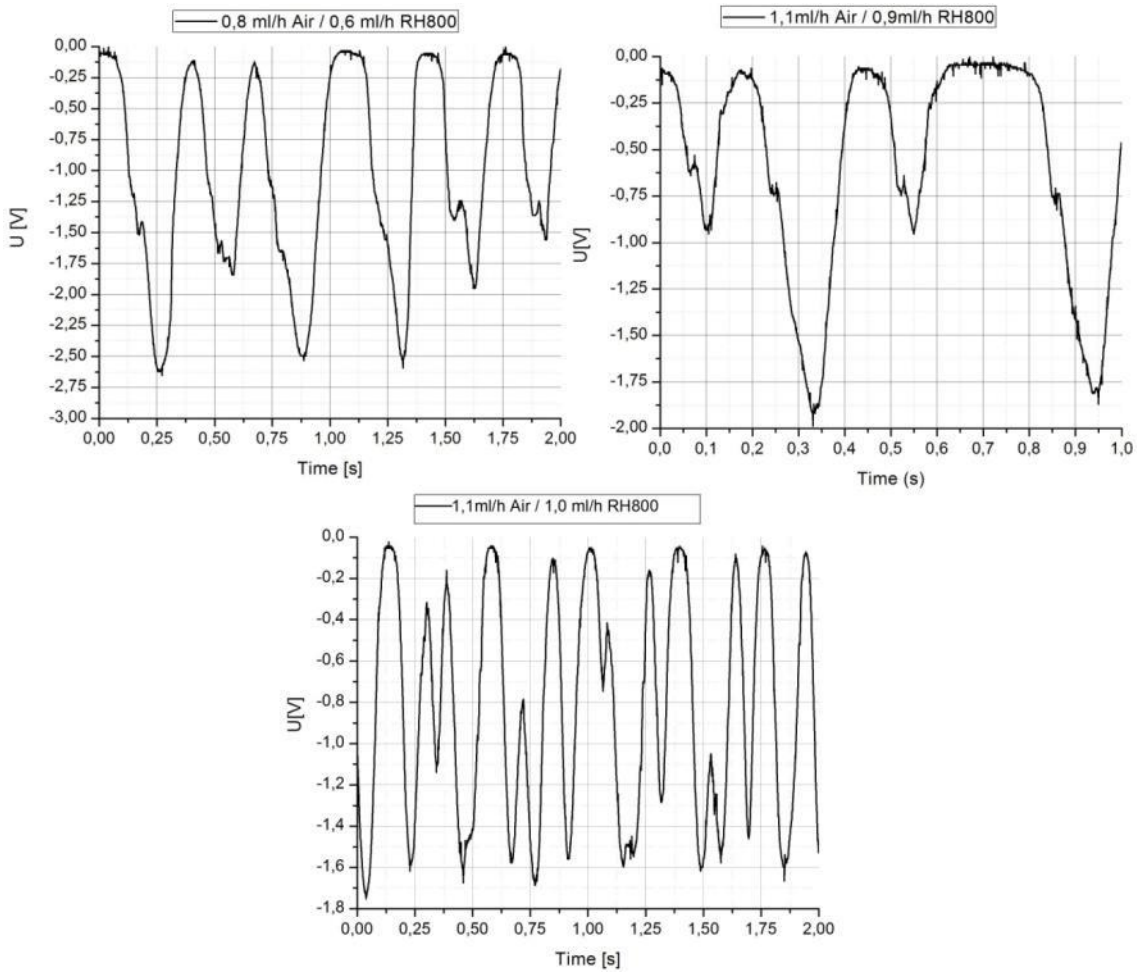

Figure 31 The set of exemplar samples of measurement for three different flow rates of mediums. The main media is Rh800 in molar concentration equal 100µM. Additional statistical calculations are presented in (Table 5).

For checking if the experiments are correct performed, the spectroscopy measurement is carried out. Principles of this stage, is to fill channels by the fluorescent liquid which will be excited by the light from the evanescent wave. In this case, the energy from the phenomenon will be absorbed by the liquid and then emitted light can be measure. To perform this experiment, the optic fibre was used with software intended for that.

Table 5 Presentation of data for different flow ratios with standard deviation, frequency with describe the number of peaks over time of experiment. Moreover, the rate of flows Q_{air} / Q_{Rh} was calculated.

	Mean value	*Standard deviation*	*%*	*frequency [no./s]*	*Flow rate: Q_{air} / Q_{Rh}*
Flow ratios: Q_{air} = 0,8ml/h Air Q_{Rh} = 0,6 ml/h 100µM					
U(V)	1,96	0,503	26%		
Time	0,15	0,044	29%	5,75	1,33
Flow ratios: Q_{air} = 1,1ml/h Air Q_{Rh} = 0,9 ml/h 100µM					
U(V)	1,20	0,450	37%		
Time	0,09	0,032	35%	4,67	1,22
Flow ratios: Q_{air} = 1,1ml/h Air Q_{Rh} = 1,0 ml/h 100µM					
U(V)	1,42	0,166	12%		
Time	0,10	0,033	34%	4,50	1,10

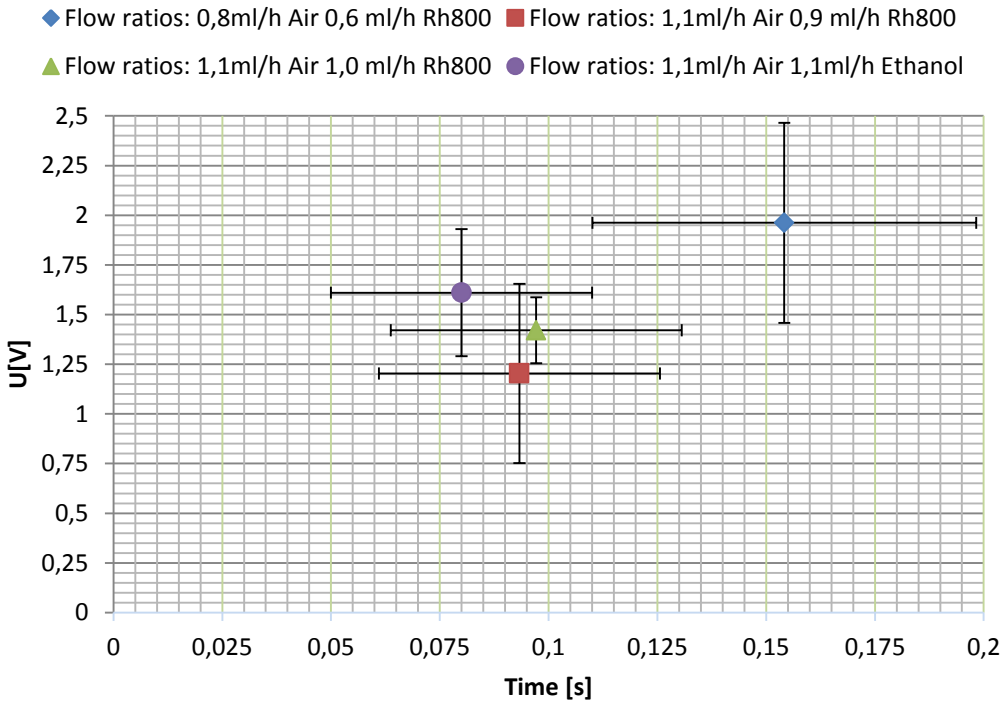

Graph 8 Presentation of data from (Table 5). Different flow ratios for Rh800 are presented with comparison with results of ethanol.

Results from measurements show that standard deviation decrease with the decreasing the ratio of flow rates. This can be explained that the size of bubbles is more uniform with smaller ratio of flows. Moreover, the time which corresponds to the time of presence of the evanescent wave is smaller for higher speeds. This can correspond to smaller size of the bubble, but not the speed, because the frequency of occurrence the bubbles are lower. However, the value of the reflected light did not reach the voltage value for ethanol. This can correspond to various kinds of scattering or it means that on the surface remain a thin layer of the solution which distorts the phenomenon.

After that, a few measurements were taken with different concentrations of Rh800. However, none of them show any significant changes or dependence in the value of the

signal from the previous measurements. The reason is that the illumination angle was adjusted for the air. It means that any disruption will only interrupt the phenomenon. It does not enter into any interactions with the liquid. Additionally, setting the angle of incidence at the critical angle for ethanol is still larger than the critical angle for the air. This means that the evanescent wave phenomenon will occur continuously.

Principles of the microfluidics with surface plasmons polaritons

Next step of developing the microfluidics system was to apply the surface plasmons polaritons (SPPs). The approach of the idea was basically the same as with the evanescent wave phenomenon. However, because SPPs occur only at the boundary of metal-dielectric, the part of the glass which corresponds to the channel had to be covered by the thin gold strip. According to calculations (p.31), the 50nm of gold layer was used.

The process of deposition of the gold stripe was presented in the part with basic fabrication process (p.21). The sealing process occurred to be more difficult than with the pure glass slide. First of all, the presence of plasma could deform planes of gold and additionally introduced into the system gold particles. That is why, only the PDMS chip was activated by the plasma and immediately after the process, the glass slide with gold was pressed to the chip. An important element of this stage was fast and efficient matching the microfluidics channel to the gold strip. That prepared system was connected to the prism with the thin layer of index matching liquid and all were applied to the cage system.

Ideally, the angle of the incident light should be adjusted to the angle which refers to the surface plasmon resonance angle (SPR angle) exactly in the middle of the gold strip. Then, like in previous experiment, the reflected light was collected by the photodiode. However, in this case the presence of the light corresponds to lack of SPPs and when required conditions for the phenomenon appear, there is no light to collect. Because SPPs characterized with high sensitivity, there should be visible response for even small changes of refractive index above the gold layer.

However, after several attempts to the experiment, there turned out that it is very difficult to obtain the SPP phenomenon with these components. First of all, it occurred that pressing the chip to the glass slide during sealing process caused shrinkage of the PDMS. Because the glass slide is very thin, it is not able to endure the tension and this result with surface curving. Because of that, it is impossible to make the smooth connection between the glass slide and the prism which disrupts the SPP. Secondly, the SPP occurs only in small range of angles. That is why it was very difficult to set the incident angle with high precision using the mirror without the rotation scale. The geometrical relations, which were used in case of the evanescent wave, were not sufficient for this phenomenon. In this case, a few changes have been introduced.

Microfluidics - improvements in the cage system

After a few tests, it was checked that deformation of the PDMS chip (after plasma activation) can be reduced by leaving the chip on the glass slide for couple of hours. This allows that the chip is bonded with the sealing part only by the gravity force. This is connected with reducing the tension in PDMS which were introduced by the pressing force. To solve the problem with controlling the angle of incident with higher precision, the *Gimbal* mirror in the cage system was replaced by the pivoting optic mount. This component has got the engraved scale with tick marks every 5°.

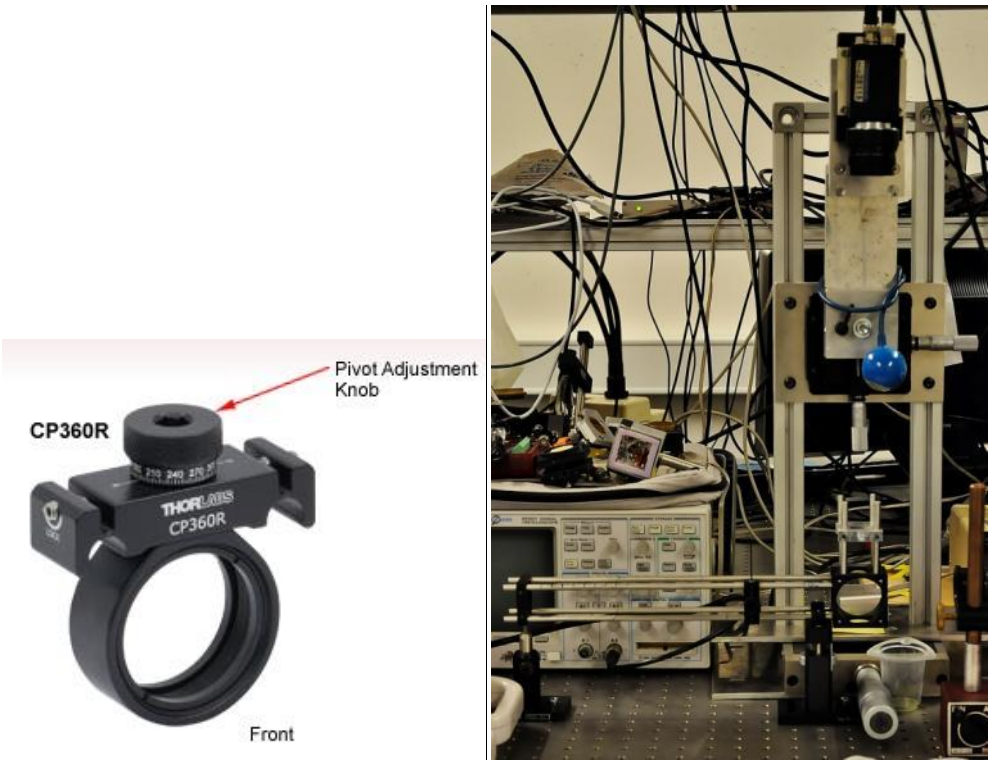

Figure 32 Presentation of the pivoting optic mount (on the left) and observation system in configuration above the PDMS chip (on the right).

Tests were performed for the same components like in both previous experiments. After a few attempts, it occurred that controlling the position of the laser beam is still difficult. One of the reason is that, the light source with 633nm wavelength is giving very bright beam, which after reaching the PDMS is giving a lot of distributed light. It is caused by the fact that the width of the laser beam is wider than the width of channel. In order to facilitate observations of beam position, the observation system was connected. However, the only possible viewpoint was just above the microfluidics system. In this case, the observation was conducted through the PDMS chip, which resulted in low quality images.

Additionally, because the new mirror mount has only one axis of rotation, it causes that the laser beam has to be controlled by changing positions of mirrors which are leading the laser beam outside the cage system. This may caused that the laser beam is no longer parallel to the table and made the adjustment process more difficult. However, after a number of attempts, it occurred that the mirror with the scale is still insufficient to reach desire angle. The experiment requires more precision during controlling the incident angle.

The lateral system for microfluidics

Due to the fact that the cage system does not allow achieving the required angle, it was decided to change the system to the lateral configuration (Figure 33). The system of mirrors which are responsible for conducting the laser beam was used from previous setup. Moreover, it was decided to change the light source for the laser with 795nm wavelength. It was caused, because this wavelength corresponds to more efficient excitation of SPPs and in the same way, better observation of them. Components like half-wave plate and the polarizer remained in the setup. The prism with entire microfluidics system is placed on the holder and is glued to the rotating plate which characterizes with precision of rotation up to 2°.

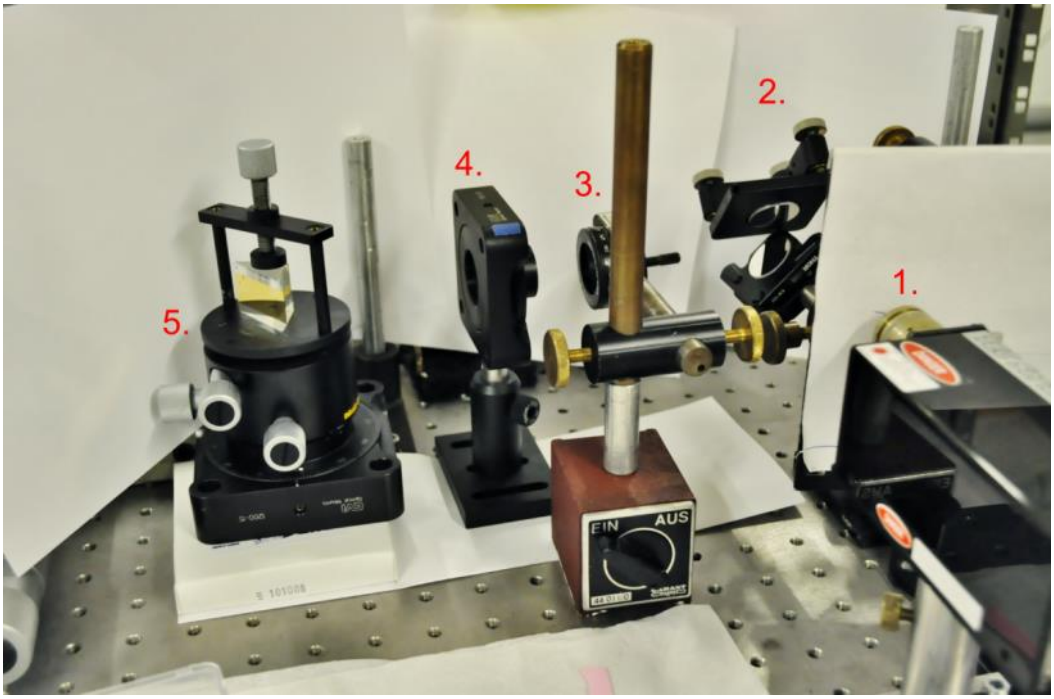

Figure 33 Presentation of the lateral system. (1.) is a laser source with 795nm wavelength, (2.) the mirror system to lead the laser beam, (3.) half-wave plate, (4.) is polarizer for used wavelength, (5.) system of rotation with 2° precision.

The next idea for improvement was used the fact, that SPPs on the gold surface are emitting the light in the visible range. In this case, the entire glass slide was covered by the gold (Figure 34). The idea was to adjust the angle for SPP and observe the dot which

appears on the gold surface. Then, the beam is controlled to the desire place in the channel. Deposition process was performed in the same way like with the gold strip. Also entire process of mounting and protecting the glass slides before deposition was similar.

However, this configuration makes a few difficulties especially with the microfluidics system. Putting the prism with fluids on the side caused that index refractive oil slowly flows from the walls of the prism. As a consequence the entire PDMS chip falls down after some time. Moreover, this setup does not provide the excitation of SPPs. In this case, it was decided to find the weak point of this system and check all steps necessary to excite SPPs one by one.

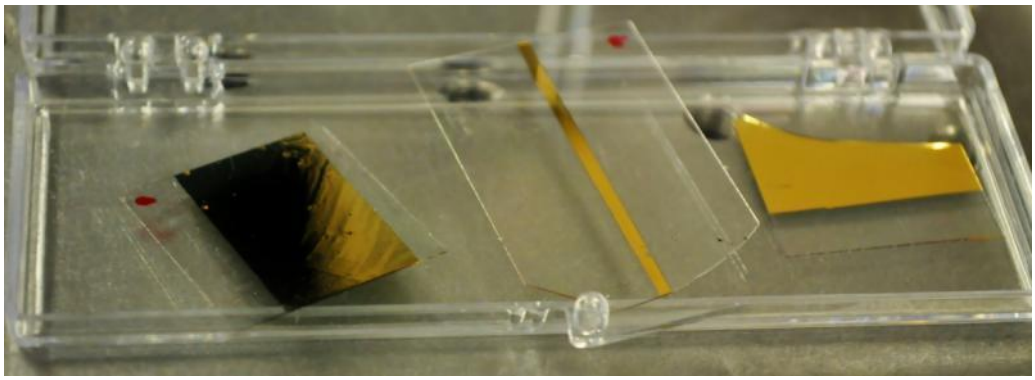

Figure 34 Presentation of different solution of the gold layer on the glass slide (the gold layer and the gold strip)

First step of verification of the setup was to adjust the incident angle to create the evanescent wave and measure the power of the reflected beam. In this case, the prism after thorough cleaning was placed on the rotating holder and adjusts the critical angle for this configuration. Power of the beam was measure by the power meter and was equal to 8,8mW. After that the droplet of index matching liquid was put on the side of the prism and a piece of clean glass slide was attached to it. The evanescent wave phenomenon was still observable.

Next, all steps in the sequence was repeated for the glass slide which is covered with gold layer. However, in this case SPPs were not observed (Figure 35 - A). Moreover, the power of reflected light was measured (Graph 9).From calculations it is known, that SPR angle is close to the 45° of the incident angle. Adjusting to the 45° is possible by checking the position of the beam which reflected from the front wall of the prism.

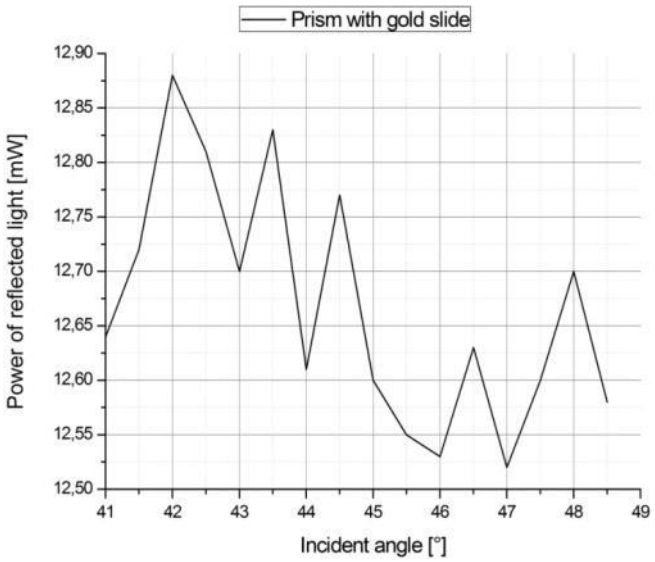

Graph 9 Results of the measurement of the reflected beam power according to the incident angle. In this experiment the prism with the glass slide with gold was measured.

In this case, the prism with directly deposited gold layer was checked. In line with expectations, SPPs were excited (Figure 35 - B). Appropriate measurements were performed (Graph 10).

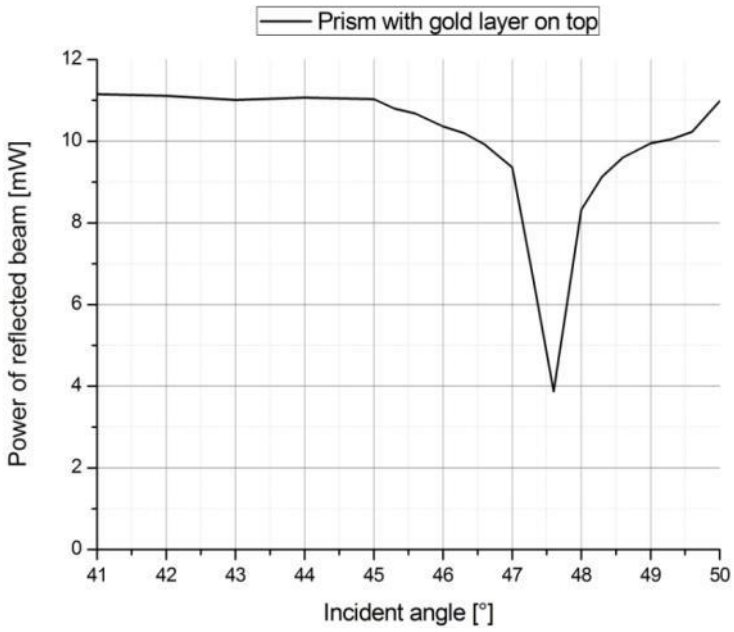

Graph 10 Results of the measurement of the reflected beam power according to the incident angle. In this experiment the prism with the gold layer on top was measured. The measurement was taken with accuracy of 0,5°.

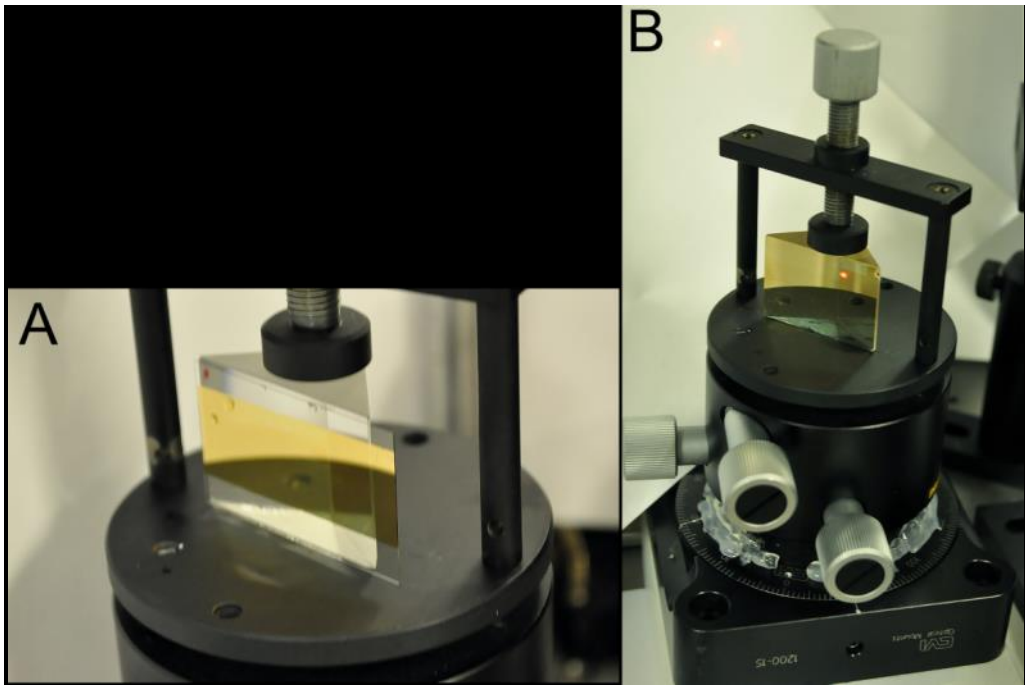

Figure 35 Presentation of the experiments (A) for the prism with glass-gold slide and (B) for the prism with gold layer on top.

Microfluidics system on the prism

In connection with all previous tests, improvements and results, it was concluded that to perform the microfluidic system with SPPs as the measuring tool, the entire system must be achieved directly on the prism. This resulted that new way of fabrication the chip system must be considered and obtained. According to the size of the prism, the entire design of channel structure had to be changed. However, the principles of the droplet-based system remained unchanged.

All processes of designing, developing and manufacturing the master for PDMS chip, remaining as described (p.21). Changes in the fabrication begin with the deposition and sealing which that were continually adjusted to the needs.

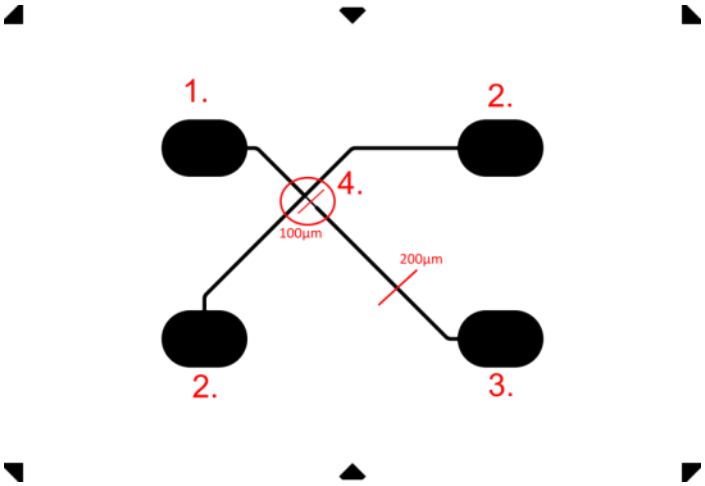

Figure 36 New design of the microfluidics structure. (1.) is an inlet and chamber for fluid which will be in droplet form in the system (in this case it is air). (2.) corresponds to chambers for main fluid (in this case it is ethanol). (3.) is a output and (4.) is a bubbles structure maker which has got thinner cross section area than the rest of channels. The width of the rest of channels is equal for everyone and is 200µm.

According to previous types of sealing, it was decided that the entire hypotenuse wall of the prism should be covered with gold layer. That requires to safely mounting the prism in order to avoid falling inside the deposition device. After that, the PDMS chip was put into the plasma cleaner and then connected with the prism. However, it was noticed that bonding between gold layer and PDMS chip is weaker than with glass slide, the prism was pressed to the chip and left for 24h with a load.

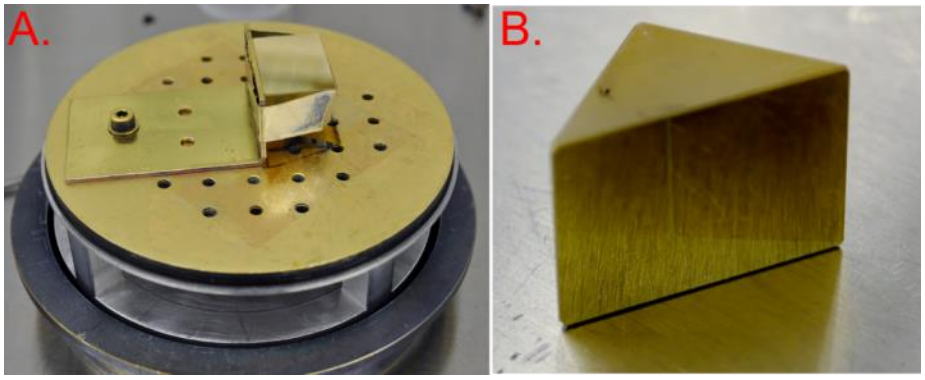

Figure 37 Method of mounting the prism to the L-shaped profile before deposition (A.). The prism with hypotenuse wall covered with gold (B.).

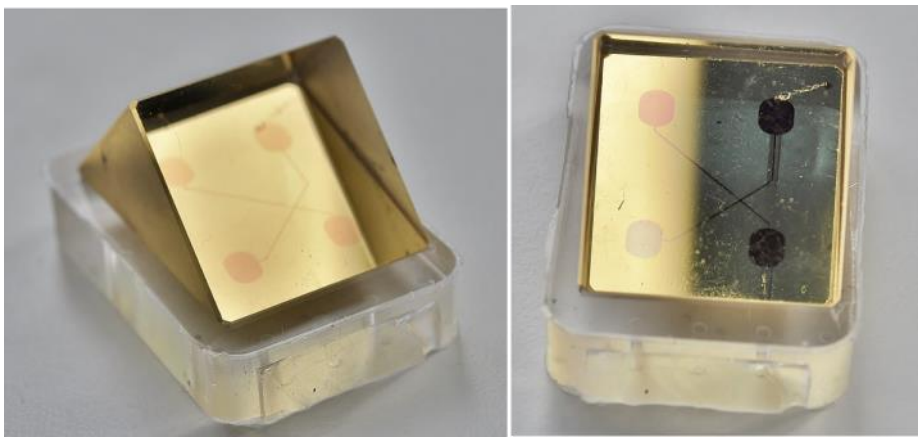

Figure 38 Prism bonded to the PDMS chip. These pictures present the good quality bonding. There are no bubbles of air between the prism and the chip. Moreover, the entire structure of channels can be seen.

After that time, it was checked if the prism is connected with the PDMS chip. It occurred that the connection is weak and the components broke away after inserting pins with rubber pipes. In this case, it was assumed that there is a need of leaving a clean area of glass to enable the PDMS to make bond with it. In order to that, the gold layer was removed in the Aqua Regina for sufficient time and a new layer of gold was deposited.

New deposition design assumed that there are parts of the prism which are not covered with the gold layer. To achieve that, after mounting to the L-shape profile, edges of the prism are covered with the special tape which can be put inside the Cryofox. Moreover, it does not leave the sticky surface and is easy to remove. At the same time two prisms were taken under the deposition process. Sealing process is the same as previously, only PDMS chip is subjected to activation by plasma. After sealing, two methods of connection were performed. First one, (similar to the previous one), the prism is pressed to the chip and left for 24h to strengthen the bonding, before putting pins to the chip (Figure 39). Second one has been subjected to the gravity force and no external forces are added.

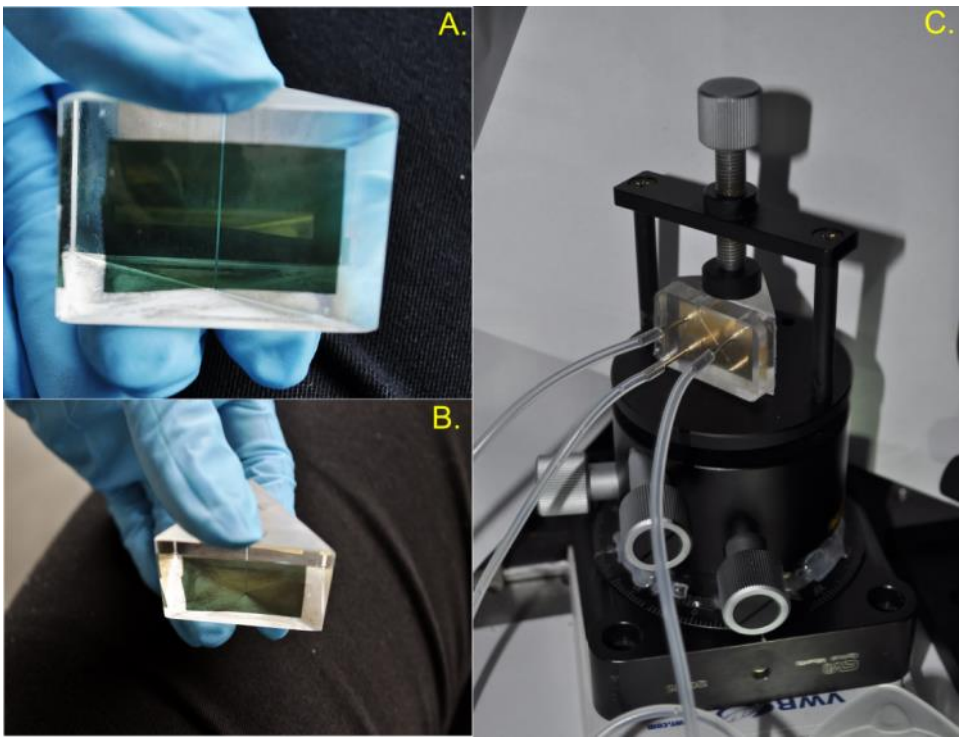

Figure 39 A and B present the prism after deposition with gold layer only in the middle of the wall. Image C. Shows the system ready for experiments, after sealing and connecting the pins.

At the beginning, this method of connection showed good quality of bonding in both cases. Moreover, putting pins inside the chip did not destroy the link. In that case, the entire system was assembled to perform the experiment and the measurement. In the first attempt, the first prism was used. After adjusting the laser beam into the channel, it occurred that SPPs excitation cannot be detected. Measurement of the reflected light did not show any changes of value during changes of incident angle.

After that, all steps of the experiment were repeated with the second prism. In this case, the excitation of SPPs could be seen by the bare eye, because of the presence of the light spot at the gold surface. Moreover, this was confirmed by the measuring the power of reflected light and compared with detailed calculations (Graph 11).

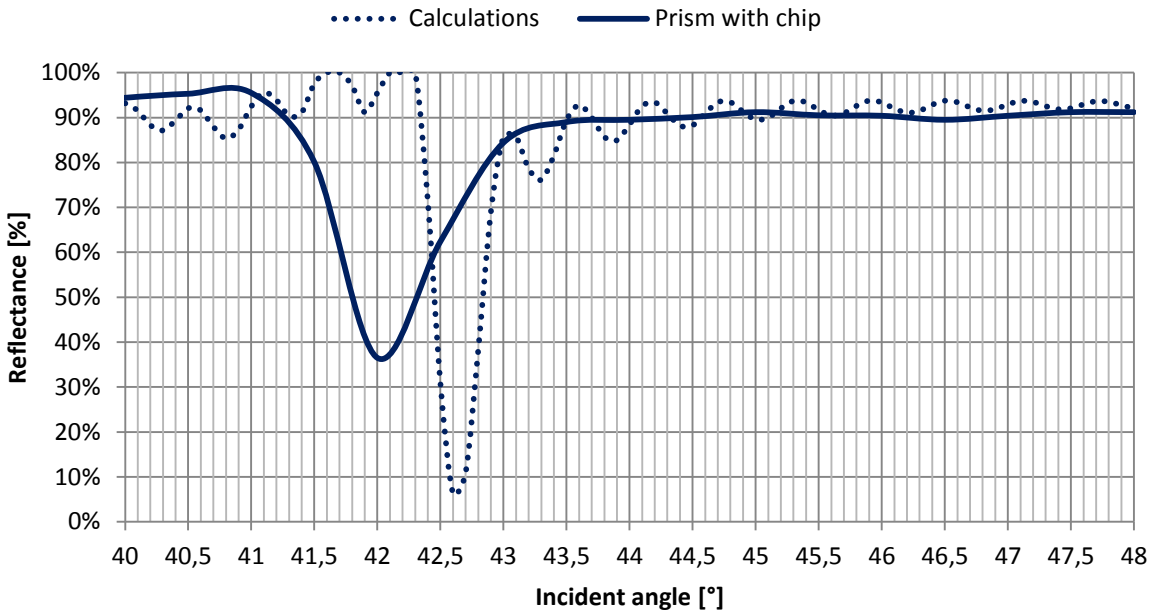

Graph 11 Presentation of achieved results. Measurement was taken with the prism with gold square at the top and sealed PDMS chip (solid line). Also there are presented results of detailed calculations for used system (dotted line). Reflectance is calculated by deviating the measured power by the max achieved power for this experiment.

The next step was to connect the flow of ethanol and create air bubbles in the middle of channel. However, it occurred that achieved bonding is not strong enough to withstand the pressure exerted by the fluid. As a consequence, the PDMS chip fell down from the prism.

Due to the fact that previous bonding was not sufficient for experiment, it was decided to verify one more deposition design. Because only PDMS chip is activated by the plasma, it was assumed that the best properties of bonding have the edges of chambers. Moreover, if this part of the microfluidics system is able to withstand the fluid pressure, the rest of the structure will not fail. That is why, gold was deposited only on the part of the prism which will cover the channels, but not chambers (Figure 40 – A.). However, during sealing process the PDMS chip was pressed to the prism and left for 24h to strengthen the bonding. It was done to be sure that connection is stable.

In this configuration it occurred that it is very difficult to control the laser beam, especially the place where it falls on gold layer. That is why; the observation system was expanded by the second CCD camera which was placed above the laser in the way that allows observing the interface prism-chip (Figure 40 - B). Moreover, the rotating plate has been changed for another with higher precision. Additionally, the focusing lens was used to increase the effectiveness of the laser light,. This allowed focusing the laser beam on the

small spot which should not be wider than width of channel. The lens was added between the polarizer and the prism in the distance which correspond to its focal point.

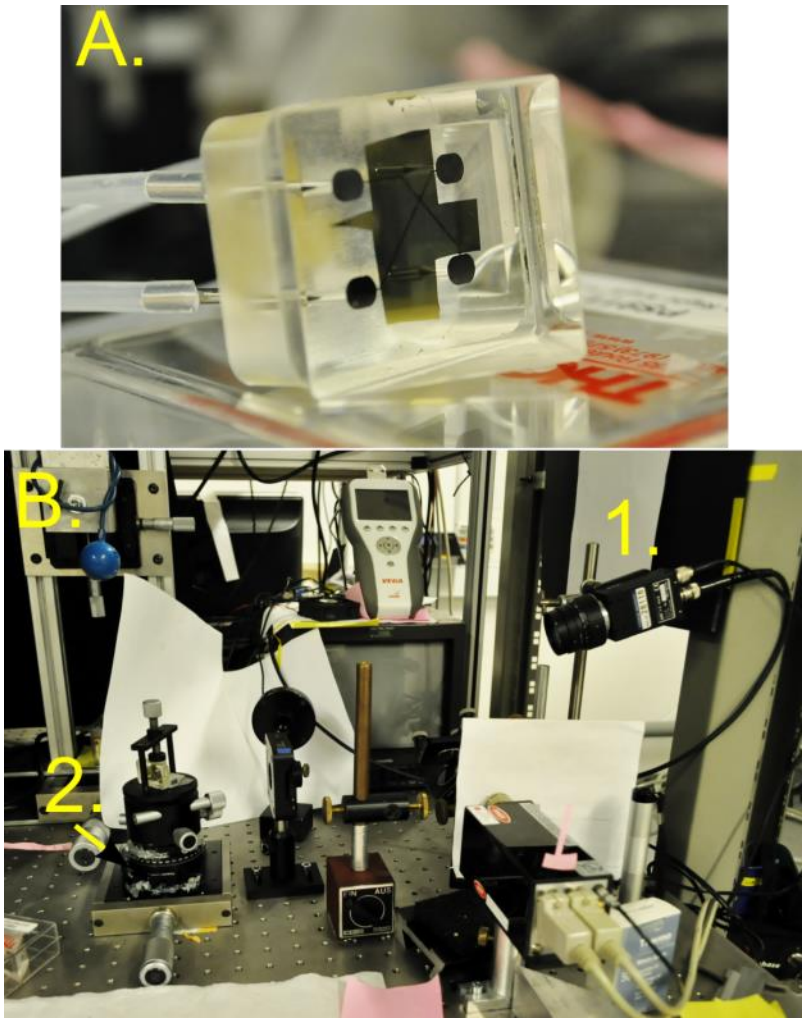

Figure 40 (A.) Presentation of the microfluidics system with gold layer only at the area of channels. (B.) presents the entire modified experimental setup with additional camera (1.) and more precise rotating table (2).

After adjusting the laser beam to the channel a number of attempts were taken to find and set the incident angle which corresponds to SPR angle. However, after finding the desired angle it occurred that SPPs were not excited with high effectiveness. It could be observe as a slight decrease in power of reflected light (a decrease of approximately 10%). Achieved results are not sufficient for perform the detection system. After presented numbers of attempts which ended with or without excitation of SPPs, a hypothesis was put forward. Some pollutants which are moving in the fluid they may deposited on the gold surface and interrupt in the phenomenon.

Observation of Surface Plasmon Polaritons

During this project many experimental attempts have been performed and each of them provided new information of the system, which gave a lot of ideas for improvement and development. However, the last experiment proposed that many of failed attempts could be caused by the left sediments. According to this hypothesis, the setup was changed in order to verify the suspicion.

The approach of this part of experiment was to use principles of Surface Plasmon Resonance Technology. In this case, the reflected light was collected by the CCD camera. This should allow observing results of excitation of SPP which appears as a dark line in the reflected beam. It was caused because the phenomenon corresponds only to specific angle. If the surface plasmons polaritons were set to resonate with the laser beam, it resulted in absorption of the light at that angle.

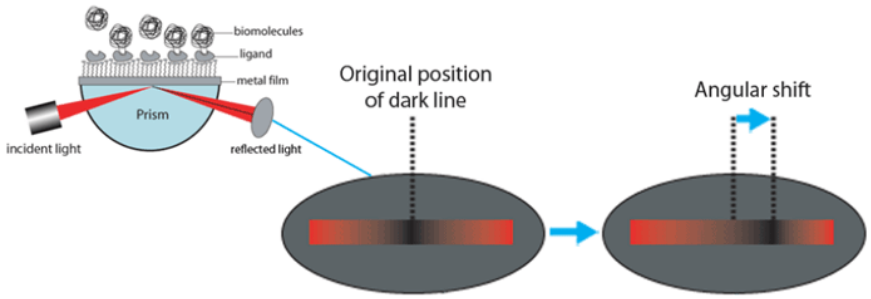

Figure 41 The excitation of SPPs results in a dark line in the reflected beam. Any angular shifts are connected with changes of the dielectric above the place of excitation [33].

This feature of SPPs excitation was used to observe a surface, which may become contaminated. Moreover, the focusing lens is helping to collect entire laser beam and focused at the desire area of the surface. For this experiment two prism with gold layer were intended. Both of them had the same thickness of gold but deposited at different times. It was possible to observe this phenomenon in two ways.

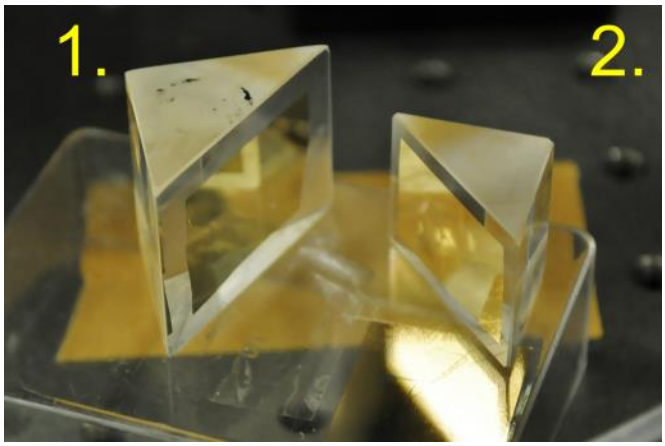

Figure 42 Two prisms which are used in the experiment. Both of them have the same thickness of gold layer, but there were taken in different deposition processes.

The first one; was about taking the images of the reflected light in traditional way. A piece of paper was put in a way of reflected light and observation of dark line could be done by bare eye. In this case, images with high resolution were taken for both prisms. Moreover, information about incidence angle was collected for pictures analyses.

At first, the prism no.1 with ethanol as a fluidic was used. The dark strip which corresponded to SPPs were easily observed before pouring the ethanol. After the evaporation of ethanol, it occurred that no SPPs were excited on the surface. That provided the assumption that some contaminations were deposited on the prism wall after evaporating the alcohol. Even after a several repetitions, the phenomenon was not achieved. Also, at the gold surface it was possible to notices a streak on the place where previously the ethanol was poured. In this case, the ethanol was changed for isopropanol (IP) which characterized with high purity and it did not leave any trails.

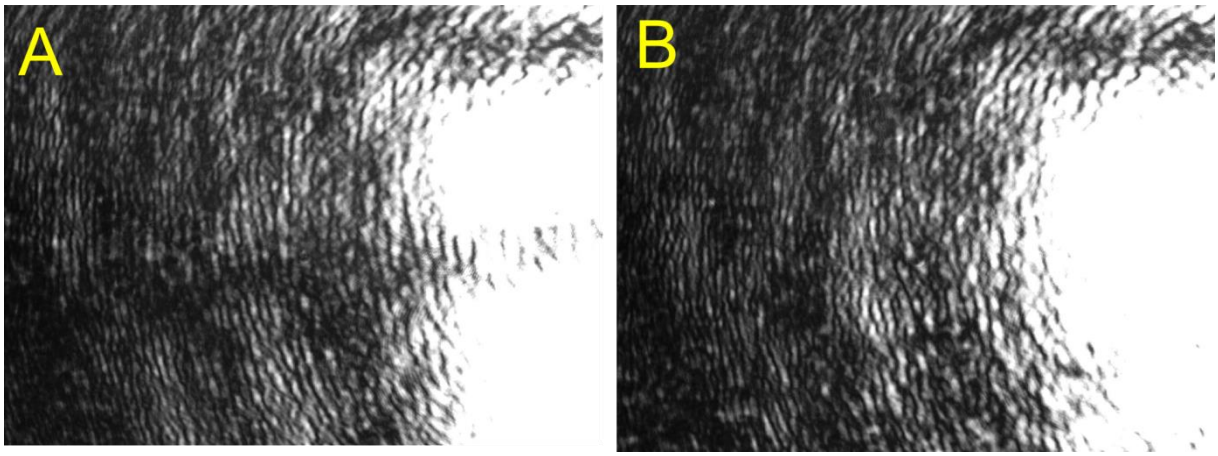

Figure 43 Images of the reflected light with 1st prism and ethanol as a fluidic. (A) Corresponds to the gold surface before pouring the ethanol, were B refers to the surface after .

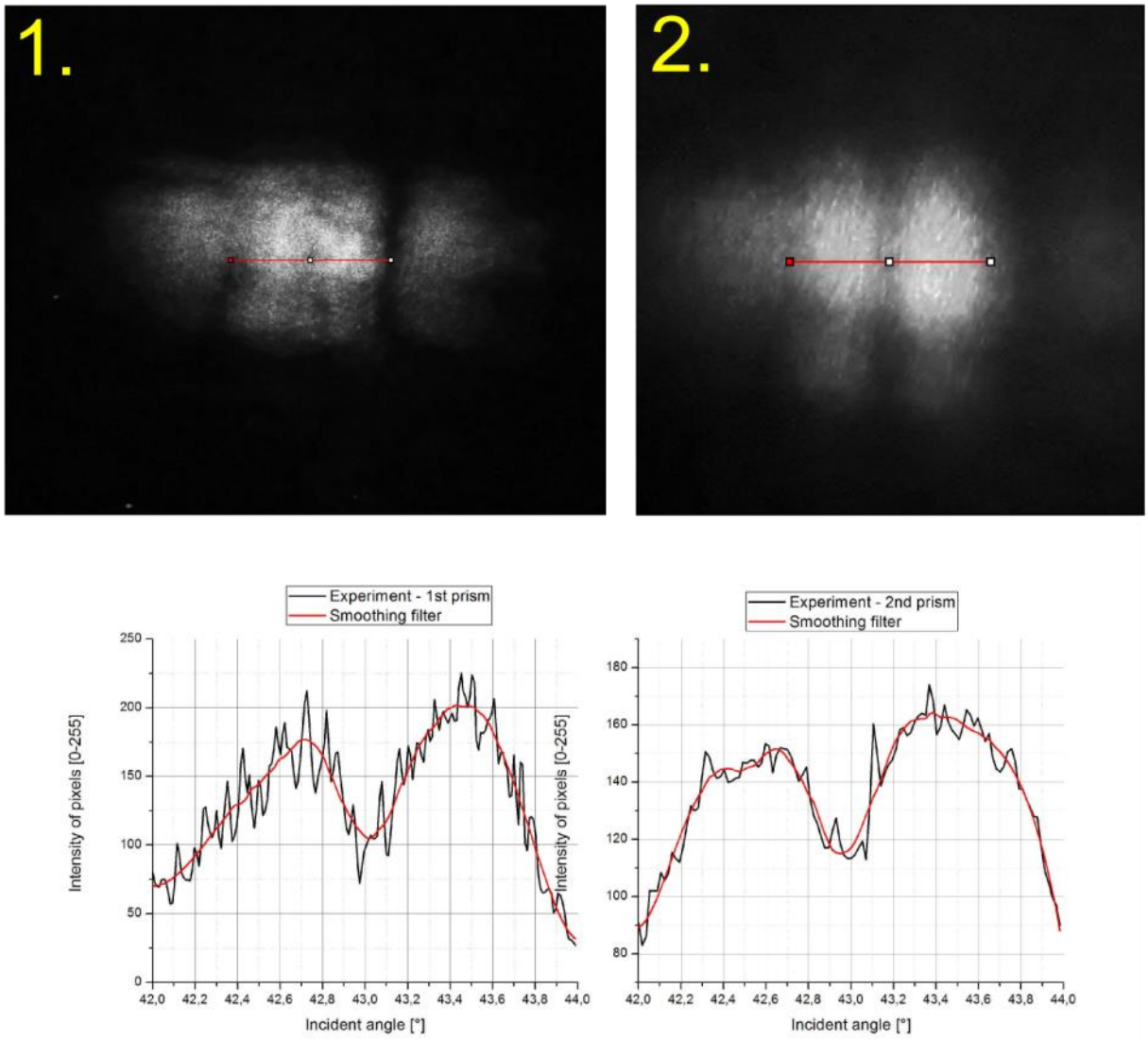

Figure 44 Examples of pictures taken during the experiment with SRL camera. Graphs present the analyses of the images by the ImageJ software. The intensity of pixels (of the red line which are marked on the images) is presented in respect to the incident angle. Values of incident were calculated according to the collected data.

Method of analyses the image should be explained in more details. During the experiment, information about incident angles were collected for 45° and also for both angles which correspond to the dark stripes on both sides (on the images). It occurred that the move from one dark stripe to another corresponded to 2° of rotation. Than red line was marked on the picture and information about intensity of pixels was taken from ImageJ software. The data was presented in the table with points and connected with them intensity of pixels. In that case dividing 2° by the number of points are giving the rough orientation of the incident angle for each of the measured point. After plotting the graph, the smoothing filter was added in order to present more clearly the relations between images and the phenomenon of SPPs.

Already on the images can be seen the difference in the quality of SPPs. Also analyses of the intensity of pixels in images give a suspicion that quality of surface is different in both cases.

Next stage of this experiment was to collect reflected light by the CMOS camera (Thorlabs - Compact USB 2.0 CMOS Camera). In this case, both prisms were also used. Moreover, a short movie has been recorded during performing the experiment.

An aim of this part was to make projection of what happening inside the microfluidic channel during the experiment. At first the SPR angle is found on the prism covered with the gold layer. Next, a droplet (around 0,05ml) of isopropanol (IP) was poured on the gold side of prism. After evaporating the alcohol, SPPs appear again on the surface. However, comparing the pictures before and after the presence of IP the place of SPPs excitation is shifted. A number of attempts were performed to check these relations. Analysis of images data was made in the same way as before in usage of ImageJ. During the experiment neither the camera nor the prism has been moved. In this case the red line was taken in the same place in both pictures (parameters of x and y which correspond to the pixels had the same value).

This experiment was performed with both prisms. Isopropanol was used in, because this type of alcohol is commonly used for cleaning the optical components. This is due to that IP doesn't leave stains on the surface after evaporation. Results are presented below.

After experiment and analyses data it occurred that the shift of the SPR angle appears. However, after a few attempts, SPPs appear at the same place as at the beginning. This is probably due to the accumulation of contaminants on the surface. It means that despite the fact that IP is very pure fluid it also leaves some contaminants on the surface which affect on the change of SPR angle. Moreover, the quality of the gold layer has a significant impact on excitation SPPs. It can be notice comparing the images from both prisms.

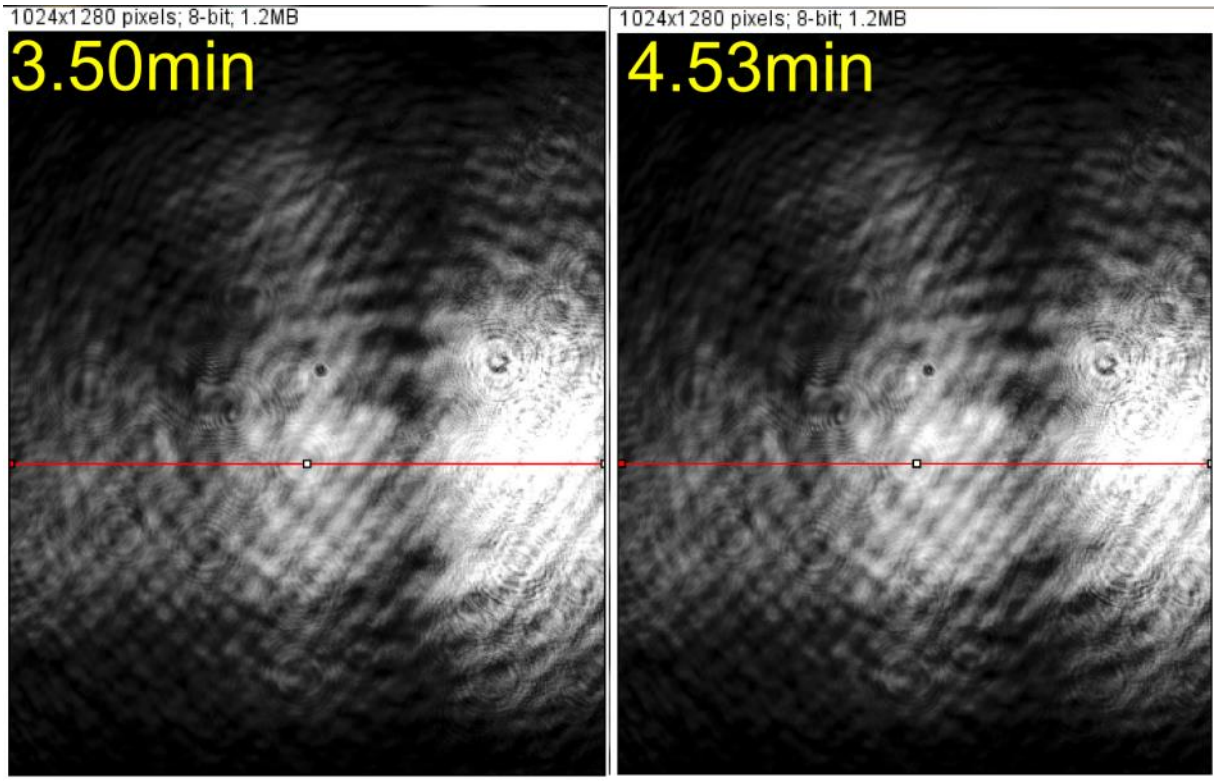

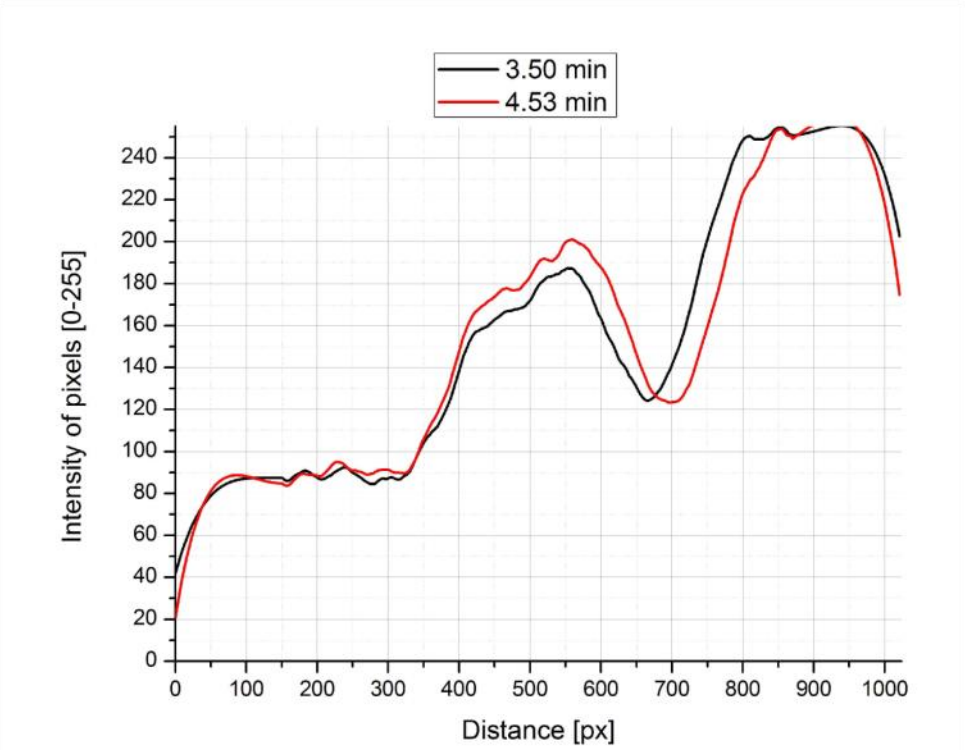

Figure 45 Snapshots from the experiment with 1st prism (Figure 42). There are presented two images of the place where SPPs occur. Image from 3:50 min presents SPPs before pouring the IP and image from 4:53min is after the evaporation. A graph presents the analyses of the intensity of pixels in both pictures at the same place.

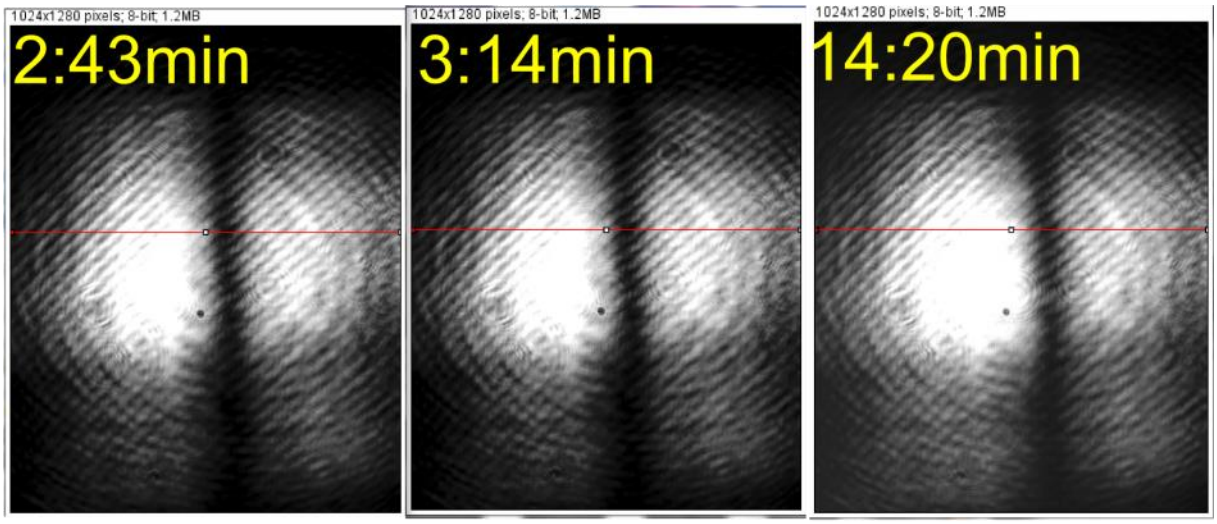

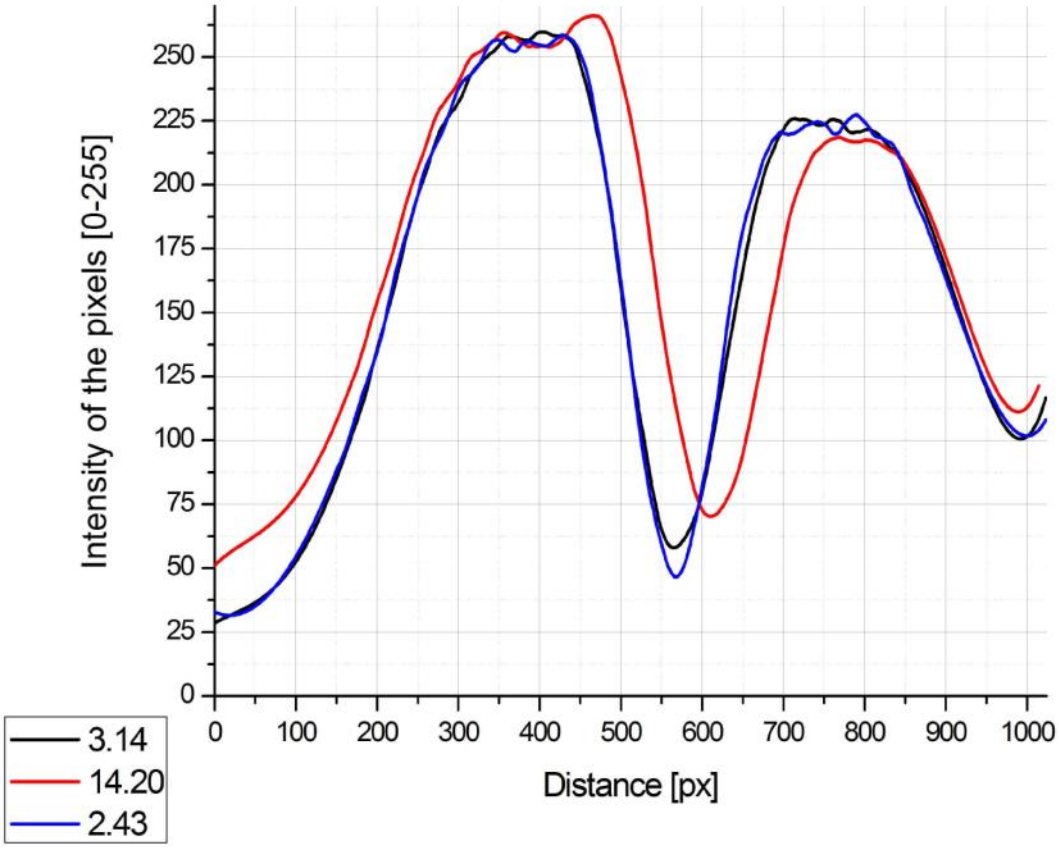

Figure 46 Snapshots from the experiment with 2nd prism (Figure 42). There are presented three images of the place where SPPs occur. Image from 2:43 min presents SPPs before pouring the IP and image from 3:14min is after the evaporation. Moreover, image from 14:20 min presents results after 20 repetitions of the experiment. Graph presents the analyses of the intensity of pixels in all pictures at the same place.

Due to the entire experiment was recorded in short movie, as samples of the results a sequence of snapshots are presented (Figure 47). For both prisms the experiment looked similar that is why results only from the 2nd one are shown.

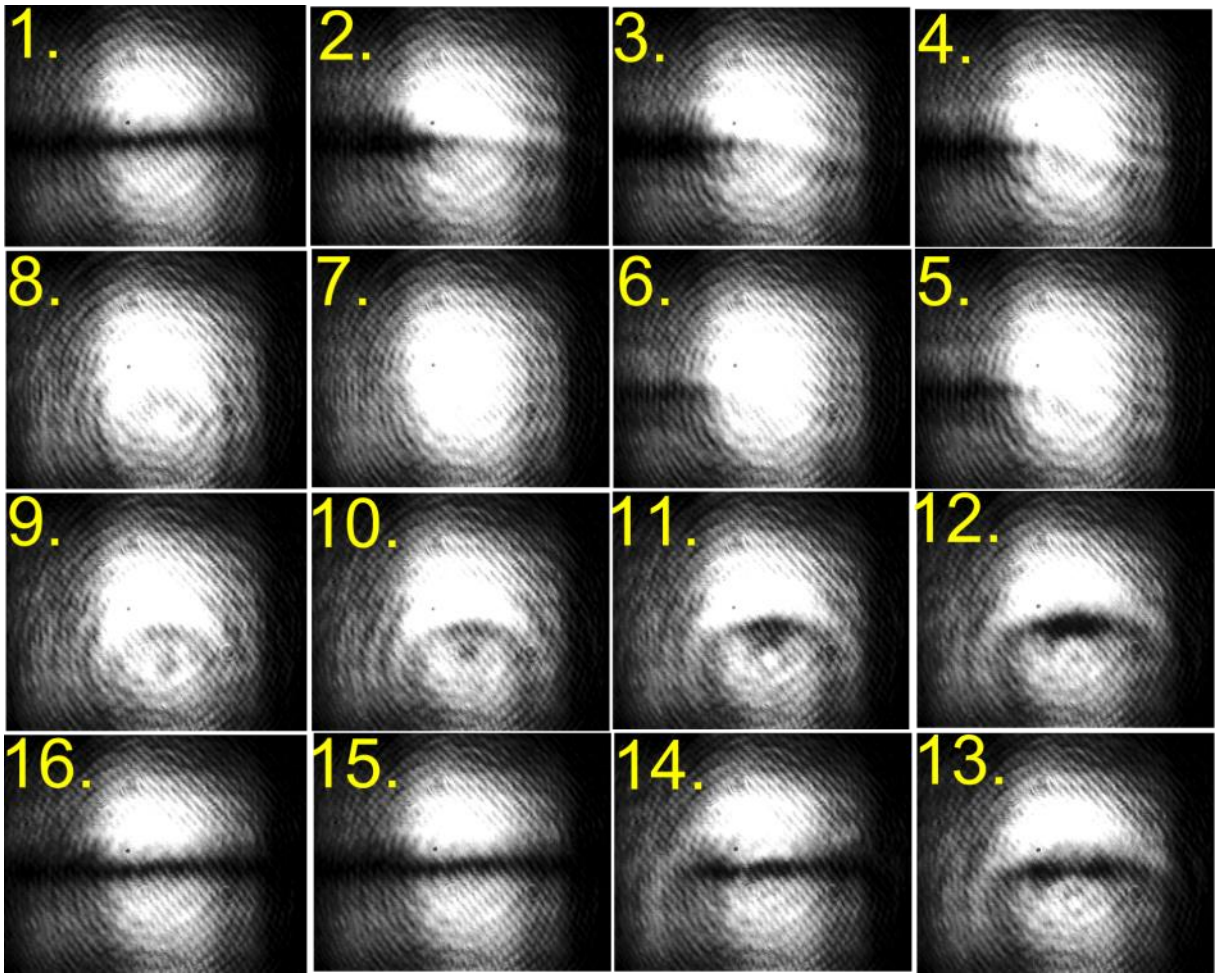

Figure 47 Snapshots of reflected light from one attempt of the experiment with 2nd prism. Snapshots no. 1 presents the surface before pouring the isopropanol (IP). Number from 2-4 present when droplet of IP was falling down and reaching the place where SPPs are excited. Number 7 and 8 show the moment were IP is on the surface. Snapshots from 6-15 show what is happening during evaporation and number 16 presents when SPPs are again excited on the dry gold surface.

VI. Conclusions

The entire project has finished with a great success. A number of performed experiments provided a lot of information about a microfluidics system and its features. An aim of the project has been confirmed when promising results on the use of optical phenomena in microfluidics sensors have been delivered. Approach of the project has been verified by experiments. Results showed a few additional conditions which must be fulfilled to achieve a highly accurate device. These requirements are related not only to fabrication of the device, but also to principles of phenomena. Improvements and analysis of obtained results are divided into three parts. The first part is connected to the experiment with basic characteristics of the evanescent wave. Next, experiments related to SPPs are discussed and finally conclusions connected to steps of chip fabrication process are presented.

The first experiment confirmed the approach of the microfluidics sensor. The PDMS chip was sealed with the glass slide and then connected to the prism by a thin layer of the index matching liquid. In this case, the evanescent wave was formed at the interface between the glass slide and the air inside the channel. The aim of this experiment was to make air bubbles inside the continue flow of ethanol and Rhodamine 800. According to the principles of the phenomenon, each of the bubble should be detected in the reflected light which was collected by the photodiode. Results of experiments confirmed the assumption. Each of the flowing bubble caused the formation of the evanescent wave, so the reflected beam could be measured.

A number of experiments with different values of flow ratios have been performed. Results were presented as peaks of signals when bubbles appeared. It has been observed that with lower values of the flow rate, measured time of each peak is longer and more uniform than for higher speeds of fluids and it is related to the size of the bubble. Larger bubble allowed performing the evanescent wave for longer time when intensity observed for the reflected light increased. This could be also related to the size of bubble, because longer bubbles give more time to remove anything what could remain after liquid flow. The values of standard deviation for both parameters are similar or higher than in other cases. This means that slower flow of fluids was performing bubbles with higher randomness when signal observed at higher speeds showed greater uniformity. This also confirmed the purpose of the experiment: the system was able to detect small objects which interrupted the phenomenon.

Moreover, this experiment was also intended to verify the molar concentration of the solution. In this case, it was not possible to observe any relevant connections between the shape of signals and the molar concentration. It is because, the critical angle which corresponds to the formation of the evanescent wave for air is very low (41,3°) and also because this phenomenon takes place at any angle greater than critical value. Which means

that to detect any changes in the molar concentration of liquid, the critical angle for this liquid has to be set when air of bubbles should not be used. Better effect is expected to be observed by using other liquid with higher critical angle than the main fluid. Another idea is to measure e.g. fluorescence of the liquid (if the solution is fluorescent) rather than the reflected light.

Experiments with SPPs provided us with a lot of information about the phenomenon and conditions of fabrication the chip. Achieved results confirmed high sensitivity of SPPs. It could be also observed that the angle which corresponds to the SPR, is dependent on many parameters of the system and used materials. Images from experiments presented the relation between the quality of gold surface and the efficiency of the phenomenon. Moreover, the purity of used fluids has significant meaning for sensors based on principles of SPPs as contaminations from the liquid may deposit on the surface after evaporation of fluid. Achieved images suggested that angle which corresponds to SPR has been shifted and achieved results may not represent highly accurate data. Also, it has been observed that using highly pure isopropanol made a significant difference in the quality and accuracy of the measured signal which showed that beside shifted angle, the intensity of the light decreased. Finding the proper material which can be deposited on top of the gold layer may be solution for this issue. Also, the gold layer should be covered by the substance which will protect it from degradation (e.g. SiO2). Another idea is to cover a gold layer with thin layer of hydrophobic material. All these solutions must undergo further, because any additional layer on top of the gold may disrupt in excitation of SPPs. Application of cleaning liquid is another idea which may solve the problem of contaminations. The additional droplet system would create droplets from the solution which absorbs any contaminations when these “cleaning droplets” would flow between droplets of main fluid. However, it must be remembered that to make droplet inside the channel, both of fluids must not mix.

All performed experiments provided a lot of information about conditions of fabrication. First of all, the approach assumed that the prism and the glass slide are connected by the thin layer of the index matching oil. However, like the experiments presented, this idea did not work with excitation of SPPs. One of the reasons is that used liquid could not perform the uniform thin film. That caused tilting the PDMS chip and as a consequence the incident angle could not be controlled. Moreover, number of attempts showed that bonding between the PDMS and glass is strong and durable. However, it has to be done only by gravity forces. In other way, additional forces introduce stresses into the chip, which resulted with bending the surface of chip and destroying uniform connection area. On the other hand, bonding between PDMS and gold layer is weak and not durable. That is why the design should take into account areas which are intended to the bonding process and the gold layer should only cover parts which are dedicated to the channels. Additionally, during experiments, it has been observed that in case of gold, the requirements for sealing process are the same and all bonding connections must be performed only by the

gravity forces. It has been concluded that the additional forces can cause deformation of the channel by changing the dimension of the design structure. This may lead to the case where changed dimensions of the channel are not sufficient for light trapping.

Each of presented experiments provided us with information how difficult it is to fulfill all requirements and achieve desire sensing system. Data and conclusions presented in this thesis confirm that idea of combining the optics with microfluidics system is worth further examination. The evanescent wave has been proved to be sufficient and accurate detection method providing satisfying results in case of detection of objects in the fluidic flow. However, further studies are necessary to prove if the evanescent wave method may be successfully used to detect changes in moles or molecules sizes. In that case, principles of SPPs fully satisfy all requirements. Results obtained in this project confirmed that sensitivity of SPPs is unrivalled in terms of detecting changes at the level of surface contaminants or in the refractive index of liquid. Results presented in this thesis are a good platform for further studies. Additionally, examinations of this field of research which can be considered as very promising and valuable despite requiring further development and continuous improvement.

VII. References

[1] Y. A. Akimov and H. S. Chu, "Plasmon–plasmon interaction: controlling light at nanoscale," *IOP science/ Nanotechnology,* vol. 23, no. 44, January 2012.

[2] H. M. Hiep, T. Endo, K. Kerman, M. Chikae, D.-K. Kim, S. Yamamura, Y. Takamura and E. Tamiya, "A localized surface plasmon resonance based immunosensor for the detection of casein in milk," *Science and Technology of Advanced Materials,* vol. 8, no. 4, 2007.

[3] C. Rockstuhl, S. Fahr and F. Lederer, "Absorption enhancement in solar cells by localized plasmon polaritons," *Journal of Applied Physics,* vol. 104, no. 12, 2008.

[4] DARPA Center of Optofluidic Integration , "What is optofluidic?," California Insititute of Technology, 2008. [Online]. Available: http://www.biophot.caltech.edu/optofluidics/optofluidics/index.html. [Accessed 2014].

[5] D. Erickson, D. Sinton and D. Psaltis, "Optofluidics for energy applications," *Nature Photonics,* no. 5, pp. 583-585, 2011.

[6] X. Fan and I. M. White, "Optofluidic microsystems for chemical and biological analysis," *Nature Photonics,* no. 5, pp. 591-594, 2011.

[7] B. C. Sih, M. O. Wolf, D. Jarvis and J. F. Young, "Surface-plasmon resonance sensing of alcohol with electrodeposited," *Journal of applied physics,* no. 98, 2005.

[8] H. R. Gwon and S. H. Lee, "Spectral and Angular Responses of Surface Plasmon Resonance Based on the Kretschmann Prism Configuration," *Materials Transactions,* vol. 51, no. 6, pp. 1150-1155, 2010.

[9] M. Okan, O. Balci and C. Kocabas, "A microfluidic based differential plasmon resonance sensor," *Sensors and Actuators B: Chemical,* no. 160, pp. 670-676, 2011.

[10] Daniel Mittleman, Rice University, "Waves and Photonics - lectures 13-14," January 2014. [Online]. Available: http://www.ece.rice.edu/~daniel/. [Accessed May 2014].

[11] E. Hecht, "Optics 4th," San Francisco, Addison Wesley, 2002, pp. 97,99-102,111,113-118.

[12] M. Born and E. Wolf, “Principles of optics 4th,” in *Electromagnetic Theory of Propagation, Interference and Diffraction of Light*, Pergamon Press, 1970, pp. 47-48.

[13] J. Y. Han, “Low-Cost Multi-Touch Sensing through Frustrated Total Internal Refl ection,” in *18th Annual ACM Symposium on User Interface Software and Technology*, Seattle, 2005.

[14] W. Ockenga, “Total Internal Reflection Fluorescence (TIRF) Microscopy,” Science Lab, 12 March 2012. [Online]. Available: http://www.leica-microsystems.com/science-lab/total-internal-reflection-fluorescence-tirf-microscopy/. [Accessed 2014].

[15] S. A. Maier, “Electromagnetics of metals,” in *Plasmonics Fundamentals and Applications*, Bath, UK, Springer, 2007, pp. 6-9.

[16] Wikipedia, “Drude model,” 7 May 2014. [Online]. Available: http://en.wikipedia.org/wiki/Drude_model. [Accessed May 2014].

[17] A. Roszkiewicz, “Generacja plazmonów polarytonów powierzchniowych na strukturach periodycznych,” Warsaw, Polska Akademia Nauk, Instytut Podstawowych Problemów Techniki, 2011, pp. 17-20, Polish.

[18] L. Novotny and B. Hecht, “Surface plasmon polaritons at plane interfaces,” in *Principles of Nano-Optics*, Cambridge University Press, 2006, pp. 382-386.

[19] S. A. Maier, “Excitation of surface plasmon polaritons on planar interfaces,” in *Plasmonics - Fundamentals and applications* , Springer, 2007, pp. 39-47.

[20] Thermal-Fluids Central, “Surface plasmon (or phonon) polaritons,” 10 February 2012. [Online]. Available: https://www.thermalfluidscentral.org/encyclopedia/index.php/Surface_plasmon_(or_phonon)_polaritons. [Accessed May 2014].

[21] A. Radenovic, “Microfludics Lab On Chip, thesis,” École polytechnique fédérale de Lausanne, Lausanne, Switzerland.

[22] Wikipedia, “Hagen–Poiseuille equation,” February 2014. [Online]. Available: http://en.wikipedia.org/wiki/Hagen%E2%80%93Poiseuille_equation. [Accessed May 2014].

[23] V. Slapar, “Microfluidics,” University of Ljubljana, Faculty of Mathematics and Physics, Ljubljana, January 2008, p. 3-4.

[24] J. N. Libii, “A Method of Evaluating the Presence of Fan-Blade-Rotation Induced Unsteadiness in Wind Tunnel Experiments,” in *Josué Njock Libii (2013). A Method of Evaluating the Presence of Fan-Blade-Rotation Induced Unsteadiness in Wind Tunnel Experiments, Wind Tunnel Designs and Their Diverse Engineering Applications, Dr. Noor Ahmed (Ed.), ISBN: 978-953-51-1047-7, InTech, DOI*, Indiana, USA, InTech, 2013, p. 97.

[25] G. M. Whitesides, “The origins and the future of microfluidics,” *Nature,* vol. 442, no. 27, pp. 368-369, July 2006.

[26] C. Kunstmann-Olsen, “Development of microfluidic sensing platforms,” University of

] Southern Denmark, Sønderborg, 2012.

[27] M. Joudenas, “Piezoelectric Actuation for microfluidic cell sorting,” Sønderborg, 2013.

[28] SPUR, *Datasheet, Speed Photography + Ultrahigh Resolution,* Langerwehe, used in may 2014, German.

[29] MicroChem., *Data sheet, SU-8 2050,* 2014.

[30] V. Sunkara, D. K. Park and Y. K. Cho, “Versatile method for bonding hard and soft materials,” *RSC Advances,* no. Issue 24, 2012, pp. 9066-9070, 2012.

[31] Mikhail Polyanskiy , “Refractive Index database,” 2013. [Online]. Available: http://refractiveindex.info/. [Accessed may 2014].

[32] K-Patetnts Process Instruments, “Refractive Index Measurement Principle p.6-7,” [Online]. Available: http://www.kpatents.com/pdf/downloads/refractive_index_principle.pdf. [Accessed April 2014].

[33] Biosensing Instrument Inc. , “Surface Plasmon Resonance Technology,” Biosensing Instrument Inc. , 2006-2013. [Online]. Available: http://www.biosensingusa.com/biosensing_instrument_technology.html. [Accessed May 2014].

Appendices

1. The software for calculation SPPs
2. Detailed recipe of fabrication the PDMS chip
3. Su-8
4. Datenblatt SPUR Docu SHC

Appendix 1 - The software for calculation SPPs

The code for the software which calculates the incident angle of surface plasmon resonance is presented below. All necessary to understand comments are applied. Sentences preceded by a hash (#) are comments which are seen in the code but are ignored by the software during compilation.

```
(below are presented values of complex refractive index for each of assumed layer with their thickness)
# Filmstack properties set WAVELENGTH  0.633
set WAVELENGTH  0.795
# prism 633nm set N1 1.5151 set K1 0.0000000012126
# prism 795nm
set N1 1.511
set K1 0.0000000092489

# index matching oil 795nm
set N2 1.500
set K2 0.0000

#Glass slide BK7 795nm
set N3 1.511
set K3 0.0000000092489

#Ti 795nm
set N4 2.9287
set K4 3.2835

#Au 795nm
set N5 0.18266
set K5 5.1075

#Au 633nm set N2 0.18344 set K2 3.4332
#Ti 633nm set N3 2.7043 set K3 3.7657
#SiO2 633nm set N3 1.5426 set K3 0.0

# air 795nm
set N6 1.00027508
set K6 0.00000

# air 633nm set N4 1.00027653 set K4 0.00000
# water 795nm set N4 1.3292 set K4 0.0000001296

#thickness
set H1 1.45
set H2 0.020
set H3 0.016
set H4 0.002
set H5 0.030
set H6 1.50

#variable for loops Value1 is for loop which is increasing thickness of AU and Value 2 is for second loop
set Value1 1
set Value2 1

#step which thickness of layers increase in each loop
set ThicknessAU 0.005
set Thickness2nd 0.001

#temporary thickness, it is useful for loop to avoid overwriting the thickness
#set H2TIME 0
set H4TIME $H4
set H5TIME $H5
```

```
#How many times loop should repeat
set MLOOP 7
set MLOOPS 4

# Yee cell size
set GRIDSIZE 0.005

#Loop to increase the thickness of Au layer
while {$Value1<=$MLOOP} {

set H4TIME $H4 (set the temporary value)

set Value2 1

#Loop to increase the thickness of 2nd layer
        while {$Value2<=$MLOOPS} {

        # Simulation domain size
        set LX $GRIDSIZE
        set LY $GRIDSIZE
        set LZ [expr $H1+$H2+$H3+$H4TIME+$H5TIME+$H6] (here must be added all defined layers)

        # Number of Yee cells
        set NX [expr int($LX/$GRIDSIZE+0.5)]
        set NY [expr int($LY/$GRIDSIZE+0.5)]
        set NZ [expr int($LZ/$GRIDSIZE+0.5)]


        # Open a file to save data
        set FILE [open "Air 795nm Au $H5TIME Ti $H4TIME $Value1 $Value2.txt" w] (creating the file)
        puts $FILE "theta R"
        close $FILE


        # Loop over polarization (TE, TM) (loop for checking the mode)
        foreach POLARIZATION {TM} {
                # Loop over incident angle (setting the range of calculation with the precision- here range is from 30 to 80 degree and precision is set to 0,5 degree)
                for {set THETA 30} {$THETA <= 80} {set THETA [expr $THETA+0.5]} {

                ### Setup FDTD grid
                emxp::grid lx=$LX ly=$LY lz=$LZ nx=$NX ny=$NY nz=$NZ n0=$N1 k0=$K1

                        ### Setup FDTD geometry (here starts the process of calculation, parameters for Z-axes (ZC) should be repeated till all the thickness of layer in z-direction is equal to sum of each of the layer)
                                set XC [expr 0.5*$LX]
                                set YC [expr 0.5*$LY]
                                set ZC [expr $H1+0.5*$H2]
emxp::solid shape=box xc=$XC yc=$YC zc=$ZC xw=[expr 200*$LX] yw=[expr 200*$LY] zw=$H2  n=$N2 k=$K2
                                set ZC [expr $H1+$H2+0.5*$H3]
 emxp::solid shape=box xc=$XC yc=$YC zc=$ZC xw=[expr 200*$LX] yw=[expr 200*$LY] zw=$H3 n=$N3 k=$K3
                                set ZC [expr $H1+$H2+$H3+0.5*$H4TIME]
emxp::solid shape=box xc=$XC yc=$YC zc=$ZC xw=[expr 200*$LX] yw=[expr 200*$LY] zw=$H4TIME n=$N4 k=$K4
                                set ZC [expr $H1+$H2+$H3+$H4TIME+0.5*$H5TIME]
emxp::solid shape=box xc=$XC yc=$YC zc=$ZC xw=[expr 200*$LX] yw=[expr 200*$LY] zw=$H5TIME n=$N5 k=$K5
                                set ZC [expr $H1+$H2+$H3+$H4TIME+$H5TIME+0.5*$H6]
```

```
 emxp::solid shape=box xc=$XC yc=$YC zc=$ZC xw=[expr 200*$LX] yw=[expr 200*$LY] zw=$H6 n=$N6
k=$K6


                                        ### Setup FDTD incident field
                                                if {$POLARIZATION == "TE"} {
                                                        set ES 1.0
                                                        set EP 0.0
                                                } else {
                                                        set ES 0.0
                                                        set EP 1.0
                                                 }
                                        set ZSRC [expr 0.5*$H1]
emxp::planewave2 wavelength=$WAVELENGTH z_source=$ZSRC theta=$THETA phi=0 ep_amp=$EP
es_amp=$ES ep_phz=0.0 es_phz=0.0

                                        ### Setup FDTD PML boundary condition
                                        emxp::pml3

                                         ### Setup FDTD convergence monitor

        emxp::convergence i=0 j=0 k=0 samples_per_cycle=0.1 sample_size=10 tolerance=0.005

                                        ### Run FDTD solver
                                        emxp::run n_cycles=100


                        ### Compute the ratio of zero diffraction order reflected energy to incident energy
                        set R00 [emxp::diffraction_efficiency field=reflected   type=individual m=0 n=0]

                                        # Save data to file
                        set FILE [open "Air 795nm Au $H5TIME Ti $H4TIME $Value1 $Value2.txt" a]
                                        puts $FILE "$THETA $R00"
                                        close $FILE


                                        ### Reset FDTD solver before next condition
                                        emxp::reset

                        }
                }

        # increaseing the loop's variable
        set Value2 [expr $Value2+1]

        # increasing the Au thickness for next loop
        set H5TIME  [expr $H5TIME +$Thickness2nd]
        }

# Increasing the value of variables used only for counting the loops
set Value1 [expr $Value1+1]
# increasing the 2nd matierial thickness for next loop
set H4TIME [expr $H4TIME+$ThicknessAU]
}
 Exit
```

Appendix 2 - Detailed recipe of fabrication the PDMS chip

1. Fabrication of master mold takes place in cleanroom.
    a. Starting wafer: Si(100), 4'', single-sided polished, thickness = 525µm
    b. Cleaning – Piranha wet etch, rinse with DI-water, dry
    c. Solvent cleaning – Alternative to 2: rinse in Acetone, IPA and DI water
       Dehydrate: bake for 5 min at 150°C on hotplate
    d. Spincoating photoresist- use resist SU-8 2050, resulting in 85µm film
        - Pour a few ml on the wafer
        - Spin at 500rpm for 5 sec (acc. 250rpm/sec)
        - Spin at 1500rpm for 60sec (acc. 500 rpm/sec)
    e. Soft bake
        - Bake for 5 min at 65°C on a hotplate
        - Bake for 10 min at 95°C for on a hotplate
    f. UV exposure –mask aligner, use photo-negative, energy=220mJ/cm^2
       Exposure time= 75sec
    g. Post exposure bake
        - Bake for 3 min at 65°C on a hotplate
        - Bake for 10 min at 95°C on a hotplate
    h. Develop
        - Dilute 35ml SU-8 developer in 15ml IPA
        - Develop for 5 min, agitation!
    i. Rinse and dry – rinse with IPA for 30s, dry with pressurized air
    j. Hard bake – bake for 10 min at 150°C on a hotplate
    k. Inspection – Optical microscope, profiler or maybe SEM.

2. PDMS mixing takes place in chemical lab:
    a. *SYLGARD 184 silicone* has 2 ingredients: base and the curing agent
    b. Mix in proposition 10:1, respectively
    c. 7g of the base for 1 chip
        i. Take pipette and plastic plate for elastomer (hardener)
        ii. Put the plate on the weight and pour desire amount
        iii. Using the pipette pour the elastomer - the 10% of the base weight
        iv. Mix all ingredients well
        v. Clean everything
    d. Outgassing in the optic lab for at least 20 min

3. Main Chip fabrication – the casting method takes place in the optic lab
    a. Put the mold with desire design in the cast
    b. Cover the mold with the second part of the cast and put alignment pins
    c. Assembly all three parts of the cast together and screw gently with screws

d. Pour PDMS slowly into the holder – to avoid unnecessary oxygenation
e. Outgassing for around 10 min (but not too long)
f. Bond with the glass slid in plasma cleaner-but don't press both together (This makes the PDMS chip bends)

4. Cleaning old PDMS chips takes place in the chemical lab
    a. Use beaker, plastic tweezers and googles
    b. Pour HCL (it should cover the chip)
    c. Leave for 8-10 min
    d. In the other beaker pour DI water and put there the chip
    e. HCL pour to the Inorganic Acids Waste
    f. Take out the chip, raise with DI water and blow with the nitrogen

5. Sealing part takes place in Optic lab with usage of the Plasma Cleaner. After adjusting all parameters of this process, the activation of surface takes place in plasma only for 1 min.